

# The ANTARES Collaboration

## Contributions to ICRC 2017

### Part II: The multi-messenger program

---

#### Contents

<b>1 Time-dependent search for neutrino emission from Mrk 421 and Mrk 501 observed by the HAWC gamma-ray observatory</b>	<b>5</b>
PoS (ICRC2017) 946	
<b>2 Searching for High Energy Neutrinos detected by ANTARES in coincidence with Gravitational Wave signals observed during LIGO Observation Run O1</b>	<b>13</b>
PoS (ICRC2017) 947	
<b>3 Time-dependent search of neutrino emission from bright gamma-ray flaring blazars with the ANTARES telescope</b>	<b>21</b>
PoS (ICRC2017) 970	
<b>4 Time-dependent search of neutrino emission from X-ray and gamma-ray binaries with the ANTARES telescope</b>	<b>28</b>
PoS (ICRC2017) 971	
<b>5 Multi-messenger real-time follow-up of transient events with the ANTARES neutrino telescope</b>	<b>36</b>
PoS (ICRC2017) 984	
<b>6 Multi-wavelength follow-up observations of ANTARES neutrino alerts</b>	<b>44</b>
PoS (ICRC2017) 985	
<b>7 Search for muon neutrinos from GRBs with the ANTARES neutrino telescope</b>	<b>52</b>
PoS (ICRC2017) 988	
<b>8 Search for neutrinos from Fast Radio Bursts with ANTARES</b>	<b>60</b>
PoS (ICRC2017) 989	
<b>9 Search for a correlation between ANTARES high-energy neutrinos and ultra high-energy cosmic rays detected by the Pierre Auger Observatory and the Telescope Array</b>	<b>67</b>
PoS (ICRC2017) 990	

*35th International Cosmic Ray Conference — ICRC2017*  
 10–20 July, 2017, Bexco, Busan, Korea

## ANTARES Collaboration Author List

A. Albert<sup>1</sup>, M. André<sup>2</sup>, M. Anghinolfi<sup>3</sup>, G. Anton<sup>4</sup>, M. Ardid<sup>5</sup>, J.-J. Aubert<sup>6</sup>, T. Avgitas<sup>7</sup>, B. Baret<sup>7</sup>, J. Barrios-Martí<sup>8</sup>, S. Basa<sup>9</sup>, B. Belhorma<sup>10</sup>, V. Bertin<sup>6</sup>, S. Biagi<sup>11</sup>, R. Bormuth<sup>12,13</sup>, S. Bourret<sup>7</sup>, M.C. Bouwhuis<sup>12</sup>, H. Brânzaş<sup>14</sup>, R. Bruijn<sup>12,15</sup>, J. Brunner<sup>6</sup>, J. Busto<sup>6</sup>, A. Capone<sup>16,17</sup>, L. Caramete<sup>14</sup>, J. Carr<sup>6</sup>, S. Celli<sup>16,17,18</sup>, R. Cherkaoui El Moursli<sup>19</sup>, T. Chiarusi<sup>20</sup>, M. Circella<sup>21</sup>, J.A.B. Coelho<sup>7</sup>, A. Coleiro<sup>7,8</sup>, R. Coniglione<sup>11</sup>, H. Costantini<sup>6</sup>, P. Coyle<sup>6</sup>, A. Creusot<sup>7</sup>, A. F. Díaz<sup>22</sup>, A. Deschamps<sup>23</sup>, G. De Bonis<sup>16</sup>, C. Distefano<sup>11</sup>, I. Di Palma<sup>16,17</sup>, A. Domi<sup>3,24</sup>, C. Donzaud<sup>7,25</sup>, D. Dornic<sup>6</sup>, D. Drouhin<sup>1</sup>, T. Eberl<sup>4</sup>, I. El Bojaddaini<sup>26</sup>, N. El Khayati<sup>19</sup>, D. Elsässer<sup>27</sup>, A. Enzenhöfer<sup>6</sup>, A. Ettahiri<sup>19</sup>, F. Fassi<sup>19</sup>, I. Felis<sup>5</sup>, L.A. Fusco<sup>20,28</sup>, P. Gay<sup>29,7</sup>, V. Giordano<sup>30</sup>, H. Glotin<sup>31,32</sup>, T. Grégoire<sup>7</sup>, R. Gracia Ruiz<sup>7,33</sup>, K. Graf<sup>4</sup>, S. Hallmann<sup>4</sup>, H. van Haren<sup>34</sup>, A.J. Heijboer<sup>12</sup>, Y. Hello<sup>23</sup>, J.J. Hernández-Rey<sup>8</sup>, J. Höfl<sup>4</sup>, J. Hofestädt<sup>4</sup>, C. Hugon<sup>3,24</sup>, G. Illuminati<sup>8</sup>, C.W. James<sup>4</sup>, M. de Jong<sup>12,13</sup>, M. Jongen<sup>12</sup>, M. Kadler<sup>27</sup>, O. Kalekin<sup>4</sup>, U. Katz<sup>4</sup>, D. Kießling<sup>4</sup>, A. Kouchner<sup>7,32</sup>, M. Kreter<sup>27</sup>, I. Kreykenbohm<sup>35</sup>, V. Kulikovskiy<sup>6,36</sup>, C. Lachaud<sup>7</sup>, R. Lahmann<sup>4</sup>, D. Lefèvre<sup>37</sup>, E. Leonora<sup>30,38</sup>, M. Lotze<sup>8</sup>, S. Loucatos<sup>39,7</sup>, M. Marcelin<sup>9</sup>, A. Margiotta<sup>20,28</sup>, A. Marinelli<sup>40,41</sup>, J.A. Martínez-Mora<sup>5</sup>, R. Mele<sup>42,43</sup>, K. Melis<sup>12,15</sup>, T. Michael<sup>12</sup>, P. Migliozzi<sup>42</sup>, A. Moussa<sup>26</sup>, S. Navas<sup>44</sup>, E. Nezri<sup>9</sup>, M. Organokov<sup>33</sup>, G.E. Pāvālaš<sup>14</sup>, C. Pellegrino<sup>20,28</sup>, C. Perrina<sup>16,17</sup>, P. Piattelli<sup>11</sup>, V. Popa<sup>14</sup>, T. Pradier<sup>33</sup>, L. Quinn<sup>6</sup>, C. Racca<sup>1</sup>, G. Riccobene<sup>11</sup>, A. Sánchez-Losa<sup>21</sup>, M. Saldaña<sup>5</sup>, I. Salvadori<sup>6</sup>, D. F. E. Samtleben<sup>12,13</sup>, M. Sanguineti<sup>3,24</sup>, P. Sapienza<sup>11</sup>, F. Schüssler<sup>39</sup>, C. Sieger<sup>4</sup>, M. Spurio<sup>20,28</sup>, Th. Stolarczyk<sup>39</sup>, M. Taiuti<sup>3,24</sup>, Y. Tayalati<sup>19</sup>, A. Trovato<sup>11</sup>, D. Turpin<sup>6</sup>, C. Tönnes<sup>8</sup>, B. Vallage<sup>39,7</sup>, V. Van Elewyck<sup>7,32</sup>, F. Versari<sup>20,28</sup>, D. Vivolo<sup>42,43</sup>, A. Vizzoca<sup>16,17</sup>, J. Wilms<sup>35</sup>, J.D. Zornoza<sup>8</sup>, J. Zúñiga<sup>8</sup>.

<sup>1</sup>GRPHE - Université de Haute Alsace - Institut universitaire de technologie de Colmar, 34 rue du Grillenbreit BP 50568 - 68008 Colmar, France

<sup>2</sup>Technical University of Catalonia, Laboratory of Applied Bioacoustics, Rambla Exposició, 08800 Vilanova i la Geltrú, Barcelona, Spain

<sup>3</sup>INFN - Sezione di Genova, Via Dodecaneso 33, 16146 Genova, Italy

<sup>4</sup>Friedrich-Alexander-Universität Erlangen-Nürnberg, Erlangen Centre for Astroparticle Physics, Erwin-Rommel-Str. 1, 91058 Erlangen, Germany

<sup>5</sup>Institut d'Investigació per a la Gestió Integrada de les Zones Costaneres (IGIC) - Universitat Politècnica de València. C/ Paranimf 1, 46730 Gandia, Spain

<sup>6</sup>Aix Marseille Univ, CNRS/IN2P3, CPPM, Marseille, France

<sup>7</sup>APC, Univ Paris Diderot, CNRS/IN2P3, CEA/Irfu, Obs de Paris, Sorbonne Paris Cité, France

<sup>8</sup>IFIC - Instituto de Física Corpuscular (CSIC - Universitat de València) c/ Catedrático José Beltrán, 2 E-46980 Paterna, Valencia, Spain

<sup>9</sup>LAM - Laboratoire d'Astrophysique de Marseille, Pôle de l'Étoile Site de Château-Gombert, rue Frédéric Joliot-Curie 38, 13388 Marseille Cedex 13, France

<sup>10</sup>National Center for Energy Sciences and Nuclear Techniques, B.P.1382, R. P.10001 Rabat, Morocco

<sup>11</sup>INFN - Laboratori Nazionali del Sud (LNS), Via S. Sofia 62, 95123 Catania, Italy

- <sup>12</sup>Nikhef, Science Park, Amsterdam, The Netherlands
- <sup>13</sup>Huygens-Kamerlingh Onnes Laboratorium, Universiteit Leiden, The Netherlands
- <sup>14</sup>Institute of Space Science, RO-077125 Bucharest, Măgurele, Romania
- <sup>15</sup>Universiteit van Amsterdam, Instituut voor Hoge-Energie Fysica, Science Park 105, 1098 XG Amsterdam, The Netherlands
- <sup>16</sup>INFN - Sezione di Roma, P.le Aldo Moro 2, 00185 Roma, Italy
- <sup>17</sup>Dipartimento di Fisica dell'Università La Sapienza, P.le Aldo Moro 2, 00185 Roma, Italy
- <sup>18</sup>Gran Sasso Science Institute, Viale Francesco Crispi 7, 00167 L'Aquila, Italy
- <sup>19</sup>University Mohammed V in Rabat, Faculty of Sciences, 4 av. Ibn Battouta, B.P. 1014, R.P. 10000 Rabat, Morocco
- <sup>20</sup>INFN - Sezione di Bologna, Viale Berti-Pichat 6/2, 40127 Bologna, Italy
- <sup>21</sup>INFN - Sezione di Bari, Via E. Orabona 4, 70126 Bari, Italy
- <sup>22</sup>Department of Computer Architecture and Technology/CITIC, University of Granada, 18071 Granada, Spain
- <sup>23</sup>Géozur, UCA, CNRS, IRD, Observatoire de la Côte d'Azur, Sophia Antipolis, France
- <sup>24</sup>Dipartimento di Fisica dell'Università, Via Dodecaneso 33, 16146 Genova, Italy
- <sup>25</sup>Université Paris-Sud, 91405 Orsay Cedex, France
- <sup>26</sup>University Mohammed I, Laboratory of Physics of Matter and Radiations, B.P.717, Oujda 6000, Morocco
- <sup>27</sup>Institut für Theoretische Physik und Astrophysik, Universität Würzburg, Emil-Fischer Str. 31, 97074 Würzburg, Germany
- <sup>28</sup>Dipartimento di Fisica e Astronomia dell'Università, Viale Berti Pichat 6/2, 40127 Bologna, Italy
- <sup>29</sup>Laboratoire de Physique Corpusculaire, Clermont Université, Université Blaise Pascal, CNRS/IN2P3, BP 10448, F-63000 Clermont-Ferrand, France
- <sup>30</sup>INFN - Sezione di Catania, Viale Andrea Doria 6, 95125 Catania, Italy
- <sup>31</sup>LSIS, Aix Marseille Université CNRS ENSAM LSIS UMR 7296 13397 Marseille, France; Université de Toulon CNRS LSIS UMR 7296, 83957 La Garde, France
- <sup>32</sup>Institut Universitaire de France, 75005 Paris, France
- <sup>33</sup>Université de Strasbourg, CNRS, IPHC UMR 7178, F-67000 Strasbourg, France
- <sup>34</sup>Royal Netherlands Institute for Sea Research (NIOZ) and Utrecht University, Landsdiep 4, 1797 SZ 't Horntje (Texel), the Netherlands
- <sup>35</sup>Dr. Reimis-Sternwarte and ECAP, Friedrich-Alexander-Universität Erlangen-Nürnberg, Sternwartstr. 7, 96049 Bamberg, Germany
- <sup>36</sup>Moscow State University, Skobeltsyn Institute of Nuclear Physics, Leninskie gory, 119991 Moscow, Russia
- <sup>37</sup>Mediterranean Institute of Oceanography (MIO), Aix-Marseille University, 13288, Marseille, Cedex 9, France; Université du Sud Toulon-Var, CNRS-INSU/IRD UM 110, 83957, La Garde Cedex, France
- <sup>38</sup>Dipartimento di Fisica ed Astronomia dell'Università, Viale Andrea Doria 6, 95125 Catania, Italy
- <sup>39</sup>Direction des Sciences de la Matière - Institut de recherche sur les lois fondamentales de l'Univers - Service de Physique des Particules, CEA Saclay, 91191 Gif-sur-Yvette Cedex, France
- <sup>40</sup>INFN - Sezione di Pisa, Largo B. Pontecorvo 3, 56127 Pisa, Italy
- <sup>41</sup>Dipartimento di Fisica dell'Università, Largo B. Pontecorvo 3, 56127 Pisa, Italy
- <sup>42</sup>INFN - Sezione di Napoli, Via Cintia 80126 Napoli, Italy
- <sup>43</sup>Dipartimento di Fisica dell'Università Federico II di Napoli, Via Cintia 80126, Napoli, Italy
- <sup>44</sup>Dpto. de Física Teórica y del Cosmos & C.A.F.P.E., University of Granada, 18071 Granada, Spain

**Acknowledgements:**

The authors acknowledge the financial support of the funding agencies: Centre National de la Recherche Scientifique (CNRS), Commissariat à l'énergie atomique et aux énergies alternatives (CEA), Commission Européenne (FEDER fund and Marie Curie Program), Institut Universitaire de France (IUF), IdEx program and UnivEarthS Labex program at Sorbonne Paris Cité (ANR-10-LABX-0023 and ANR-11-IDEX-0005-02), Labex OCEVU (ANR-11-LABX-0060) and the A\*MIDEX project (ANR-11-IDEX-0001-02), Région Île-de-France (DIM-ACAV), Région Alsace (contrat CPER), Région Provence-Alpes-Côte d'Azur, Département du Var and Ville de La Seyne-sur-Mer, France; Bundesministerium für Bildung und Forschung (BMBF), Germany; Istituto Nazionale di Fisica Nucleare (INFN), Italy; Stichting voor Fundamenteel Onderzoek der Materie (FOM), Nederlandse organisatie voor Wetenschappelijk Onderzoek (NWO), the Netherlands; Council of the President of the Russian Federation for young scientists and leading scientific schools supporting grants, Russia; National Authority for Scientific Research (ANCS), Romania; Ministerio de Economía y Competitividad (MINECO): Plan Estatal de Investigación (refs. FPA2015-65150-C3-1-P, -2-P and -3-P, (MINECO/FEDER)), Severo Ochoa Centre of Excellence and MultiDark Consolider (MINECO), and Prometeo and Grisolia programs (Generalitat Valenciana), Spain; Ministry of Higher Education, Scientific Research and Professional Training, Morocco. We also acknowledge the technical support of Ifremer, AIM and Foselev Marine for the sea operations and the CC-IN2P3 for the computing facilities.

# Time-dependent search for neutrino emission from Mrk 421 and Mrk 501 observed by the HAWC gamma-ray observatory

---

## Mukharbek Organokov

*IPHC - Institut Pluridisciplinaire Hubert Curien - Universite de Strasbourg et CNRS/IN2P3,  
23 rue du Loess, BP 28, 67037 Strasbourg Cedex 2, France*

*E-mail: [mukharbek.organokov@iphc.cnrs.fr](mailto:mukharbek.organokov@iphc.cnrs.fr)*

## Agustin Sanchez-Loza\*

*INFN - Sezione di Bari, Via Edoardo Orabona 4, 70125 Bari, Italy*

*E-mail: [agustin.sanchez@ba.infn.it](mailto:agustin.sanchez@ba.infn.it)*

## Thierry Pradier

*IPHC - Institut Pluridisciplinaire Hubert Curien - Universite de Strasbourg et CNRS/IN2P3,  
23 rue du Loess, BP 28, 67037 Strasbourg Cedex 2, France*

*E-mail: [thierry.pradier@iphc.cnrs.fr](mailto:thierry.pradier@iphc.cnrs.fr)*

## on behalf of the ANTARES Collaboration

The principles of a search for high energy neutrino emission in coincidence with very high energy (VHE; 0.1-100 TeV) gamma-ray flares from two bright extragalactic sources, based on the data collected in 2012-2016 by the ANTARES neutrino detector and High Altitude Water Cherenkov (HAWC) gamma-ray observatory, are presented. The ANTARES telescope observes with high duty cycle an instantaneous field of view of  $2\pi$ . To study variable sources like blazars, it is crucial to achieve unbiased monitoring and an instrument like HAWC is capable of long term and continuous monitoring of the source with nearly 100% duty cycle. Markarian 421 (Mrk 421) and Markarian 501 (Mrk 501) are the brightest and the closest BL Lac objects known. In contrast to other types of active galactic nuclei (AGN), BL Lacs are characterized by rapid and large-amplitude flux variability. Such radio-loud AGNs with collimated jets aligned to the line of sight, are candidate sources of the observed high energy cosmic rays and of accompanying neutrinos and gamma rays produced in hadronic interactions with the surrounding medium.

*35th International Cosmic Ray Conference — ICRC2017*

*10–20 July, 2017*

*Bexco, Busan, Korea*

---

\*Speaker.

## 1. Introduction

The VHE extragalactic sky is dominated by emission from blazars [1], a class of non-thermal jet-powered AGN known as radio-loud AGN. The spectral energy distribution (SED) of blazars can be described with two components: one low-energy from radio to X-ray and one high-energy from X-ray to TeV. The low energy component is commonly assumed to come from synchrotron emission of accelerated emitted. The origin of the high-energy part is still under discussion: either from inverse compton in the leptonic processes or imbeded protons [2]. Some hadronic scenarios introduce relativistic protons to explain the high-energy bump generally seen in the MeV to TeV range for BL Lac objects. In the hadronic framework, this component attributed to either proton-synchrotron emission or radiation from secondary products of  $p\gamma$  or  $pp$  interactions [2, 3, 4]. Acceleration of protons is assumed to occur by the first-order diffusive Fermi mechanism at the shock, resulting in a generic  $E^{-2}$  differential spectrum. Energy loss processes which occur during acceleration include  $p\gamma \rightarrow N\pi$  and  $p\gamma \rightarrow p + e^+e^-$  in the dense radiation fields and  $pp$  collisions in the gas. All three processes contribute to an energetic electromagnetic component, either through  $\pi^0 \rightarrow \gamma\gamma$  or by production of electrons. Both photo-meson production and  $pp$  collisions also give rise to neutrinos via  $\pi^\pm \rightarrow \mu^\pm \nu_\mu \bar{\nu}_\mu \rightarrow e^\pm \bar{\nu}_e \nu_\mu \bar{\nu}_\mu$  decay chain [3].

This analysis focuses on the search of spatial/temporal correlation between neutrinos detected by ANTARES and  $\gamma$ -ray emission from flares detected by HAWC from Mrk 421 and Mrk 501, the first and the second extragalactic object discovered in the TeV energy band. Moreover, these are two of four sources detected in the 0.6-2.0 TeV band by *Fermi*-LAT out of the Galactic plane,  $|\text{bl}| > 5^\circ$ , and at low redshift,  $z < 0.3$  [5]. Both sources have been significantly detected in the 2HAWC catalog [6], and flare information were recently reported in [7] (see section 3.1).

Mrk 421 and Mrk 501 are the brightest and closest BL Lac objects known, at luminosity distances  $d_L = 134$  Mpc with redshift  $z = 0.031$  and  $d_L = 143$  Mpc with redshift  $z=0.033$  respectively. Both are classified as high-peaked BL Lac objects (HBL). Mrk 421 is known to exhibit a high degree of variability in its emission and yearly average fluxes are known to vary between a few tenths and 1.9 times the flux of the Crab Nebula. Variability of Mrk 421 has been observed down to time scales of hours or less and its spectral shape is known to vary with its brightness. Various studies of Mrk 501 at TeV energies have shown different features of low flux states emission and extreme outbursts [7]. The VHE spectrum of Mrk 421 has been successfully modeled with both leptonic and hadronic models and conclusive results have been achieved yet about origin and both models are still under debate [8]. As the nearest blazars to Earth, both are excellent sources to test the blazar-neutrino connection scenario, especially during flares where time-dependent neutrino searches may have a higher detection probability.

The IceCube collaboration has performed a time integrated search for the most significant a priori source candidates selected on the basis of  $\gamma$ -rays observations or astrophysical modeling that predicts neutrino emission [9]. No significant excess was found leading to an differential flux limit of  $dN/dE \leq 11.71 \times 10^{-12} \text{TeV}^{-1} \text{cm}^{-2} \text{s}^{-1}$  for Mrk 421 and  $dN/dE \leq 8.11 \times 10^{-12} \text{TeV}^{-1} \text{cm}^{-2} \text{s}^{-1}$  for Mrk 501. Additional searches in IceCube [10] show no correlated neutrinos.

Similar time-dependent analyses have been performed in the past using ANTARES data, in particular for flaring blazars [11].

## 2. The ANTARES neutrino telescope

The ANTARES Neutrino Telescope (Astronomy with a Neutrino Telescope and Abyss environmental RESearch) is a Cherenkov detector located in the Mediterranean sea, 40 km off the coast of Toulon, France ( $42^{\circ}48' \text{ N } 6^{\circ}10'$ ), at a depth of 2,475 meters. Currently, ANTARES is the largest neutrino telescope in the Northern Hemisphere and it is designed primarily to search for  $E > 100 \text{ GeV}$  muons resulting from the charged-current (CC) interactions of  $\nu_{\mu}$  in the vicinity of the detector. The median angular resolution for  $E^{-2}$  for tracks is  $\sim 0.5^{\circ}$  [12]. The search of such astrophysical neutrinos origin has become a key mission in high-energy astrophysics after the discovery from IceCube of a cosmic neutrino flux of still unknown origin [13].

### 2.1 Data selection

The data set covers the period from the January 1<sup>st</sup>, 2012 to December 31<sup>st</sup>, 2016 (MJD: 55927-57753) leading to effective detector livetime of 1209 days, covering the same period of observation as HAWC. The search relies on track-like event signatures, so only CC interactions of muon neutrinos considered. Atmospheric neutrinos are the main source of background. An additional source of background is due to the mis-reconstructed atmospheric muons. The muon track reconstruction returns two quality parameters, namely the track-fit quality parameter,  $\Lambda$ , and the estimated angular uncertainty on the fitted muon track direction,  $\beta$ . Cuts on these parameters are used to improve the signal-to-noise ratio.  $\Lambda$  will be optimised source by source. To ensure a good directional reconstruction of the selected  $\nu$  candidates,  $\beta < 1$  is required [14].

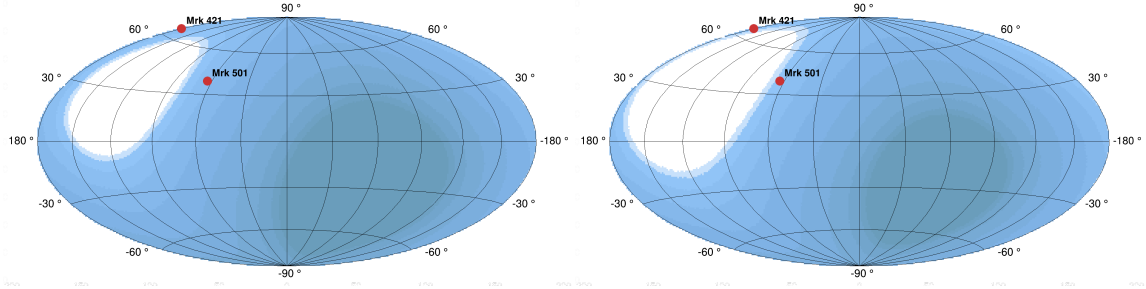


**Figure 1:** ANTARES visibility of the sky ranging from 0 (white) to 100% (dark blue) with 10% step. Left: Upgoing and slightly downgoing (angle above the horizon below  $8.62^{\circ}$ ) for  $\cos(\theta) > -0.15$ ; Right: Only Upgoing  $\cos(\theta) > 0$ .

Due to the fact that Mrk 421 and Mrk 501 are located at the edge of ANTARES visibility (see Fig. 1) and sources are below the horizon only  $\sim 6$  hours per day, a small amount of down-going events can be accepted to gain  $\sim 15\%$  in visibility (see Fig. 1), and increase an observation time (see Fig. 2). This is done by application of the cut on cosine of zenith angle of the events. In this analysis events with  $\cos(\theta) > -0.15$  are selected.

## 3. The HAWC gamma-ray telescope

The HAWC Observatory is located at an elevation of 4,100 m above sea level on the flanks of the Sierra Negra volcano in the state of Puebla, Mexico ( $18^{\circ}99' \text{ N, } 97^{\circ}18' \text{ W}$ ). The detector

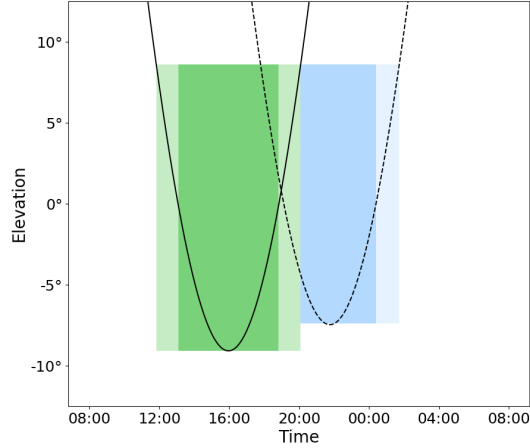


**Figure 2:** Source elevation as a function of time for Mrk 421 (solid) and for Mrk 501 (dash) at the ANTARES position for January 1<sup>st</sup>, 2016. Corresponding color boxes represent the elevation ranges (height) and source observation time by ANTARES (width) for  $\cos(\theta) > 0$  (dark) and  $\cos(\theta) > -0.15$  (light).

array installation began in February 2012; HAWC-300 fully operational began operation on March 20, 2015. Covering an area of  $22,000 \text{ m}^2$ , the array consists of 300 water Cherenkov detectors (WCDs), with 190,000 liters each and instrumented with 4 PMTs to detect Cherenkov light from charged particles in extensive air showers. The design of HAWC is optimized for the detection of air showers induced by  $\gamma$ -rays in 0.1-100 TeV. With field of view  $\sim 2$  steradians HAWC can monitor any source over  $2/3$  of the sky for up to 6 hours per day and most sensitive to sources between declinations  $-26^\circ$  and  $+64^\circ$  [7, 15, 16]. Such capabilities make unprecedented TeV light curve data available for studying flaring behavior of blazars. In addition, scanning a large part of the sky with such sensitivity increase the chances to find bright flare events from established and new extragalactic sources [7].

### 3.1 Light curves of blazars

HAWC has made clear detections of Mrk 421 and Mrk 501. Preliminary blazar light curves from data taken in 2013-2014 with the partial HAWC array were shown in [16]. In this analysis HAWC-300 data of first long-term TeV light curve studies with single-transit intervals are used, collected over 17 months between November 26<sup>th</sup>, 2014 and April 20<sup>th</sup>, 2016 [7].

In [7] the maximum-likelihood approach was used to test if the daily flux measurements in a light curve are consistent with a source flux that is constant in time over the whole period under consideration. The best-fit flux value  $F_i$  for time interval  $i$  is fitted from the minimisation of the following likelihood function [7]:

$$dN/dE = F_i (E/(1\text{TeV}))^{-\gamma} \exp(-E/E_{\text{cut}}) \quad (3.1)$$

converted to Crab Units by dividing by the HAWC measurement of the average Crab Nebula  $\gamma$ -ray flux  $1.89 \times 10^{-11} \text{ ph cm}^{-2} \text{ s}^{-1}$  above 1 TeV in order to allow comparisons between the sources. The main characteristics of the gamma-ray flux for the two sources are summarised in Table 1.



**Table 1:** Some parameters from [7]

	Mrk 421	Mrk 501
Highest daily flux*	$26.94 \pm 3.7$	$16.7 \pm 2.3$
Average flux*	$4.53 \pm 0.14$	$1.74 \pm 0.08$
$\Gamma^{**}$	$2.21 \pm 0.14_{\text{stat}} \pm 0.20_{\text{sys}}$	$1.60 \pm 0.30_{\text{stat}} \pm 0.20_{\text{sys}}$
$E_{\text{cut}}^{**}$	$E_0 = 5.4 \pm 1.1_{\text{stat}} \pm 1.0_{\text{sys}}$	$E_0 = 5.7 \pm 1.6_{\text{stat}} \pm 1.0_{\text{sys}}$

\* in  $10^{-12} \text{ ph cm}^{-2} \text{ s}^{-1}$  units; fluxes calculated above 2 TeV for Mrk 421 and above 3 TeV for Mrk 501.

\*\*Spectral index and exponential cut-off, derived from spectral fit.

If a light curve is variable, the Bayesian blocks algorithm can be used to find an optimal data segmentation into regions that are well represented by a constant flux, within the statistical uncertainties. Bayesian blocks algorithm is used to identify distinct flux states (see Fig. 3), both Mrk 421 and Mrk 501 show clear variability on time scales of one day. Taking advantage of gamma-ray flux variation time information from potential neutrino emitters as in Fig. 3, significantly reduce the  $\nu$  background and improve the signal-to-noise discrimination.

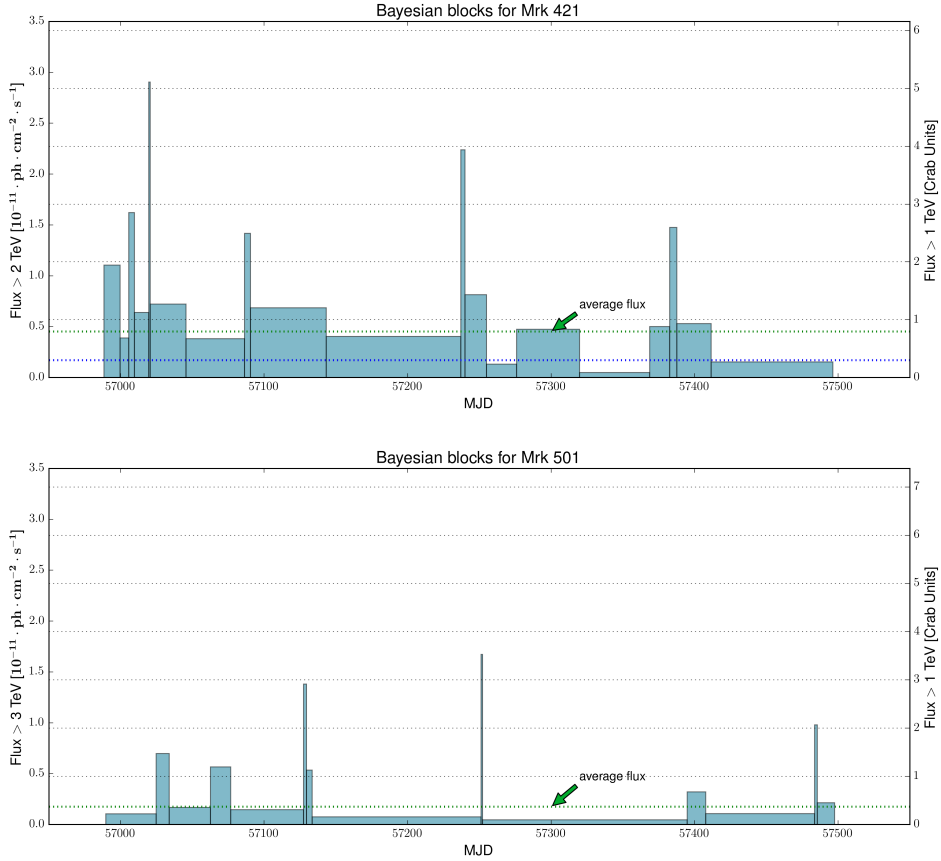


**Figure 3:** Flux light curve for Mrk 421 (top) and Mrk 501 (bottom) for 17 months; the green dotted lines represent the average fluxes,  $\sim 0.8$  CU and  $\sim 0.3$  CU respectively. The value for Mrk 421 is higher than previous estimates for an upper limit to the baseline flux  $\sim 0.3$  CU (blue). Adapted from [7]

#### 4. Time-dependent search method

A time-dependent search for neutrino candidates in coincidence with  $\gamma$ -rays from astrophysical sources is performed using an unbinned likelihood-ratio maximization method [11]. This is done via the test statistics,  $\lambda$ , defined as the ratio of the probability for the hypothesis of the background and signal ( $H_{\text{sig+bkg}}$ ), called  $H_1$ , over the probability of only background ( $H_{\text{bkg}}$ ), called  $H_0$ :

$$\lambda = \sum_{i=1}^N \ln \frac{P(x_i | H_{\text{sig+bkg}}(N_S))}{P(x_i | H_{\text{bkg}})}, \quad (4.1)$$

where  $N_S$  (unknown) and  $N$  (known) are expected number of signal events and total number of events in the considered data sample,  $x_i$  are observed event properties ( $\delta_i$ ,  $RA_i$ ,  $dE/dX_i$ , and  $t_i$ ).

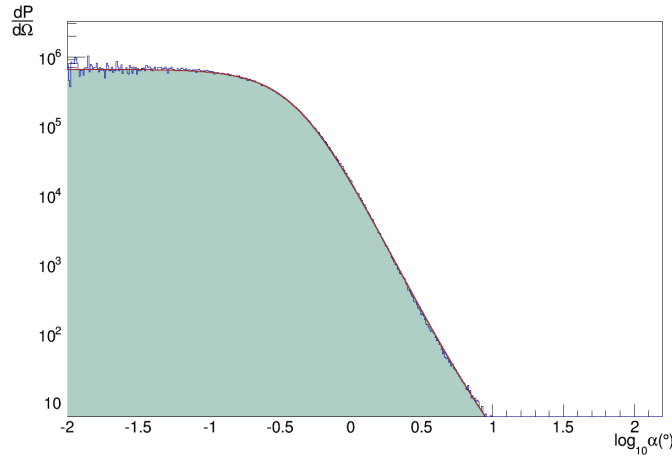


**Figure 4:** Sample of PSF parametrization for Mrk 421. The PSF parametrization before normalisation (red line) with  $\log_{10}\alpha$  distribution (shaded rea) for  $E^{-2}$  spectrum and  $\Lambda_{\text{cut}} > -5.2$ .

To perform the analysis, the ANTARES data sample is parametrized as two-component mixture of signal and background. The signal is expected to be small so that the full data direction scrambled can be used as an estimation of background.  $S_i$  and  $B_i$  are defined as the probability density functions (PDF) respectively for signal and background for an event  $i$ , at time  $t_i$ , energy, declination  $\delta_i$ . The logarithm of the likelihood  $L$  is:

$$\ln(L) = \left( \sum_{i=1}^N \ln[N_S S_i + N_B B_i] \right) - [N_S + N_B] \quad (4.2)$$

To distinguish the signal-like events from the background ones, for each event three types of PDFs are used, based on: direction  $P_s(\alpha_i)$  and  $P_b(\delta_i)$  for signal and background part respectively, where parameter  $\alpha_i$  represents the angular distance between the direction of the event  $i$  and direction to the source, and  $\delta_i$  is the declination of the event  $i$ ; energy  $P_s(E)$  and  $P_b(E)$ ; time  $P_s(t + \text{lag})$  and  $P_b(t)$ . These ingredients are determined using the ANTARES Monte Carlo simulations (MC) and data (see section 2.1). The background PDFs are all computed using data only. The shape of the time PDF for the signal event is extracted directly from the  $\gamma$ -ray light curve assuming a proportionality

between the  $\gamma$ -ray and the neutrino fluxes. A possible lag up to  $\pm 5$  days has been introduced in the likelihood. The energy PDF for the signal event is produced according to the studied energy spectrum. One of the most important parameter in point source search is the angular distance to the source, characterized by the Point Spread Function (PSF) -  $P_s(\alpha_i)$  (see Fig. 4), which is defined as the probability density of  $\alpha$  per unit solid angle,  $\Omega$ :

$$P_s(\alpha_i) = \frac{dP}{d\Omega} = \frac{d\alpha_i}{d\Omega} \frac{dP}{d\alpha_i} = \frac{1}{2\pi \sin \alpha_i} \frac{dP}{d\alpha_i}, \quad (4.3)$$

where  $\alpha_i = |\alpha_i^{true} - \alpha_i^{rec}|$  is the difference between simulated neutrino direction  $\alpha_i^{true}$  and reconstructed muon direction  $\alpha_i^{rec}$ .

Combining all terms considered before, the final likelihood is:

$$\ln(L) = \left( \sum_{i=1}^N \ln[N_S \cdot P_s(\alpha) \cdot P_s(E) \cdot P_s(t + \text{lag}) + N_B \cdot P_b(\sin(\delta)) \cdot P_b(E) \cdot P_b(t)] \right) - [N_S + N_B] \quad (4.4)$$

The test statistics is evaluated by generating pseudo-experiments (PEX) simulating background and signal around the considered source according to  $H_0$  and  $H_1$  hypothesis. The obtained value of  $\lambda$  for the data is compared to the value obtained by PEX. The discovery potential is the average number of signal events required to achieve a p-value lower than  $5.7 \cdot 10^{-7}$  for  $5\sigma$  discovery.

## 5. Conclusion

The HAWC detector operates nearly continuously and it is currently the most sensitive wide field-of-view telescope in the very promising VHE band  $\sim 0.1$  and  $\sim 100$  TeV. Therefore, it opens prospects to study the most energetic astrophysical phenomena in the Universe as well as understand the mechanisms that power them and endeavour to break the mystery of their origin. Taking into account the flare timing information given by gamma-ray observations, even for long-duration flares, should improve the efficiency of the search for a neutrino counterpart with ANTARES. The next generation KM3NeT neutrino telescope [17], currently being built in the Mediterranean Sea, will provide more than an order of magnitude improvement in sensitivity [18]; therefore, such sources are promising candidates as high energy neutrino emitters for an improved future time-dependent search.

## References

- [1] M. Cerruti et al. [HESS Collaboration], "Target of Opportunity observations of blazars with H.E.S.S.", AIP Conf.Proc. 1792 (2017) no.1, 050029 [arXiv:1610.05523][astro-ph.HE]
- [2] A. Zech, M. Cerruti, D. Mazin, "Expected signatures from hadronic emission processes in the TeV spectra of BL Lacertae objects", Astron.Astrophys. 602 (2017) A25 [arXiv:1703.05937][astro-ph.HE]
- [3] T.K. Gaisser, F. Halzen, T. Stanev, "Particle Physics with High Energy Neutrinos", Phys. Rep. 258 (1995) 173 [arXiv:hep-ph/9410384]
- [4] J.G. Learned, K. Mannheim, "High-energy neutrino astrophysics", Ann. Rev. Nucl. Part. Sci. 50 (2000) 679-749

- [5] M. Ackermann et al., "*2FHL: The Second Catalog of Hard Fermi-LAT Sources*", *Astrophys. J.*, 222, 5. (2016) [[arXiv:1508.04449](#)][astro-ph.HE]
- [6] A. Abeysekara et al. [HAWC Collaboration], "*The 2HWC HAWC Observatory Gamma Ray Catalog*", *Astrophys.J.* 843 (2017) no.1, 40 [[arXiv:1702.02992](#)][astro-ph.HE].
- [7] A. Abeysekara et al. [HAWC Collaboration], "*Daily monitoring of TeV gamma-ray emission from Mrk 421, Mrk 501, and the Crab Nebula with HAWC*", *Astrophys.J.*, 841 (2017) no.2, 100 [[arXiv:1703.06968](#)][astro-ph.HE]
- [8] A. Marinelli, B. Patricelli, N. Fraija, "*Hadronic flares and associated neutrinos for Markarian 421*", Published in *IAU Symp.* 313 (2015) 177-178 [[arXiv:1505.03165](#)][astro-ph.HE]
- [9] Abbasi et al. [IceCube Collaboration], "*Time-Integrated Searches for Point-like Sources of Neutrinos with the 40-String IceCube Detector*", *Astrophys J.*, 732 (2011), no.1, 18 [[arXiv:1012.2137](#)][astro-ph.HE]
- [10] Aartsen et al. [IceCube Collaboration], "*Searches for Extended and Point-like Neutrino Sources with Four Years of IceCube Data*", *Astrophys.J.*, 796 (2014), no.2, 109 [[arXiv:1406.6757](#)][astro-ph.HE]
- [11] A. Albert et al. [ANTARES Collaboration], "*Time-dependent search for neutrino emission from x-ray binaries with the ANTARES telescope*", *JCAP* 1704 (2017) no.04, 019 [[arXiv:1609.07372](#)][astro-ph.HE]
- [12] A. Albert et al. [ANTARES collaboration], "*New Constraints on all flavour Galactic diffuse neutrino emission with the ANTARES telescope*" [[arXiv:1705.00497](#)][astro-ph.HE]
- [13] Aartsen M G et al. [IceCube Collaboration], "*Observation of High-Energy Astrophysical Neutrinos in Three Years of IceCube Data*", *Phys. Rev. Lett.* 113 (2014) 101101 [[arXiv:1405.5303](#)][astro-ph.HE]
- [14] A. Albert et al. [ANTARES collaboration], "*First all-flavour Neutrino Point-like Source Search with the ANTARES Neutrino Telescope*", Submitted to: *Phys.Rev.D* [[arXiv:1706.01857](#)][astro-ph.HE]
- [15] A. Abeysekara et al. [HAWC Collaboration], "*The HAWC Gamma-Ray Observatory: Design, Calibration, and Operation*", *Proc. 33rd ICRC* (2013) [[arXiv:1310.0074](#)][astro-ph.IM]
- [16] R. J. Lauer and P. W. Younk [HAWC Collaboration], "*Results from monitoring TeV blazars with HAWC*", *PoS ICRC2015* (2016) 716, [[arXiv:1508.04479](#)][astro-ph.HE]
- [17] S. Adrian-Martinez et al. [KM3NeT Collaboration], "*Letter of intent for KM3NeT 2.0*", *J. Phys. G43* no. 8, (2016) 084001 [[arXiv:1601.07459](#)][astro-ph.IM].
- [18] A. Heijboer, on behalf of the ANTARES and KM3NeT Collaborations, "*Highlights from ANTARES and KM3NeT*", Highlight talk, these Proceedings.

# Searching for High Energy Neutrinos detected by ANTARES in coincidence with Gravitational Wave signals observed during LIGO Observation Run O1

---

**Thierry Pradier**\*<sup>†</sup>

*Université de Strasbourg, CNRS, IPHC UMR 7178, F-67000 Strasbourg, France*

*E-mail: [thierry.pradier@iphc.cnrs.fr](mailto:thierry.pradier@iphc.cnrs.fr)*

**Bruny Baret**

*APC, Université Paris Diderot, CNRS/IN2P3, CEA/IRFU, Observatoire de Paris, Sorbonne Paris Cité, 75205 Paris, France*

*E-mail: [bruny.baret@apc.univ-paris7.fr](mailto:bruny.baret@apc.univ-paris7.fr)*

**Alexis Coleiro**

*APC, Université Paris Diderot, CNRS/IN2P3, CEA/IRFU, Observatoire de Paris, Sorbonne Paris Cité, 75205 Paris, France*

*now at IFIC - Instituto de Física Corpuscular (CSIC - Universitat de València) c/ Catedrático José Beltrán, 2 E-46980 Paterna, Valencia, Spain*

*E-mail: [alexis.coleiro@apc.univ-paris7.fr](mailto:alexis.coleiro@apc.univ-paris7.fr)*

## on behalf of the ANTARES Collaboration

The ANTARES Neutrino Telescope can determine the arrival direction of a muonic High Energy Neutrino (HEN) with a precision well below  $1^\circ$  above 1 TeV. The detection of such a HEN in coincidence with a Gravitational Wave (GW) event would then improve the localization of the GW source, facilitating the search for electromagnetic counterparts. The results of such targeted HEN searches for the 3 GW events (GW150914, GW151226, both confirmed signals, and LVT151012, an event candidate) detected during the Observation Run O1 of ADVANCED LIGO in 2015-2016 are presented. The principles of a sub-threshold analysis, which looks for time and space correlations between HEN detected by ANTARES or ICECUBE and GW candidates of low signal-to-noise ratio detected by LIGO during O1 are presented. The specific procedure optimized to select HEN candidates in ANTARES data is emphasized.

*35th International Cosmic Ray Conference — ICRC2017*

*10–20 July, 2017*

*Bexco, Busan, Korea*

---

\*Speaker.

<sup>†</sup>The GW+HEN analyses presented here are the results of a collaborative work between the ANTARES Collaboration, the LIGO Scientific Collaboration, the VIRGO Collaboration and the ICECUBE Collaboration. Thanks in particular to I. Bartos (Columbia University, New-York, USA) for LIGO/VIRGO, and C. Finley (Oskar Klein Centre and Dept. of Physics, Stockholm, Sweden), for ICECUBE.

## 1. Introduction

The observation of three significant gravitational wave (GW) sources by ADVANCED LIGO on Sept. 14<sup>th</sup>, 2015, Dec. 26<sup>th</sup>, 2015 and Jan. 4<sup>th</sup>, 2017 [1, 2, 3] represents an important step forward in the study of the latest stage of massive star binary system evolution. By involving a number of observatories from the radio to the gamma-rays and also neutrino detectors to search for a potential counterpart associated to these events, the detection of the first GW events opened the era of time domain multi-messenger astrophysics.

The three signals correspond to the coalescence of stellar-mass black hole binary (BBH) systems at distances ranging from 400 Mpc to about 900 Mpc. While an electromagnetic counterpart (presumably associated with a neutrino emission) is generally expected from a neutron star/black hole or neutron star/neutron star merger [4], current consensus is that black hole/black hole merger does not produce electromagnetic or neutrino counterpart. However, in a dense enough hadronic environment, an accretion disk might form, and relativistic outflow connected to the accretion could be released. Energy dissipation in this outflow would consequently lead to a gamma-ray emission with a potential high-energy neutrino (HEN, of energy  $\gg$  GeV) counterpart [5]. The detection of HEN from GW sources would provide a better determination of the origin of the GW signal, thanks to the comparatively much more accurate pointing accuracy of neutrino telescopes, of the order of (or below) the degree - and would subsequently help the electromagnetic follow-up campaign.

ANTARES is currently the largest high-energy neutrino telescope in the Northern hemisphere [6]. Located in the Mediterranean Sea, 40 km off the Southern coast of France, it is composed of 12 detection lines that detect the Cherenkov light emitted by relativistic upgoing muons, signature of a neutrino interaction close to the detector. After the discovery from ICECUBE of a cosmic neutrino flux of still unknown origin [7], observing campaigns relying both on electromagnetic and multi-messenger facilities may be decisive to identify the origin of these neutrino events.

Joint searches of common sources of HEN and GW have already been performed in the past with both ANTARES and ICECUBE neutrino telescopes [8, 9, 10]. In these proceedings are reported the results of the HEN follow-ups performed during the first Observation Run O1 of LIGO (September 2015-January 2016), i.e. the searches for neutrinos in temporal and spatial coincidence with GW150914, detailed in [11], and with GW151226 and the event candidate LVT151012, presented in [12]. Using GW data collected during O1, a so-called "sub-threshold" analysis is being performed, which searches for time and space correlations between HEN detected by ANTARES or ICECUBE and GW candidates of low signal-to-noise ratio; it is presented in the last section, with an emphasis on the specific procedure optimized to select HEN candidates in ANTARES data.

## 2. HEN follow-ups of GW150914, GW151226 and LVT151012

We searched for directional and temporal coincidences between the GW signals and reconstructed HEN candidates from both ANTARES and ICECUBE. Relying on the methodology defined in [13], we searched for (*i*) temporal coincidences within a  $\pm 500$  s time window around the

GW alert and (ii) spatial overlap between the 90% positional probability contour associated to each signal (see Fig. 1) and neutrino point spread function.

The search time window, which was used in previous GW+HEN searches, is a conservative, observation-based upper limit on the plausible emission of GW and HEN in the case of GRBs which are thought to be driven by a stellar-mass black hole-accretion disk system [14]. Directionally, we searched for overlap between the GW sky map (shown in Fig. 1) and the neutrino point spread functions, assumed to be Gaussian.

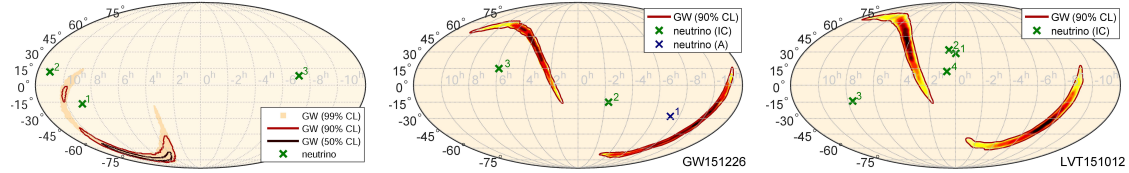


**Figure 1:** GW skymaps in equatorial coordinates, showing the reconstructed probability density contours of the GW events for GW150914 (left, [11]), GW151226 (middle, [12]), LVT151012 (right, [12]), and the reconstructed directions of high-energy neutrino candidates detected by ICECUBE (green crosses) or ANTARES (blue crosses) during a  $\pm 500$  s time window around the GW events. The neutrino directional uncertainties are below  $1^\circ$  and are not shown. GW shading indicates the reconstructed probability density of the GW events, darker regions corresponding to higher probability.

## 2.1 HEN analysis for GW150914

The ANTARES online reconstruction pipeline was used, which selects upgoing neutrino candidates with atmospheric muon contamination less than 10%. An energy cut is also applied to reduce the background of atmospheric neutrinos which finally leads to an event rate of 1.2 events/day. Consequently, the expected number of neutrino candidates within 1000s is 0.014, corresponding to a Poisson probability of observing at least one background event of  $\sim 1.4\%$ . No neutrino candidates temporally coincident with GW150914 were found, which is fully consistent with the background expectation. The search for HEN counterpart with ICECUBE used the online event stream with an event selection similar to the one applied for point source searches, but optimized for real-time search. The expected background rate is equal to 2.2 atmospheric neutrino events in the Northern sky (atmospheric neutrinos) and 2.2 high energy atmospheric muons from the Southern sky. Within  $\pm 500$  s around GW150914, three events were found, which are shown in Fig. 1 [11]. This observed event rate and the energy of these three events are compatible with the background expectations.

## 2.2 HEN analysis for GW151226 and LVT151012

We searched for coincident neutrinos within ANTARES data by selecting up-going events. The search was performed with the most recent official offline data set, incorporating dedicated calibrations, in terms of positioning, timing and efficiency. This sample is dominated by background events from mis-reconstructed down-going atmospheric muons. It was optimized for each GW event individually so that one event that passes the search criteria and is located within the 90% GW probability contour would lead to a detection with a significance level of  $3\sigma$ . For GW151226, a total of  $1.4 \times 10^{-2}$  atmospheric neutrino candidates are expected in the field of view within  $\pm 500$  s,



while the number of misreconstructed down-going muons amounts to  $8 \times 10^{-2}$  events in the same time window. We found one event that is temporally coincident with GW151226, located outside the 90% GW probability contour. The Poissonian probability of detecting at least one such background event when  $9.4 \times 10^{-2}$  are expected is  $\sim 9\%$ . Thus, this detection is consistent with the expected background muon rate and we conclude that this event is likely a misreconstructed down-going muon. Its estimated deposited energy is 9 TeV, in agreement with what is expected from an atmospheric down-going muon. The sky location of the event is shown in Fig. 1 [12].

For LVT151210, the atmospheric neutrino candidate rate expected from the southern sky within  $\pm 500$  s is equal to  $1.8 \times 10^{-2}$  while the number of misreconstructed down-going muons amounts to  $4 \times 10^{-2}$ . These are somewhat different from the values obtained for GW151226 as the sensitivity of ANTARES varies with time. No neutrino candidates temporally coincident with LVT151012 were found with ANTARES.

For ICECUBE, the detector online event stream was used. This event selection consists primarily of cosmic-ray-induced background events, with an expectation of 2.2 events in the northern sky (atmospheric neutrinos) and 2.2 events in the southern sky (high-energy atmospheric muons) per 1000 seconds. In the search window of  $\pm 500$  s centered on the GW alert times, 2 and 4 neutrino candidates were found by IceCube in correspondence of GW151226 and LVT151012, respectively. This result is consistent with the expected background. The sky location of the neutrino candidates are shown in Fig. 1 [12].

### 2.3 Constraints on neutrino emission

We use the non-detection of joint GW and neutrino events to constrain neutrino emission from the GW source. Since the sensitivity of neutrino detectors is highly dependent on source direction, upper limits were calculated as a function of source direction for the whole sky. The obtained spectral fluence upper limits as a function of source direction are shown in Fig. 2, for a model with a spectral cutoff at high energies:  $dN/dE \propto E^{-2} \exp[-\sqrt{(E/100\text{TeV})}]$ . The latter model is expected for sources with exponential cutoff in the primary proton spectrum. A pure  $E^{-2}$  was also considered and the results reported in [11, 12]. For a given direction, we adopt the upper limit from ICECUBE or ANTARES, whichever is more constraining.

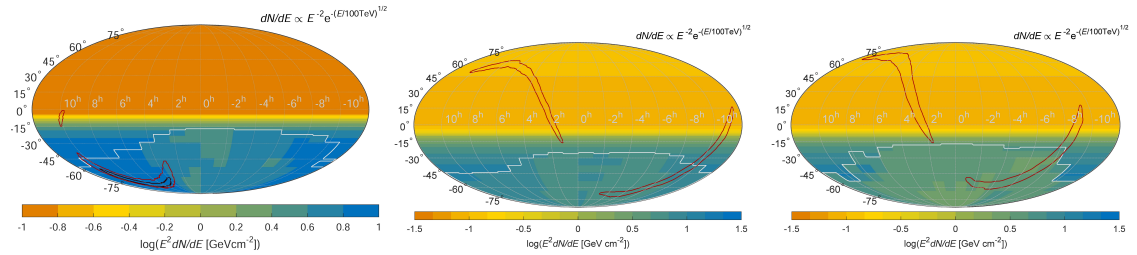


**Figure 2:** Upper limit on the high-energy neutrino spectral fluence ( $\nu_\mu + \bar{\nu}_\mu$ ) from GW150914 (left [11]), GW151226 (middle [12]), and LVT151012 (right [12]) as a function of source direction, assuming  $dN/dE \propto E^{-2} \exp[-\sqrt{(E/100\text{TeV})}]$  neutrino spectrum. The region surrounded by a white line shows the part of the sky in which ANTARES is more sensitive (close to nadir). For comparison, the 50% CL (for GW150914) and 90% CL contours (for the 3 events) of the GW sky maps are also shown.



A constraint on the total energy emitted in neutrinos by the source can be obtained from the fluence upper limits, by integrating the emission within [100 GeV, 100 PeV] for each considered source model. The obtained constraint will vary with respect to source direction, and also on the uncertain source distance. To account for these uncertainties for GW150914, we provide in Table 1 the range of energy values from the lowest to the highest possible within the 90% confidence intervals with respect to source direction and the 90% credible interval with respect to source distance (luminosity distance  $D_{\text{GW}} = 410_{-180}^{+160}$  Mpc). For GW151226, the source position was constrained to within a 3D volume - the lower limit  $D_{\text{low}}^{95\%}(\vec{x})$  on the source distance for a given direction  $\vec{x}$  such that the source is located within this distance at 95% credible level is used to calculate the upper limit on the total isotropic-equivalent energy emitted in neutrinos by the source,  $E_{\nu, \text{iso}}^{\text{ul}}(\vec{x}) = 4\pi [D_{\text{low}}^{95\%}(\vec{x})]^2 \int \frac{dN}{dE} E dE$ . To quantify the range of the upper limits over the skymap, the minimum and maximum upper limit values over the whole GW skymap, separately for the two spectral models, are shown in Table 1. Constraints for LVT151012, not shown, are about a factor of 4 weaker as its expected distance is about twice that of GW151226 [2], while both their skymaps similarly lie over a large declination range, corresponding to similar neutrino detector sensitivities.

GW Event	$D_L^{\text{GW}}$ [Mpc]	$E_{\text{GW}}^{\text{iso}}$ [erg]	$E^{-2} : E_{\text{HEN}}^{\text{iso}}/E_{\text{GW}}^{\text{iso}}$	$E^{-2}$ with cutoff : $E_{\text{HEN}}^{\text{iso}}/E_{\text{GW}}^{\text{iso}}$	Ref
GW150914	$410_{-180}^{+160}$	$5 \times 10^{54}$	0.11% – 26%	0.13% – 74%	[11]
GW151226	$440_{-190}^{+180}$	$1.8 \times 10^{54}$	0.11% – 17%	0.17% – 100%	[12]

**Table 1:** Minimum and maximum upper limits on the total energy radiated in neutrinos, for the pure  $E^{-2}$  HEN spectrum, and the HEN spectrum with 100 TeV-cutoff, for GW150914 and GW151226 [11, 12].

### 3. Searching for an association of weak GW signals and HEN candidates

The GW signals for which we performed dedicated HEN followups were highly significant events (GW150914 and GW151226) or event candidates (LVT151012), with particularly high signal-to-noise ratios, shown in Fig. 3. Apart from these signals, LIGO search pipelines identified  $\mathcal{O}(1000)$  potential signals, or triggers, characterized by low signal-to-noise ratios, as can be seen on Fig. 3. It is thus natural to search for a possible time and space correlation between these "sub-threshold" GW candidates (i.e., not significant enough to be claimed as "events") and HEN detected by ANTARES and ICECUBE, by performing a joint analysis, which method is presented in [14], and already applied for previous GW+HEN searches [10]. The joint analysis aims to identify GW events and HEN that originate from a common astrophysical source, by determining the significance of a GW+HEN event; this is obtained by a combination of the significances and directional distributions of GW events, neutrinos and galaxies (each galaxy is assigned a weight that reflects the probability of detecting an astrophysical HEN from the given galaxy, the distribution of GW sources being expected to be non-uniform in the volume probed by LIGO). The flow diagram of the joint GW+neutrino analysis algorithm is presented on Fig. 3, taken from [10]. Neutrinos detected by ANTARES and ICECUBE during O1 are used in this particular, still ongoing analysis. This section will concentrate on the specific process that has been developed for the selection of ANTARES HEN candidates.

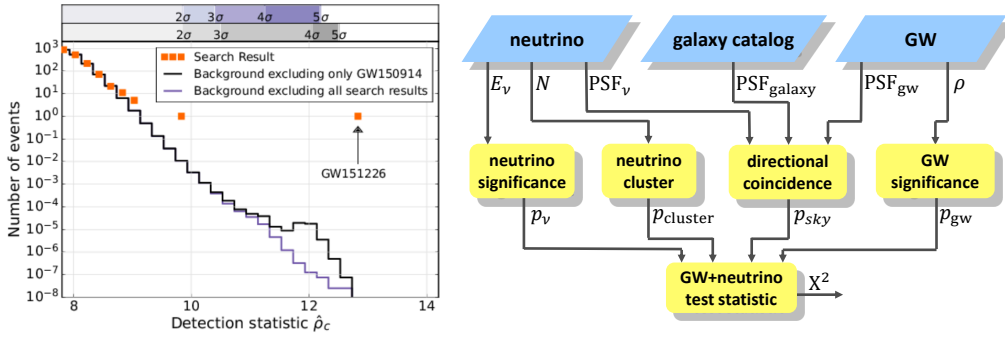


**Figure 3:** Left : As an illustration, GW detection statistics (related to the signal-to-noise ratio) distribution during O1, excluding GW150914, for the Binary Black-Hole search pipeline [15]. Right : Flow diagram of the joint GW+HEN analysis algorithm, showing how information on neutrinos, galaxies and GW are combined into one test statistic [10].

The selection of ANTARES  $\nu_\mu$  candidates is data-driven : it is optimized in order to obtain a  $3\sigma$  significance for a HEN event in a sliding window of 1000s and within the expected reconstructed GW 90% probability contour for typical GW signals.

**Time-dependent selection of the HEN candidates:** In order to optimize the HEN search, we rely on [16] for a sample of realistic GW events, which allows to extract a relationship between the signal-to-noise ratio  $\rho$  of a signal to the area of 90% confidence region  $A_{90}$  for the GW localization, of the form  $\log_{10} A_{90} = a \log \rho + b$ , used to extrapolate the size of the confidence region to sub-threshold GW events. This size is then convolved with ANTARES visible sky (ANTARES is only sensitive to up-going neutrinos in this analysis), and its local acceptance, to obtain the typical sizes reported in Table 2 below.

50%	90%	99%
524 deg <sup>2</sup>	744 deg <sup>2</sup>	1036 deg <sup>2</sup>

**Table 2:** 50%, 90% and 99% quantiles of the distribution of effective sizes (i.e. when the HEN detector effects, visibility and acceptance, are taken into account) of GW 90% probability regions.

A time-dependent selection criterium, based on the quality of the muon track reconstruction  $\Lambda$ , taking into account the time-dependence of the sensitivity of ANTARES, is then determined so that a selected HEN event in a time window of 1000s, in a space angle corresponding to these typical GW-contour regions will yield a significance of  $3\sigma$  - the results for the time-dependent cut are shown in Fig. 4. For the final selection, the value corresponding to the median effective size has been used, which yields a total of 906 selected HEN candidates for ANTARES, for the period covering the entire O1 observation run from Sep 12 2015 to Jan 19 2016, corresponding to a rate of 8 neutrinos/day.

**Characterization of HEN selected candidates:** Each HEN candidate is characterized by its detection time, its arrival direction and reconstruction uncertainty, and a probability of being of atmospheric origin based on the number of detected photons  $N_{\text{hit}}$  (an estimator of the event deposited

energy), shown in Fig. 4. At time of printing, the joint analysis, combining ANTARES and ICECUBE selected neutrinos, is still ongoing.e

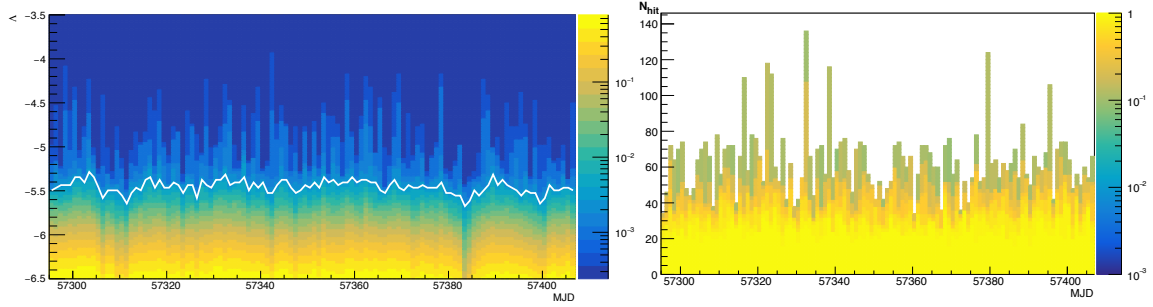


**Figure 4:** Left : probability to have  $\geq 1$  background event with a value of the reconstruction parameter  $\Lambda$  above a given value, in a 1000s time window, in a space area corresponding to the median of all 90% GW-contour regions. The white line marks the  $3\sigma$  significance level. Right :  $p$ -value of the HEN event being of atmospheric origin based on the data time-dependent distribution of the number of detected photons  $N_{\text{hit}}$ .

**Importance of a time-dependent analysis:** Using a time-dependent selection criterium instead of a constant value as used in point-source searches [17] allows to increase the number of selected signal events, for a  $E^{-2}$  spectrum, by  $45\% \pm 15\%$ , varying with time and data taking conditions. This optimization improves by a factor 1.5 to 2 the volume of universe probed by the joint analysis, and correspondingly the number of detectable joint GW+HEN sources.

#### 4. Conclusions & Perspectives

Searching in data recorded by the ANTARES Neutrino Telescope and ICECUBE concomittant with LIGO Observation Run O1, we detected no neutrino emission associated with the 2 confirmed signals GW150914 and GW151226, and event candidate LVT151012 [11, 12]. The total neutrino emission from the GW sources have been constrained, allowing for different possible neutrino spectra. HEN and/or electromagnetic emission induced by BBH systems can be expected in the case of significant gas accretion, which would trigger an energetic outflow. Such searches represent a promising way in comprehensively probing high-energy emission also for sources outside of the field of view of electromagnetic telescopes. Given the precise direction reconstruction of HEN ( $\lesssim 1\text{deg}^2$ ) compared to GW ( $\gtrsim 100\text{deg}^2$ ), a joint detection would provide a greatly reduced sky area for follow-up observatories.

The principles of an analysis combining GW and HEN data have been presented, using low-significance GW signals and neutrinos detected by ANTARES and ICECUBE. The data-driven optimized procedure to select ANTARES neutrino candidates improves by a factor 1.5 to 2 the number of detectable joint GW+HEN sources. Such a search relies on the improved sensitivity of a combined GW+HEN search as compared to a single-messenger search, as already shown in [10].

Such follow-up searches and extended "sub-threshold" analyses will also be performed using data taken during the ongoing Observation Run O2 of LIGO, and soon VIRGO, with increased sensitivity, which has already led to the detection of GW170104 [3]. A dedicated HEN followup all-sky search for GW170104 using ANTARES data is presented in these Proceedings [18].

## References

- [1] Abbott B. P. et al. *Phys. Rev. Lett.* **116** 061102 (2016).
- [2] Abbott B. P. et al. *Phys. Rev. Lett.* **116** 241103 (2016).
- [3] Abbott B. P. et al. *Phys. Rev. Lett.* **118** 221101 (2017).
- [4] e.g. Metzger B. D. and Berger E. *Astroph. Journal* **746** 48 (2012).
- [5] e.g. Perna R., Lazzati D. and Giacomazzo B. *Astroph. Journal Letters* **821** 18 (2016).
- [6] Heijboer A., on behalf of the ANTARES and KM3NET Collaborations, *Highlights from ANTARES and KM3NET*, Highlight talk, these Proceedings.
- [7] Aartsen M. G. et al. *Phys. Rev. Lett.* **113** 101101 (2014).
- [8] Adrián-Martínez S. et al. *JCAP* **6** 008 (2013).
- [9] Baret B., Proceedings of the *Rencontres de Moriond: Gravitation* (2015).
- [10] Aartsen M. G. et al. *Phys. Rev. D* **90** 102002 (2014).
- [11] Adrián-Martínez S. et al. *Phys. Rev. D* **93** 122010 (2016).
- [12] Albert A. et al., <https://arxiv.org/abs/1703.06298>, accepted by *Phys. Rev. D*.
- [13] Baret B. et al. *Astropart. Phy.* **35** 1:7 (2011).
- [14] Baret B. et al. *Phys. Rev. D* **85** 103004 (2012)
- [15] Abbott B. P. et al. *Phys. Rev. X* **6** 041015 (2016)
- [16] Singer L. P. et al. *ApJ* **795** 105 (2014)
- [17] Adrián-Martínez S. et al. *Astroph. Journal* **823** 65 (2016).
- [18] Coleiro A., Dornic D., on behalf of the ANTARES Collaboration, *Multi-messenger real-time analysis of transient events with the ANTARES neutrino telescope*, presented as a Poster, these Proceedings.

1 **Time-dependent search of neutrino emission from**  
2 **bright gamma-ray flaring blazars with the ANTARES**  
3 **telescope**

---

**Agustín Sánchez Losa\***

*INFN - Sezione di Bari*

*E-mail: agustin.sanchez@ba.infn.it*

**Damien Dornic**

*CPPM*

*E-mail: dornic@cppm.in2p3.fr*

**on the behalf of the ANTARES Collaboration**

The ANTARES telescope is well suited for detecting astrophysical transient neutrino sources as it can observe with high duty cycle an instantaneous field of view of  $2\pi$  sr. The background due to atmospheric muons and neutrinos can be drastically reduced, and the point-source sensitivity improved, by selecting a narrow time window around possible neutrino production periods. Blazars, radio-loud active galactic nuclei with their jets pointing almost directly towards the observer, are particularly attractive potential neutrino point sources, since they are among the most likely sources of the very high-energy cosmic rays. Neutrinos and gamma rays may be produced in hadronic interactions with the surrounding medium. Blazars generally show high time variability in their light curves at different wavelengths and on various time scales. Using ANTARES data a time-dependent analysis has been carried out searching for neutrino events from a selection of flaring gamma-ray blazars previously observed by the FERMI/LAT experiment and by TeV imaging Cherenkov telescopes. The results of these searches will be presented. If no signal will be discovered upper limits on neutrino fluxes, their comparisons with the published gamma-ray spectral energy distribution and with prediction from astrophysical models will also be reported.

*35th International Cosmic Ray Conference — ICRC2017*

*10–20 July, 2017*

*Bexco, Busan, Korea*

---

\*Speaker.

## 4 1. Introduction

5 Active galactic nuclei (AGN) are among the most likely sources of the very high-energy cos-  
6 mic rays. High-energy neutrino detection from them would confirm such hypothesis [1]. The  
7 debate is still open if AGN gamma-ray emission is due by leptonic [2, 3, 4, 5] or hadronic pro-  
8 cesses [6, 7]. In the second scenario, neutrinos are expected to be produced in correlation with  
9 gamma-rays from pion-decays.

10 Blazars are among the best candidates for being the source of the very high-energy cosmic  
11 rays [8, 9]. Several neutrino emission models are proposed [10, 11, 12, 13, 14, 15, 16], characterised  
12 by different spectral indexes and normalisation constants. While  $E^{-2}$  is among the most commonly  
13 proposed spectrum, in certain cases harder spectral indexes up to one are proposed [17, 18]. In  
14 analogy to what has been observed for several gamma-ray sources also for the neutrino spectra  
15 is possible to conceive a high energy cutoff. For the present analysis is considered the following  
16 neutrino spectra:  $E^{-1}$ ,  $E^{-2}$ ,  $E^{-2} \times \exp(\sqrt{-E/10 \text{ TeV}})$  and  $E^{-2} \times \exp(\sqrt{-E/1 \text{ TeV}})$ .

17 We report here about results obtained analysing a data sample, collected by the ANTARES  
18 telescope [19, 20], searching for neutrinos, with energy dependences as the ones described above  
19 and from a selection of flaring gamma-ray blazars. The search is performed in restricted time win-  
20 dows under the hypothesis of a time-correlation between neutrino and gamma fluxes. Searching for  
21 neutrinos in a limited time interval around the gamma flare time, increases the Signal/Background  
22 ratio and, if compared with analogous time integrated searches elsewhere reported by ANTARES [21,  
23 22], reduces by a factor 2–3 the number of signal events required for a discovery. This approach  
24 has been carried out in previous similar analyses [23, 24] where, in order to test the blazar source  
25 hypothesis, a correlation between the most energetic observed gamma-ray flares of the brightest  
26 blazars with neutrino emission has been studied (see Sec. 3). The main update with respect to  
27 the previous analyses is the inclusion of the shower channel in addition to the track one from the  
28 ANTARES data taken from 2008 to 2016 with  $\sim 2413$  days of live-time.

## 29 2. Time-dependent analysis

30 The analysis is done evaluating a test statistic built from an unbinned extended likelihood  
31 maximised ratio. The likelihood ( $\mathcal{L}$ ) treats the ANTARES data as a composition of background  
32 ( $\mathcal{N}_{bk}$ ) and signal ( $\mathcal{N}_{sg}$ ) events, properly weighted by their different probability density functions  
33 (PDFs,  $P_{sg/bk}$ ):

$$34 \ln \mathcal{L}_{sg+bk} = \sum_{ch} \sum_i \ln \left[ \mathcal{N}_{sg}^{ch} \cdot P_{sg}^{ch} + \mathcal{N}_{bk}^{ch} \cdot P_{bk}^{ch} \right] - [\mathcal{N}_{sg} + \mathcal{N}_{bk}]$$

35 The likelihood is extended over all the events ( $i$ ) for both considered channels ( $ch$ ), i.e. tracks and  
36 showers.

37 The  $P_{sg}$  for the track channel is defined as the product of three probability functions: one  
38 related to the neutrino direction (the point spread function probability, PSF,  $PSF_{sg}^{tr}(\alpha)$ , with  $\alpha$  the  
39 angular distance to the source), the second related to the energy ( $P_{sg}^{tr}(dE/dX)$ , being  $dE/dX$  the  
40 energy estimator used in the track channel) and the third related to the time ( $P_{sg}(t)$ ):

$$P_{sg}^{tr} = PSF_{sg}^{tr}(\alpha, \delta_S) \cdot P_{sg}^{tr}(dE/dX) \cdot P_{sg}(t + lag)$$

41 The PSF is estimated for each source declination ( $\delta_S$ ) and both  $PSF_{sg}^{tr}(\alpha)$  and  $P_{sg}^{tr}(dE/dX)$  are  
 42 function of the assumed neutrino energy spectrum. Additionally, a *lag* of  $\pm 5$  days is allowed  
 43 on the neutrino signal arrival time  $t$  in order to allow possible offsets between the neutrino and  
 44 gamma-ray emission at leaving the source.

45 The neutrino time probability is obtained directly by the observed gamma-ray light curve  
 46 assuming the correlation between gamma-rays and neutrinos, i.e. the neutrino time probability  
 47 follows the gamma-ray detection time, PDF extracted from the gamma ray emission of the studied  
 48 source (see Sec. 3). This time PDF is the same for both track and shower channels.

49 The  $P_{sg}$  for the shower channel is the product of the shower PSF, the energy and the time PDF:

$$P_{sg}^{sh} = PSF_{sg}^{sh}(\alpha, \delta_S) \cdot P_{sg}^{sh}(n_{hits}) \cdot P_{sg}(t + lag)$$

50 where the number of hits used in the shower reconstruction,  $n_{hits}$ , is used as the energy estimator  
 51 and again both  $PSF_{sg}^{sh}(\alpha)$  and  $P_{sg}^{sh}(n_{hits})$  are function of the assumed neutrino energy spectrum.

52 The  $P_{bk}$  for each channel is the corresponding product of the background PDF at a certain  
 53 declination ( $P_{bk}^{tr}(\delta)$ ), the background energy estimator PDF and the background time PDF:

$$P_{bk}^{tr} = P_{bk}^{tr}(\delta) \cdot P_{bk}^{tr}(dE/dX, \delta) \cdot P_{bk}(t)$$

54

$$P_{sg}^{sh} = P_{bk}^{sh}(\delta) \cdot P_{bk}^{sh}(n_{hits}) \cdot P_{bk}(t)$$

55 These probabilities are derived from data using, respectively, the observed declination distribution  
 56 of selected events in the sample, the measured distribution of the energy estimator, and the observed  
 57 time distribution of all the reconstructed events.

58 The amount of signal for each channel is determined by the ratio contribution of each channel  
 59 to the global acceptance of the detector at source declination:

$$\mathcal{N}_{sg}^{ch} = \mathcal{N}_{sg} \cdot (A_{cc}^{ch}(\delta_S) / A_{cc}^{TOTAL}(\delta_S))$$

60 and the total signal or background is the sum of each channel:

$$\mathcal{N}_{sg/bk} = \mathcal{N}_{sg/bk}^{sh} + \mathcal{N}_{sg/bk}^{tr}$$

61 The likelihood is maximised by varying the  $\mathcal{N}_{sg}$  and *lag* parameters and the test statistic  $\mathcal{Q}$  is  
 62 built from the ratio of this maximised likelihood with the null hypothesis:

$$\mathcal{Q} = \log \mathcal{L}_{sg+bk}^{max} - \log \mathcal{L}_{bk}$$

63 The significance of this test statistic is evaluated via pseudo-experiment simulation. Cut optimi-  
 64 sation is realised for each source and for each assumed energy spectrum in order to optimise the  
 65 track quality parameter cut on the track-like event selection and to improve the analysis model dis-  
 66 covery potential at  $3\sigma$ . Well established quality cuts used in previous analyses, and in point source  
 67 analyses for the shower channel, are kept.



### 68 3. Source and gamma-ray flare selection

69 Potentially interesting blazars are selected from the 3FHL FermiLAT high-energy catalogue [25,  
70 26], where are listed all sources significantly detected in the 10 GeV–2 TeV range during the first  
71 7 years of the Fermi mission using the Pass 8 event-level analysis. From this list, the following  
72 sources are selected:

- 73 • Blazars of the flat spectrum radio quasars (FSRQ) type or BL Lac objects (BLL).
- 74 • Blazars with a detection significance above 10.
- 75 • Blazars with more than one Bayesian block emission, which implies to be variable at 99% of  
76 confidence level.
- 77 • The brightest sources, with a flux above  $10^{-10}$  photons  $\text{cm}^{-2} \text{s}^{-1}$ .
- 78 • Sources with declination below  $35^\circ$ , i.e. visible in the track channel of ANTARES.

79 This criteria results in a preliminary selection of 46 BLLs and 32 FSRQs. A subsequent selection  
80 of sources is done regarding they flare or not in the light curves (LCs) described below.

81 The time PDF to be used for each source is build from the 2nd FAVA catalogue [27], the Fermi  
82 all-sky variability analysis done with 7.4 years of Fermi mission, from 2008/08/04 to 2016/01/04.  
83 LCs with weekly time bin and in two energy bands (100–800 MeV and 0.8–300 GeV) are analysed.  
84 The detection threshold for a source to be include in the catalogue is of  $6\sigma$  pre-trial. Sources from  
85 the preliminary selection showing more than one flare in the FAVA catalogue with more than a  
86  $5\sigma$  excess over the baseline emission are selected for the analysis: 17 BLLs and 23 FSRQs (see  
87 Table 1). The time PDFs are build up with the flares above a  $5\sigma$  significance from the LCs of  
88 the FAVA catalogue, complemented with the online FAVA search. Each flare is weighted by its  
89 significance in the time PDF.

### 90 4. Results

91 Preliminary sensitivities for the track only channel considering a  $E^{-2}$  spectrum have been pre-  
92 sented at the conference (see some specific cases in Table 2). Sensitivity to the neutrino flux during  
93 the flares is improved by a factor of  $\sim 2$  on average with respect to the previous analysis upper lim-  
94 its. In function of the source declination, shower channel inclusion would improve neutrino limits  
95 even a 10%. The corresponding neutrino fluence estimate is also provided in the tables according  
96 to its definition:

$$\mathcal{F} = \iint E \frac{dN}{dE} dE dt = \phi_0 \Delta t \int_{5\%}^{95\%} E E^{-2} dE$$

97 with  $\phi_0$  the spectrum normalisation,  $\Delta t$  the flaring livetime and the integral performed in the 5–95%  
98 ANTARES sensibility energy range of each source.



**Table 1:** List of the 40 blazars selected for the analysis. For each source are given its coordinates, flaring days and average daily significance.

Name	R.A. (°)	$\delta$ (°)	Flaring days	Ave. sig.
1ES 1215+303	184.5	30.1	21.0	7.5
3C 279	194.0	-5.8	231.0	9.9
3C 454.3	343.5	16.1	336.0	15.6
4C +14.23	111.3	14.4	70.0	8.7
4C +21.35	186.2	21.4	133.0	13.5
4C +28.07	39.5	28.8	77.0	7.7
AO 0235+164	39.7	16.6	217.0	8.2
B2 0716+33	109.9	33.1	49.0	7.0
B2 1520+31	230.5	31.7	49.0	8.1
CTA 102	338.2	11.7	616.0	11.4
MG1 J021114+1051	32.8	10.9	7.0	8.2
MG2 J043337+2905	68.4	29.1	14.0	7.3
OJ 287	133.7	20.1	56.0	8.7
ON 246	187.6	25.3	119.0	10.0
PKS 0301-243	45.9	-24.1	21.0	11.5
PKS 0426-380	67.2	-37.9	273.0	6.7
PKS 0454-234	74.3	-23.4	147.0	7.2
PKS 0507+17	77.5	18.0	63.0	15.8
PKS 0537-441	84.7	-44.1	98.0	7.3
PKS 0727-11	112.6	-11.7	7.0	8.1
PKS 0805-07	122.1	-7.9	56.0	10.0
PKS 0829+046	128.0	4.5	14.0	7.5
PKS 1124-186	171.8	-19.0	126.0	6.5
PKS 1441+25	221.0	25.0	399.0	8.4
PKS 1502+106	226.1	10.5	259.0	8.1
PKS 1510-08	228.2	-9.1	287.0	11.1
PKS 1717+177	259.8	17.8	112.0	7.5
PKS 1730-13	263.3	-13.1	84.0	8.0
PKS 2142-75	326.8	-75.6	105.0	7.6
PKS 2155-304	329.7	-30.2	14.0	8.4
PKS 2233-148	339.1	-14.6	98.0	10.2
PKS B1424-418	217.0	-42.1	728.0	9.5
PMN J0531-4827	83.0	-48.5	63.0	10.6
PMN J0622-2605	95.6	-26.1	21.0	6.8
PMN J1802-3940	270.7	-39.7	70.0	6.5
PMN J2345-1555	356.3	-15.9	182.0	7.9
RX J1754.1+3212	268.5	32.2	28.0	8.2
Ton 599	179.9	29.2	49.0	9.1
TXS 0518+211	80.4	21.2	70.0	6.8
TXS 1530-131	233.2	-13.3	140.0	9.0

**Table 2:** Preliminary sensitivities for some specific blazars for the track only channel assuming a  $E^{-2}$  spectrum. For each source are given the neutrino flux sensitivity during the flare ( $\phi_0$ , in  $10^{-8} \text{ GeV}^{-1} \text{ cm}^{-2} \text{ s}^{-1}$ ), the flare livetime ( $\Delta t$ , in days), the integral in the 5–95% ANTARES sensibility energy range ( $I_{5\%}^{95\%} = \int_{5\%}^{95\%} E^{-1} dE$ ) and the fluence ( $\mathcal{F}$ , in  $\text{GeV cm}^{-2}$ ).

Name	$\phi_0$	$\Delta t$	$I_{5\%}^{95\%}$	$\mathcal{F}$	Name	$\phi_0$	$\Delta t$	$I_{5\%}^{95\%}$	$\mathcal{F}$
3C 279	10	182	7.0	11	PKS 0426–380	6.4	191	7.4	8
4C +14.23	52	41	7.0	13	PKS 1441+25	6.2	383	7.0	14
CTA 102	4.0	526	7.0	13	PKS 1510–08	8.3	219	7.0	11
OJ 287	55	41	7.0	14	PKS B1424–418	1.9	594	7.3	7

## 99 References

- 100 [1] J.K. Becker, *High-energy neutrinos in the context of multimessenger physics*, *Phys. Rep.* **548** (2008)  
101 173 [astro-ph/0710.1557].
- 102 [2] S.D. Bloom, A.P. Marscher, *ApJ* **461** (1996) 657 .
- 103 [3] L. Maraschi, G. Ghisellini, A. Celotti, *ApJL* **397** (1992) L5 .
- 104 [4] C.D. Dermer, R. Schlickeiser, *ApJ* **416** (1993) 458 .
- 105 [5] M. Sikora, M.C. Begelman, M.J. Rees, *ApJ* **421** (1994) 153 .
- 106 [6] T.K. Gaisser, F. Halzen, T. Stanev, *Phys. Rep.* **258** (1995) 173 .
- 107 [7] J.G. Learned, K. Mannheim, *Ann. Rev. Nucl. Part. Sci.* **50** (2000) 679 .
- 108 [8] F. Halzen, D. Hooper, *Rep. Prog. Phys.* **65** (2002) 1025 .
- 109 [9] K. Mannheim, *A&A* **269** (1993) 67 .
- 110 [10] M. Böttcher, *Astrophys. Space Sci.* **309** (2007) 95 .
- 111 [11] K. Mannheim, P.L. Biermann, *A&A* **253** (1992) L21 .
- 112 [12] M. Böttcher, A. Reimer, K. Sweeney, A. Prakash, *ApJ* **768** (2013) 54 .
- 113 [13] M. Reynoso, G.E. Romero, M.C. Medina, *A&A* **545** (2012) .
- 114 [14] A. Mücke et al. , *Astropart. Phys.* **18(6)** (2003) 593 .
- 115 [15] A. Atayan, C. Dermer, *New Astron. Rev.* **48(5)** (2004) 381 .
- 116 [16] A. Neronov, M. Ribordy, *Phys.Rev.* **D80** (2009) 083008 .
- 117 [17] A. Mücke, R.J. Protheroe, in proceedings of *ICRC2001* [astro-ph/0105543] .
- 118 [18] A. Mücke, R.J. Protheroe, *Astropart. Phys.* **15** (2011) 121 .
- 119 [19] J.A. Aguilar et al. (the ANTARES Collaboration), *ANTARES: the first undersea neutrino telescope*,  
120 *Nuclear Inst. and Methods in Physics Research A* **656** (2011) 11 [astro-ph/1104.1607] .
- 121 [20] A. Heijboer, *Highlights from the ANTARES neutrino telescope*, in proceedings of *ICRC2017*,  
122 PoS (ICRC2017) 002 (2017).
- 123 [21] A. Albert et al. (the ANTARES Collaboration), *First all-flavour Neutrino Point-like Source Search*  
124 *with the ANTARES Neutrino Telescope*, astro-ph/1706.01857 .

- 125 [22] G. Illuminati, *All-flavor Neutrino Point-like Source Search with the ANTARES Neutrino Telescope*, in  
126 proceedings of *ICRC2017*, PoS (ICRC2017) NU055 (2017).
- 127 [23] S. Adrián-Martínez et al. (the ANTARES Collaboration), *Search for Neutrino Emission from*  
128 *Gamma-Ray Flaring Blazars with the ANTARES Telescope*, *Astropart. Phys.* **36** (2012) 204  
129 [astro-ph/1111.3473].
- 130 [24] S. Adrián-Martínez et al. (the ANTARES Collaboration), *Search for muon-neutrino emission from*  
131 *GeV and TeV gamma-ray flaring blazars using five years of data of the ANTARES telescope*, *JCAP* **12**  
132 (2015) 014 [astro-ph/1506.07354].
- 133 [25] M. Ajello et al. (the Fermi LAT Collaboration), *3FHL: The Third Catalog of Hard Fermi-LAT*  
134 *Sources*, astro-ph/1702.00664.
- 135 [26] The 3FHL homepage: <https://fermi.gsfc.nasa.gov/ssc/data/access/lat/3FHL/>
- 136 [27] The 2FAVA homepage: [https://fermi.gsfc.nasa.gov/ssc/data/access/lat/fava\\_catalog/](https://fermi.gsfc.nasa.gov/ssc/data/access/lat/fava_catalog/)

1 **Time-dependent search of neutrino emission from**  
2 **X-ray and gamma-ray binaries with the ANTARES**  
3 **telescope**

---

**Agustín Sánchez Losa\***

*INFN - Sezione di Bari*

*E-mail: agustin.sanchez@ba.infn.it*

**Damien Dornic**

*CPPM*

*E-mail: dornic@cppm.in2p3.fr*

**Alexis Coleiro**

*IFIC*

*E-mail: alexis.coleiro@ific.uv.es*

**on the behalf of the ANTARES Collaboration**

ANTARES is currently the largest neutrino telescope operating in the Northern Hemisphere, aiming at the detection of high-energy neutrinos from astrophysical sources. Such observations would provide important clues about the processes at work in those objects, and possibly help to understand the origin of very high-energy cosmic rays. By design, neutrino telescopes constantly monitor at least one complete hemisphere of the sky and are thus well set to detect neutrinos produced in transient astrophysical events. The flux of high-energy neutrinos from a transient source is lower than if is an steady one, but the background originating from interactions of charged cosmic rays in the Earth's atmosphere can be drastically reduced by requiring a directional and temporal coincidence of the astrophysical phenomenon detected by electromagnetic instruments. Time-dependent point-source searches have been applied to a list of X-ray and gamma-ray binary systems detected by satellites or TeV imaging Cherenkov telescopes using ANTARES data. The results of these searches are presented. Upper limits on neutrino fluxes, their comparisons with the published gamma-ray spectral energy distribution and with prediction from astrophysical models are also reported.

*35th International Cosmic Ray Conference — ICRC2017*

*10–20 July, 2017*

*Bexco, Busan, Korea*

---

\*Speaker.

## 4 1. Introduction

5 X-ray and gamma-ray binaries (XRBs and  $\gamma$ RBs) are binary star systems composed of a com-  
 6 pact object (e.g. neutron star or stellar mass black hole candidate) orbiting a companion non-  
 7 degenerate star and that are luminous in X-rays and gamma-rays respectively. The high-energy  
 8 photon emission of XRBs is due to the matter falling from the companion star into the compact  
 9 object. On the other hand, in  $\gamma$ RB systems the responsible of the high-energy emission is the inter-  
 10 action of the pulsar wind with the intense stellar wind of the companion massive star. Despite the  
 11 non-thermal emission is probably dominated by leptonic processes, a hadronic component could  
 12 also be present. High-energy neutrino emission detection would confirm this possibility and pro-  
 13 vide insights about the involved acceleration mechanisms that would confirm cosmic ray produc-  
 14 tion on these sources [1]. In a hadronic scenario, the decay of the charged pions produce a neutrino  
 15 emission correlated with the very high-energy gamma rays from  $\pi^0$  decays when  $\gamma\gamma$  annihilation  
 16 is negligible. Up to know, a hadronic component has been identified in only two cases [2, 3]. Sev-  
 17 eral estimations of the neutrino flux production in these sources are proposed, with very different  
 18 spectral indexes, cutoffs and normalisations [4, 5, 6]. In order to cover the variety of models ac-  
 19 cessible to the ANTARES sensitivity, the following neutrino spectra have been considered:  $E^{-2}$ ,  
 20  $E^{-2} \times \exp(\sqrt{-E/100 \text{ TeV}})$  and  $E^{-2} \times \exp(\sqrt{-E/10 \text{ TeV}})$ , with  $E$  the neutrino energy.

21 In this contribution is presented a time-dependent analysis realised on the ANTARES [7, 8]  
 22 neutrino telescope data testing the above hypothesis. This analysis method reduces in a factor of  
 23 2–3 the signal required for a discovery with respect to a time integrated search [9, 10] under the  
 24 assumption of correlation of the neutrino signal with high-energy electromagnetic emission, as is  
 25 carried out in previous similar analyses [11, 12]. The hadronic hypothesis is tested by looking for  
 26 a correlation between the neutrino emission and the observed X-ray and gamma-ray flares of the  
 27 brightest variable XRBs and  $\gamma$ RBs (see Sec. 3). The main update with respect to previous analyses  
 28 is the inclusion of the shower channel in addition to the track one from the ANTARES data taken  
 29 from 2008 to 2016 with  $\sim 2413$  days of live-time.

## 30 2. Time-dependent analysis

31 The analysis is done evaluating a test statistic built from a maximised unbinned extended  
 32 likelihood ratio. The likelihood ( $\mathcal{L}$ ) treats the ANTARES data as a composition of background  
 33 ( $\mathcal{N}_{bk}$ ) and signal ( $\mathcal{N}_{sg}$ ), properly weighted by their different probability density functions (PDFs,  
 34  $P_{sg/bk}$ ):

35

$$\ln \mathcal{L}_{sg+bk} = \sum_{ch} \sum_i \ln \left[ \mathcal{N}_{sg}^{ch} \cdot P_{sg}^{ch} + \mathcal{N}_{bk}^{ch} \cdot P_{bk}^{ch} \right] - [\mathcal{N}_{sg} + \mathcal{N}_{bk}]$$

36 where the likelihood is extended over all the different events ( $i$ ) of each considered channel ( $ch$ ),  
 37 i.e. tracks and showers.

38 The  $P_{sg}$  for the track channel is defined as the product of the direction (the point spread function  
 39 probability,  $PSF_{sg}^{tr}(\alpha)$ , with  $\alpha$  the angular distance to the source), the energy ( $P_{sg}^{tr}(dE/dX)$ , being  
 40  $dE/dX$  the energy estimator used in the track channel) and the time ( $P_{sg}(t)$ ) probabilities:

$$P_{sg}^{tr} = PSF_{sg}^{tr}(\alpha, \delta_s) \cdot P_{sg}^{tr}(dE/dX) \cdot P_{sg}(t + lag)$$

41 where the PSF is estimated for each source declination ( $\delta_S$ ) and both  $PSF_{sg}^{tr}(\alpha)$  and  $P_{sg}^{tr}(dE/dX)$   
 42 are dependent of the evaluated spectrum. Additionally, a lag of  $\pm 5$  days is allowed on the neutrino  
 43 signal arrival time  $t$  in order to allow possible offsets between the neutrino and X-ray/gamma-ray  
 44 emission at leaving the source.

45 The time probability is the assumed correlation between X-rays/gamma-rays and neutrinos,  
 46 i.e. the detected signal neutrino time probability is proportional to the X-ray/gamma-ray detection  
 47 time, PDF extracted from the X-ray/gamma-ray emission of the studied source (see Sec. 3). This  
 48 time PDF is the same for both track and shower channels.

49 The term  $P_{sg}$  for the shower channel is the product of the shower PSF, the energy and the time  
 50 PDF:

$$P_{sg}^{sh} = PSF_{sg}^{sh}(\alpha, \delta_S) \cdot P_{sg}^{sh}(n_{hits}) \cdot P_{sg}(t + lag)$$

51 where the number of hits used in the shower reconstruction,  $n_{hits}$ , is used as the energy estimator  
 52 and again both  $PSF_{sg}^{sh}(\alpha)$  and  $P_{sg}^{sh}(n_{hits})$  are signal spectrum dependent.

53 The  $P_{bk}$  for each channel are the corresponding products of the background PDF at a certain  
 54 declination ( $P_{bk}^{tr}(\delta)$ ), the background energy estimator PDF and the background time PDF (build  
 55 from a loser cut on the data sample):

$$P_{bk}^{tr} = P_{bk}^{tr}(\delta) \cdot P_{bk}^{tr}(dE/dX, \delta) \cdot P_{bk}(t)$$

56

$$P_{sg}^{sh} = P_{bk}^{sh}(\delta) \cdot P_{bk}^{sh}(n_{hits}) \cdot P_{bk}(t)$$

57 where the dependence of the background  $dE/dX$  with respect to the declination has been consid-  
 58 ered.

59 The amount of signal of each channel is determined by the ratio contribution of each channel  
 60 to the global acceptance of the detector at source declination:

$$\mathcal{N}_{sg}^{ch} = \mathcal{N}_{sg} \cdot (A_{cc}^{ch}(\delta_S) / A_{cc}^{TOTAL}(\delta_S))$$

61 and the total signal or background is the sum of each channel:

$$\mathcal{N}_{sg/bk} = \mathcal{N}_{sg/bk}^{sh} + \mathcal{N}_{sg/bk}^{tr}$$

62 The likelihood is maximised by varying the  $\mathcal{N}_{sg}$  and  $lag$  parameters and the test statistic  $\mathcal{Q}$   
 63 is built from the ratio of this maximised likelihood with the likelihood value corresponding to the  
 64 null hypothesis:

$$\mathcal{Q} = \log \mathcal{L}_{sg+bk}^{max} - \log \mathcal{L}_{bk}$$

65 The significance of this test statistic is evaluated via pseudo-experiments. Track quality cuts are  
 66 optimized on a source and spectrum basis in order to maximize the model discovery potential at  
 67  $3\sigma$ . For the shower channels, the quality cuts optimized for the latest point source analysis are  
 68 considered.

### 69 3. Source and flare selection

70 Under the assumption of correlated high-energy neutrino and electromagnetic productions,  
 71 X-ray and gamma-ray variable emissions from XRBs and  $\gamma$ RBs are used to build the neutrino  
 72 emission time PDFs. The approach for each kind of source differs due to their emissions at different  
 73 energies.

74 **3.1 X-ray binary source and flare selection**

75 XRBs exhibiting outburst periods are selected from the Swift [13] and MAXI [14] catalogues,  
76 extended with Rossi [15] data when available. XRB light curves (LCs) are obtained from:

- 77 • Swift/BAT Hard X-ray Transient Monitor<sup>1</sup>: any high-mass XRB (HMXR) and low-mass  
78 XRB (LMXB) with significant time variabilities are initially selected. Their daily LCs are  
79 denoised with a maximum likelihood block [16] procedure and their flare significance char-  
80 characterised as done in previous analyses [12, 17]. Sources with more than one flare above a  
81 5 standard deviation significance are selected for the analysis.
- 82 • MAXI Light Curves<sup>2</sup>: The same procedure as for Swift LCs is followed for select MAXI  
83 galactic compact binary flares.
- 84 • RXTE/ASM Light Curves<sup>3</sup>: Because X-ray data are not always available for all the sources  
85 from the above detectors, in order to cover possible flares previously to 2012, Rossi LCs have  
86 been also considered in the same way as the other telescopes.

87 Depending on the time period and the availability of the different instruments, outbursts are better  
88 observed in one apparatus compared to others. Therefore, Swift flare selection is completed with  
89 the flares only observed in the other telescopes. The merging of the different LCs is done by  
90 normalising each detector LC to its relative significance.

91 The final source list comprises 36 XRBs (see Table 1), including 14 HMXBs and 19 LMXBs,  
92 half in common with the previous analysis [12] since faint sources are removed and XRBs flaring  
93 in 2014–2016 added.

94 **3.2 Gamma-ray binary source and flare selection**

95 Four  $\gamma$ RBs compatible with ANTARES up-going visibility have been selected for the study at  
96 very high-energy gamma-rays: 1FGL J1018.6–5856 [18], HESS J0632+057 [19], LS 5039–63 [20]  
97 and PSR B1259–63 [21]. Using their periodic emission established in the literature, simple on/off  
98 LCs (considering the parameter uncertainties in the flare period definition) are used for their time  
99 PDFs (see Table 2), using for LS 5039 its TeV flaring information and not the GeV one.

100 Additionally, the Cyg X–3 XRB has been detected outbursting at gamma-ray energies [22] by  
101 the Fermi-LAT telescope [23]. Thus, Cyg X–3 is included in the analysis using the multiwave-  
102 length flare observations published in [22] (Table 2, Y+ and Y– criteria) and updated with two  
103 astronomic alerts<sup>4</sup>: 57398–54412MJD (#ATel 8591) and 57646–57647MJD (#ATel 9502). The  
104 same on/off criteria used for the other  $\gamma$ RBs is applied also here for the LC construction, adding  
105  $\pm 0.5$  day on the begin and end of the flare definition periods.

<sup>1</sup><https://swift.gsfc.nasa.gov/results/transients>

<sup>2</sup><http://134.160.243.77/top/lc.html>

<sup>3</sup>[http://xte.mit.edu/ASM\\_lc.html](http://xte.mit.edu/ASM_lc.html)

<sup>4</sup><http://www.astronomerstelegam.org>



**Table 1:** List of the 36 XRBs selected for the analysis. For each source the satellite LC used (Swift, MAXI or Rossi), the number of flares (#flares), the flaring days, the source right ascension and its declination are listed.

Name	Satellite (#flares days)	R.A. (°)	$\delta$ (°)
1A 0535+262	S(#11 417) + M(#2 30)	84.7	26.3
1A 1118-61	S(#1 141)	170.2	-61.9
1A 1742-294	S(#1 3) + M(#5 284)	266.5	-29.5
4U 1630-472	S(#6 437) + M(#3 278)	248.5	-47.4
Aql X-1	S(#7 460) + M(#10 95)	287.8	0.6
AX J1749.1-2639	S(#1 85)	267.3	-26.6
Cir X-1	S(#10 205) + M(#18 478)	230.2	-57.2
Cyg X-1	S(#9 1965)	299.6	35.2
EXO 1745-248	S(#3 191) + M(#4 237)	267.0	-24.8
GRO J1008-57	S(#12 614)	152.4	-58.3
GRS 1739-278	S(#1 143) + M(#2 264)	265.7	-27.8
GS 0834-430	S(#1 1427) + M(#2 13)	129.0	-43.2
GS 1354-64	S(#1 136) + M(#3 16)	209.5	-64.7
GX 1+4	S(#9 661) + M(#2 58) + R(#1 93)	263.0	-24.7
GX 304-1	S(#16 579) + M(#1 10)	195.3	-61.6
GX 339-4	S(#5 525) + M(#5 121)	255.7	-48.8
H 1417-624	S(#1 107)	215.3	-62.7
H 1608-522	S(#7 967) + M(#12 384)	243.2	-52.4
H 1743-322	S(#12 772) + M(#3 33)	266.6	-32.2
IGR J17473-2721	S(#1 9) + R(#1 61)	266.8	-27.3
KS 1947+300	S(#4 324) + M(#10 242)	297.4	30.2
MAXI J0556-332	M(#2 475)	89.2	-33.2
MAXI J1543-564	M(#3 131)	235.8	-56.4
MAXI J1659-152	S(#2 125) + R(#2 96)	254.8	-15.3
MAXI J1836-194	S(#1 83) + M(#2 18)	278.9	-19.3
MXB 0656-072	S(#1 37) + M(#1 2) + R(#1 4)	104.6	-7.2
SAX J1747.0-2853	M(#6 382)	266.8	-28.9
SMC X-3	S(#1 90) + M(#1 3)	13.0	-72.4
SWIFT J1539.2-6227	S(#1 46)	234.8	-62.5
SWIFT J1745.1-2624	S(#1 198)	266.3	-26.4
SWIFT J1842.5-1124	S(#1 133) + R(#1 356)	280.6	-11.4
SWIFT J1910.2-0546	S(#2 52) + M(#2 14)	287.6	-5.8
V404 Cyg	S(#2 89) + M(#1 28) + R(#4 19)	306.0	33.9
XTE J1752-223	S(#2 210) + M(#12 229)	268.1	-22.3
XTE J1810-189	M(#2 277)	272.6	-19.1
XTE J1946+274	S(#1 61) + M(#1 12)	296.4	27.4



**Table 2:** List of the 4  $\gamma$ RBs selected for the analysis. For each source are given its coordinates and are listed the period, flaring phase and periastron extracted from the bibliography and used to build their time PDFs.

Name	R.A. (°)	$\delta$ (°)	Period (days)	Flaring phase	Periastron (MJD)
1FGL J1018.6–5856	154.7	–58.9	$16.58 \pm 0.02$	0.70–0.40	$55387.5 \pm 0.4$
HESS J0632+057	98.2	5.8	$315 \pm 5$	0.20–0.45	$54587.0 \pm 0.5$
LS 5039–63	276.6	–14.8	$3.91 \pm 8 \cdot 10^{-5}$	0.45–0.95	$51942.59 \pm 0.05$
PSR B1259–63	195.7	–63.8	$1236.7 \pm 2 \cdot 10^{-5}$	0.92–0.08	$55545.0 \pm 0.5$

## 106 4. Results

107 Preliminary sensitivities for the track only channel considering a  $E^{-2}$  spectrum have been  
 108 presented at the conference. Some specific cases are presented in Tables 3 and 4 for both XRBs and  
 109  $\gamma$ RBs respectively. Sensitivity to the neutrino flux during the flares, source dependent, is improved  
 110 by a factor of  $\sim 4$  on average with respect to the previous analysis upper limits. In function of  
 111 the source declination, shower channel inclusion would improve neutrino limits even a 10%. The  
 112 corresponding neutrino fluence estimate is also provided in the tables according to its definition:

$$\mathcal{F} = \iint E \frac{dN}{dE} dE dt = \phi_0 \Delta t \int_{5\%}^{95\%} E E^{-2} dE$$

113 with  $\phi_0$  the spectrum normalisation,  $\Delta t$  the flaring livetime and the integral performed in the 5–95%  
 114 ANTARES sensibility energy range of each source. The whole sample is expected to be unblinded  
 115 in the near future.

**Table 3:** Preliminary sensitivities for some specific XRBs for the track only channel assuming a  $E^{-2}$  spectrum. For each source are given the neutrino flux sensitivity during the flare ( $\phi_0$ , in  $10^{-8} \text{ GeV}^{-1} \text{ cm}^{-2} \text{ s}^{-1}$ ), the flare livetime ( $\Delta t$ , in days), the integral in the 5–95% ANTARES sensibility energy range ( $I_{5\%}^{95\%} = \int_{5\%}^{95\%} E^{-1} dE$ ) and the fluence ( $\mathcal{F}$ , in  $\text{GeV cm}^{-2}$ ).

Name	$\phi_0$	$\Delta t$	$I_{5\%}^{95\%}$	$\mathcal{F}$	Name	$\phi_0$	$\Delta t$	$I_{5\%}^{95\%}$	$\mathcal{F}$
1A 0535+262	8.6	278	7.0	14	GX 339–4	2.5	464	7.2	7.1
4U 1630–472	2.0	579	7.2	7.1	H 1743–322	2.1	665	7.4	8.9
Cir X–1	2.0	572	6.8	6.8	SMC X–3	13	88	6.5	6.3
Cyg X–1	1.8	1521	7.1	17	V404 Cyg	22	120	7.1	17

**Table 4:** Preliminary sensitivities for the studied  $\gamma$ RBs for the track only channel assuming a  $E^{-2}$  spectrum. For each source are given the neutrino flux sensitivity during the flare ( $\phi_0$ , in  $10^{-8} \text{ GeV}^{-1} \text{ cm}^{-2} \text{ s}^{-1}$ ), the flare livetime ( $\Delta t$ , in days), the integral in the 5–95% ANTARES sensibility energy range ( $I_{5\%}^{95\%} = \int_{5\%}^{95\%} E^{-1} dE$ ) and the fluence ( $\mathcal{F}$ , in  $\text{GeV cm}^{-2}$ ).

Name	$\phi_0$	$\Delta t$	$I_{5\%}^{95\%}$	$\mathcal{F}$	Name	$\phi_0$	$\Delta t$	$I_{5\%}^{95\%}$	$\mathcal{F}$
1FGL J1018.6–5856	0.5	2259	6.7	6.8	LS 5039–63	1.1	1564	7.1	10
Cyg X–3	146	20	7.2	18	PSR B1259–63	3.0	377	6.6	6.5
HESS J0632+057	1.6	1219	7.0	12					

116 **References**

- 117 [1] J.K. Becker, *High-energy neutrinos in the context of multimessenger physics*, *Phys. Rep.* **548** (2008)  
118 173 [astro-ph/0710.1557].
- 119 [2] S. Migliari, R. Fender, M. Mendez, *Iron emission lines from extended x-ray jets in SS 433: reheating*  
120 *of atomic nuclei*, *Science* **297** (2002) 1673 .
- 121 [3] M.D. Trigo, J.C.A. Miller-Jones, S. Migliari, J.W. Broderick, T. Tzioumis, *Baryons in the Relativistic*  
122 *Jets of the Stellar-Mass Black-Hole Candidate 4U 1630-47*, *Nature* **504** (2013) 260 .
- 123 [4] C. Distefano, D. Guetta, E. Waxman, A. Levinson, *ApJ* **575** (2002) 378 .
- 124 [5] G.E. Romero, D.F. Torres, M.M. Kaufman Bernadó, I.F. Mirabel, *A&A* **410** (2003) L1 .
- 125 [6] A. Levinson, E. Waxman, *Physical Review Letters* **87** (2001) 171101 .
- 126 [7] J.A. Aguilar et al. (the ANTARES Collaboration), *ANTARES: the first undersea neutrino telescope*,  
127 *Nuclear Inst. and Methods in Physics Research A* **656** (2011) 11 [astro-ph/1104.1607].
- 128 [8] A. Heijboer, *Highlights from the ANTARES neutrino telescope*, in proceedings of ICRC2017,  
129 PoS (ICRC2017) 002 (2017).
- 130 [9] A. Albert et al. (the ANTARES Collaboration), *First all-flavour Neutrino Point-like Source Search*  
131 *with the ANTARES Neutrino Telescope*, astro-ph/1706.01857 .
- 132 [10] G. Illuminati, *All-flavor Neutrino Point-like Source Search with the ANTARES Neutrino Telescope*, in  
133 proceedings of ICRC2017, PoS (ICRC2017) NU055 (2017).
- 134 [11] S. Adrián-Martínez et al. (the ANTARES Collaboration), *A search for time dependent neutrino*  
135 *emission from microquasars with the ANTARES telescope*, *JHEAp* **3-4** (2014) 9  
136 [astro-ph/1402.1600].
- 137 [12] A. Albert et al. (the ANTARES Collaboration), *Time-dependent search for neutrino emission from*  
138 *X-ray binaries with the ANTARES telescope*, *JCAP* **04** (2017) 019 [astro-ph/1609.07372].
- 139 [13] The Swift homepage: <http://swift.gsfc.nasa.gov/>
- 140 [14] The MAXI homepage: <http://maxi.riken.jp>
- 141 [15] The Rossi homepage: <http://heasarc.gsfc.nasa.gov/docs/xte/XTE.html>
- 142 [16] J.D. Scargle, J.P. Norris, B. Jackson, J. Chiang, *Studies in Astronomical Time Series Analysis. VI.*  
143 *Bayesian Block Representations*, *The Astrophysical Journal* **764** (2013) 167  
144 [astro-ph/1207.5578].
- 145 [17] S. Adrián-Martínez et al. (the ANTARES Collaboration), *Search for muon-neutrino emission from*  
146 *GeV and TeV gamma-ray flaring blazars using five years of data of the ANTARES telescope*, *JCAP* **12**  
147 (2015) 014 [astro-ph/1506.07354].
- 148 [18] M.J. Coe, F. Di Mille, P.G. Edwards, M.D. Filipović, J.L. Payne, J. Stevens, M.A.P. Torres (the Fermi  
149 LAT Collaboration), *Periodic Emission from the Gamma-ray Binary 1FGL J1018.6–5856*, *Science*  
150 **335** (2012) 6065 [astro-ph/1202.3164].
- 151 [19] S. Bongiorno, A. Falcone, M. Stroh, J. Holder, J. Skilton, J. Hinton, N. Gehrels, J. Grube, *A New TeV*  
152 *Binary: The Discovery of an Orbital Period in HESS J0632+057*, *The Astrophysical Journal Letters*  
153 **737** (2011) 1 [astro-ph/1104.4519].
- 154 [20] J. Casares, M. Ribo, I. Ribas, J.M. Paredes, J. Martí, A. Herrero, *A possible black hole in the*  
155 *gamma-ray microquasar LS 5039*, *Mon Not R Astron Soc* **364** (2005) 3 [astro-ph/0507549].

- 156 [21] A. Abramowski et al. (the H.E.S.S. Collaboration), *H.E.S.S. Observations of the Binary System*  
157 *PSR B1259–63/LS 2883 around the 2010/2011 Periastron Passage*, *A&A* **551** (2013) A94  
158 [astro-ph/1301.3930].
- 159 [22] A. Bodaghee, J.A. Tomsick, K. Pottschmidt, J. Rodriguez, J. Wilms, G.G. Pooley, *Gamma-ray*  
160 *observations of the microquasars Cygnus X–1, Cygnus X–3, GRS 1915+105, and GX 339–4 with*  
161 *the Fermi Large Area Telescope*, *The Astrophysical Journal* **775** (2013) 2 [astro-ph/1307.3264]  
162 .
- 163 [23] The Fermi LAT homepage: <https://www-glast.stanford.edu/>

## Multi-messenger real-time follow-up of transient events with ANTARES neutrino telescope

---

### D. Dornic\*

*Aix Marseille Univ, CNRS/IN2P3, CPPM, Marseille, France*  
E-mail: [dornic@cppm.in2p3.fr](mailto:dornic@cppm.in2p3.fr)

### A. Coleiro

*APC, Univ Paris Diderot, CNRS/IN2P3, CEA/Irfu, Obs de Paris, Sorbonne Paris Cité, France*  
*IFIC - Instituto de Física Corpuscular (CSIC - Universitat de València) c/ Catedrático José Beltrán, 2 E-46980 Paterna, Valencia, Spain*  
E-mail: [alexis.coleiro@ific.uv.es](mailto:alexis.coleiro@ific.uv.es)

### on behalf of the ANTARES Collaboration

By constantly monitoring at least one complete hemisphere of the sky, neutrino telescopes are well designed to detect neutrinos emitted by transient astrophysical events. Real-time searches for ANTARES neutrino candidates coincident with gamma-ray bursts, High-Energy Starting Events and Extremely High-Energy Events detected by IceCube and gravitational wave (GW) candidates observed by LIGO/Virgo are performed. By requiring coincident detection, this approach increases the sensitivity of the telescope and the significance of a potential discovery. The latest results of these analyses will be presented. In particular, a neutrino follow-up is performed after the detection of GW events by the LIGO/Virgo collaboration. Because of the good angular accuracy of neutrino telescopes compared to current GW detectors with two interferometers, a coincident detection would drastically constrain the position of the GW source on the sky, bringing valuable information for subsequent electromagnetic follow-ups. Since no coincident ANTARES event has been detected so far, the neutrino fluence and the total energy emitted in neutrinos are constrained for each GW alert.

*35th International Cosmic Ray Conference — ICRC2017*  
*10–20 July, 2017*  
*Bexco, Busan, Korea*

---

\*Speaker.

## 1. Introduction

Time-domain astroparticle physics has entered an exciting period with the recent development of wide-field-of-view instruments, communication strategies and low latency alert triggering of gravitational wave and high-energy neutrino (HEN) signals, but also across the electromagnetic spectrum. In particular, neutrinos represent unique probes to study high-energy cosmic sources. They are neutral, stable and weakly interacting. Contrary to cosmic rays (CRs), they are not deflected by the magnetic fields and unlike high-energy photons, they are not absorbed by pair production via  $\gamma\gamma$  interactions with cosmic microwave and infrared backgrounds. A HEN diffuse flux of cosmic origin has been identified by the IceCube telescope (see e.g. [1]), the sources of which have still to be identified. In this context, multi-messenger approaches consisting in simultaneously looking for the same sources with both neutrino telescopes, gravitational wave interferometers and/or multi-wavelength facilities can constitute a viable mean of locating HEN/CR sources and thus further understanding the acceleration mechanisms at play in these sources.

Search for transient sources of HEN is promising since the short timescale of emission drastically reduces the background level, mainly composed of atmospheric muons and neutrinos and consequently increases the sensitivity and discovery potential of neutrino telescopes. In particular, specific strategies are developed to look for neutrino events in both time and space coincidence with transient events announced by public alerts distributed through the Gamma-ray Coordinated Network (GCN) or by private alerts transmitted via special channels. Offline analyses are performed to search for neutrino counterparts to catalogued flaring sources and will be presented at this conference [2]. Hereafter, we describe the real-time follow-up analyses performed with ANTARES after the detection of transient events which require low latency follow-up: gravitational wave events by LIGO/Virgo (Section 3), high-energy neutrino candidates by IceCube (Section 4) and Gamma-Ray Bursts and Fast Radio Bursts (Section 5).

## 2. Data acquisition and real-time alert reception in ANTARES

The data acquisition system of the ANTARES detector is based on the "all-data-to shore" concept [3]. The time and charge amplitude of all the photomultiplier (PMT) signals above a threshold of 0.3 photoelectrons are sent to a computing farm onshore for processing. A filter is applied on shore to select the physics events among the raw dataset structured in time slices of 104.85 ms and dominated by hits due to the optical background produced by bioluminescence and radioactive decay of  $^{40}\text{K}$ . Two filtering algorithms look for a combination of local clusters of hits within a time window of  $2.2 \mu\text{s}$ . The first one selects events made of five local causally connected clusters anywhere in the detector, while the second one requires at least two clusters on nearby PMT storeys. The selected events are finally kept for online and offline reconstruction as described in [4]. In particular, a fast and robust online algorithm reconstructs tracks in nearly real time [5]. The remaining sample of events is then sent to a more accurate reconstruction algorithm [6] which improves the angular resolution of each event in less than 5 s. Both algorithms use an idealised geometry of the detector that does not take into account the dynamical positioning of the optical modules due to sea current variations. For high-energy tracks, this use limits the angular resolution by about

0.1°. These online data are routinely used to look for neutrino counterparts to various astrophysical transient events whose detection is notified directly to ANTARES through both VOEvents<sup>1</sup> and/or GCN socket and also to send alerts after the detection of interesting neutrino events (as presented in another proceedings [7]). The latest results of these studies are presented hereafter.

### 3. Follow-up of gravitational wave events

The observation of two significant gravitational wave (GW) sources by Advanced LIGO on September 14<sup>th</sup> and December 26<sup>th</sup>, 2015 [9, 10] represents an important step forward in the era of multi-messenger astrophysics.

Since the beginning of the second observing run of Advanced LIGO interferometers on November 30, 2016, ANTARES is receiving gravitational wave alerts in real time. The angular resolution of ANTARES ( $\sim 0.4^\circ$  at  $\sim 10$  TeV) compared to the size of the gravitational wave error box (a few hundreds of square degrees on the sky) offers the possibility to drastically reduce the size of the region of interest in case of a coincident neutrino detection.

About 74 days of LIGO/Hanford and LIGO/Livingston simultaneous science data have been collected up to June 2017. The average reach of the LIGO network for binary merger events is around 70 Mpc for 1.4+1.4  $M_\odot$ , 300 Mpc for 10+10  $M_\odot$  and 700 Mpc for 30+30  $M_\odot$  mergers, with relative variations in time of the order of 10%. Prior to a commissioning break that occurred in May 2017, 7 triggers, identified by online analysis using a loose false-alarm-rate threshold of one per month, were identified and shared with partner collaborations who have signed memoranda of understanding with LIGO/Virgo for electromagnetic and neutrino follow-up. Each of the 7 alerts were followed by the ANTARES neutrino telescope by searching for a potential neutrino counterpart.

A thorough investigation of the data via an offline GW analysis enabled to confirm a first significant detection which occurred on January 04 2017 and produced after the merger of two black holes with 31.2 and 19.4 solar masses respectively [11]. We used ANTARES's online reconstruction pipeline [4] which selects up-going neutrino candidates with atmospheric muon contamination less than 10%. Directional and temporal coincidences between GW170104 and reconstructed HEN candidates were searched for. Relying on the methodology defined in [12], we looked for (i) temporal coincidences within a  $\pm 500$  s time window around the GW alert and (ii) spatial overlap between the 90% probability contour of GW150914 and the neutrino point spread function. No neutrino candidates temporally coincident with GW170104 were found with ANTARES within the  $\pm 500$  s time window. The results of the nearly real-time analysis has been transmitted to LIGO/Virgo follow-up community through a GCN (now publicly available [13]) less than 24 hours after the release of the alert<sup>2</sup>. The absence of neutrino candidate both temporally and positionally coincident with GW170104 allowed us to derive a preliminary upper limit on the spectral fluence emitted in neutrinos by the source at 90% confidence level, as a function of the location of the source in equatorial coordinates and assuming a standard  $dN/dE \propto E^{-2}$  spectral model. Figure 1

<sup>1</sup>standardized language adopted by the International Virtual Observatory Alliance.

<sup>2</sup>An automated notification was not generated by LIGO/Virgo after the detection of this event as the calibration of Handford detector's had to be checked beforehand. A first alert was distributed to collaborating astronomers 6 hours after the detection.

(left) shows in each direction of the sky the most stringent fluence upper limit (U.L.) as provided to the LIGO/Virgo follow-up community on January 24, 2017.

Using the constraints on the distance of the GW source and the neutrino fluence U.L., we derived the U.L. on the total energy emitted in neutrinos by this source. This was obtained by integrating the emission between 100 GeV and 100 PeV for each spectral model and each location in the sky map. The total energy U.L. depends on the source distance and equatorial coordinates and is shown in Figure 1 (right) inside the 90% GW error box.

An optimized offline search for a neutrino counterpart to GW170104 is currently performed in the ANTARES collaboration. Results should be published soon, as it has been done previously for GW150914, GW151226 and LVT151012 [14, 15].

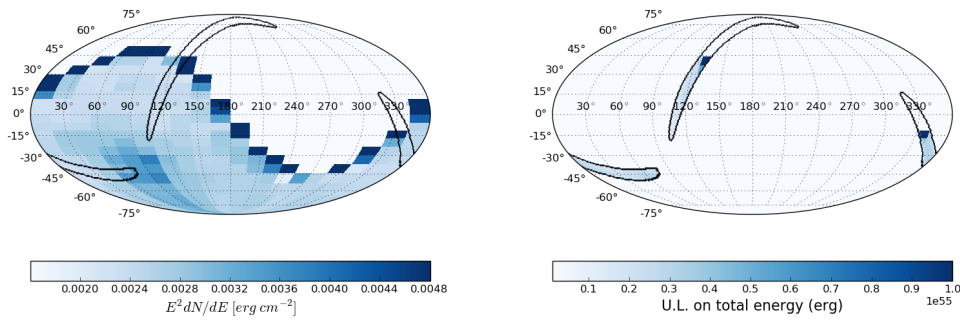


**Figure 1:** ANTARES 90% C.L. upper limits on the HEN spectral  $\nu_\mu + \bar{\nu}_\mu$  fluence (left) and on the total energy emitted through neutrinos (right) from GW170104 assuming a  $dN/dE \propto E^{-2}$  spectral model. Maps in equatorial coordinates. The black contours show the 90% C.L. contour for the GW skymap.

#### 4. Follow-up of IceCube HEN events

IceCube is currently the largest neutrino telescope. Located at the geographic South Pole, it is composed of 86 detection lines distributed over a cubic-kilometer of ice. High-energy events starting into the detector (HESE, see e.g. [1]) and extremely high-energy ones (EHE, with energy above 1 PeV) are received by the Astrophysical Multi-messenger Observatory Network (AMON, [16]) and distributed to the community via an alert of the GCN<sup>3</sup>. A coincident detection by both IceCube and ANTARES would be a significant proof of the astrophysical origin of these neutrino candidates and would point directly to the position of the source in the sky. In this context, the ANTARES collaboration is performing a follow-up analysis of each IceCube event whose position is below the horizon of ANTARES (which could consequently yield to an up-going event at the time of the alert). Up to now, ANTARES has followed the four alerts (3 HESE and 1 EHE) in the field-of-view of the telescope (see Figure 2). Two other events occurred in the field-of-view of ANTARES but were retracted by IceCube after further analysis which revealed a background origin. No neutrino candidates were found compatible with one of the alerts within a time window

<sup>3</sup><https://gcn.gsfc.nasa.gov/amon.html>



up to  $\pm 1$  hour. We used these non-detections to derive preliminary 90% confidence level upper limits on the radiant neutrino fluence of these events of the order of  $\sim 15 \text{ GeV cm}^{-2}$  and  $\sim 30 \text{ GeV cm}^{-2}$  for the  $E^{-2}$  and the  $E^{-2.5}$  spectral models respectively (see Table 1). These results have been published as GCN circulars within some hours after the alerts [17, 18, 19, 20].

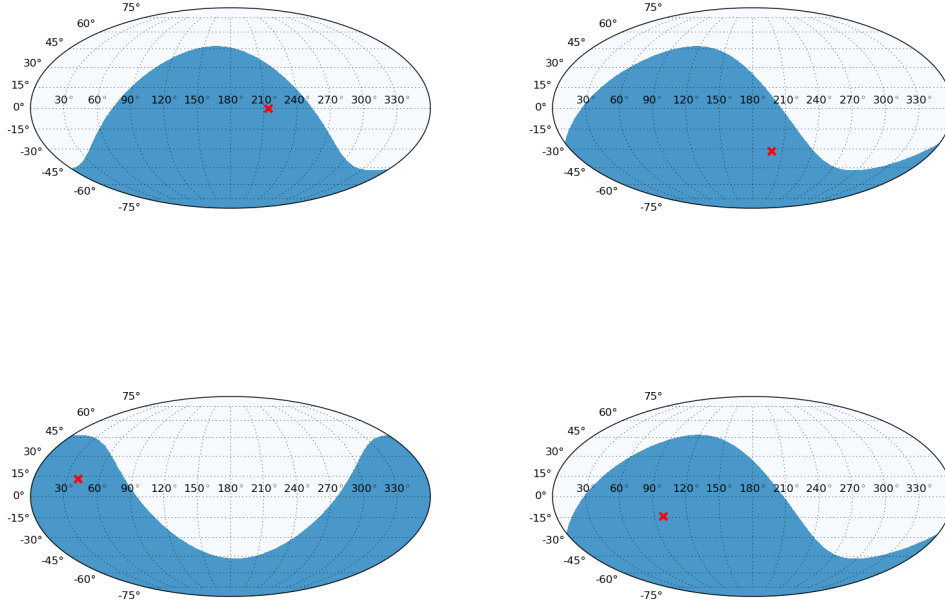


**Figure 2:** Visibility map of the IceCube alerts (top left: IC160731A, top right: IC160814A, bottom left: IC161103A, bottom right: IC170321A) in equatorial coordinates showing the field-of-view of the ANTARES neutrino telescope at the event time (blue part of the map). The red cross indicates the position of the neutrino candidate observed by IceCube.

IceCube event	Fluence U.L. ( $\text{erg cm}^{-2}$ )	
	$dN/dE \propto E^{-2}$	$dN/dE \propto E^{-2.5}$
IC160731A (EHE)	$2.2 \cdot 10^{-2}$	$4.3 \cdot 10^{-2}$
IC160814A (HESE)	$2.5 \cdot 10^{-2}$	$7.0 \cdot 10^{-2}$
IC161103A (HESE)	$2.1 \cdot 10^{-2}$	$5.1 \cdot 10^{-2}$
IC170321A (HESE)	$2.6 \cdot 10^{-2}$	$4.2 \cdot 10^{-2}$

**Table 1:** ANTARES fluence upper limits at 90% C.L. for each IceCube neutrino candidate.

## 5. Follow-up of Gamma-Ray Bursts and Fast-Radio Bursts

Transient astrophysical events are observed all over the electromagnetic spectrum and in particular at both ends of the spectrum, in the radio and gamma-ray domains where we respectively



observe fast radio bursts (FRBs) and gamma-ray bursts (GRBs). While the latter are probably related to either the collapse of massive stars or the merger of two compact objects, the sources producing the former are still unknown. If hadrons are accelerated in relativistic outflows of both GRBs and FRBs, TeV-PeV neutrinos might be produced by photo-hadronic interactions. Dedicated offline analyses are performed by the ANTARES collaboration (see e.g. [21, 22, 23]) and preliminary results of the more recent ones will be presented at this conference [24, 25]. In particular, a stacked analysis based on the full ANTARES data sample from 2008 to 2016 enables to constrain the contribution of GRBs to the diffuse flux of cosmic neutrinos. On the other hand, looking for individual GRBs and FRBs helps to constrain theoretical models of neutrino emission.

ANTARES is able to react to external alerts sent through GCN after the detection of a GRB. More than 500 GRBs detected by Swift and Fermi have been followed by ANTARES in realtime so far (see Figure 3). Data analysis can be done in two alternative ways. A search for muon-track neutrino counterpart in the standard online dataset described in Section 2 is performed in real-time within 15 min around the detection and  $2^\circ$  from the GRB position. To ensure the quality of the data at the alert time, the detector stability is checked over several hours before the alert. The result of the search is sent by email within 15 min after the release of the GCN. In case of a coincident neutrino detection, a dedicated offline analysis is run to confirm the result and compute its significance (expected to be higher than  $3\sigma$  in most of the cases).

Alternatively, a specific data taking mode is activated jointly with the standard one in case of a GRB alert. All raw data covering a preset period (typically 2 min, depending on the background rate, the number of data processing computers, and the size of the RAM) are saved to disk without any filtering [26]. Data buffering in the filter processors enables to store the data up to about one minute before the actual GCN alert. In most cases, it consequently includes data collected by ANTARES before the GRB occurred, which can be used to search for a neutrino signal occurring before the gamma ray emission. These unfiltered data can be analysed with a less strict filtering compared to the standard online filtering and a reconstruction algorithm optimised for energies below 1 TeV [27] can be applied to increase the detection efficiency (by a factor of  $\sim 2$  at 100 GeV and  $\sim 30\%$  at 10 TeV). A dedicated algorithm searching for time and space correlations in a small region of interest around the GRB position is finally used as in standard offline analyses. An analysis based on this approach has recently been published by the ANTARES collaboration to test the photospheric model of neutrino emission in GRBs [21].

As for FRBs, the Parkes radiotelescope, located in Australia, is the main discovery instrument so far and the SURvey for Pulsars and Extragalactic Radio Bursts (SUPERB) is underway on this instrument [28]. One of the main obstacles for constraining the nature of the FRBs is the latency between the detection of the burst and the starting of multi-wavelength and multi-messenger follow-up observations aimed to identify a FRB counterpart. The SUPERB program was designed to drastically reduce the time needed to send a notification to the community. In this context, ANTARES is receiving alerts issued by the SUPERB collaboration in case of a Fast Radio Burst detection since 2015. The ANTARES collaboration has recently been involved in the multi-wavelength and multi-messenger study of FRB 150215 detected with the Parkes radiotelescope by SUPERB [29]. The datastream was searched for upgoing track events from a point-like source within a time window of up to  $\pm 1$  day around the FRB detection in a region of interest of  $2^\circ$

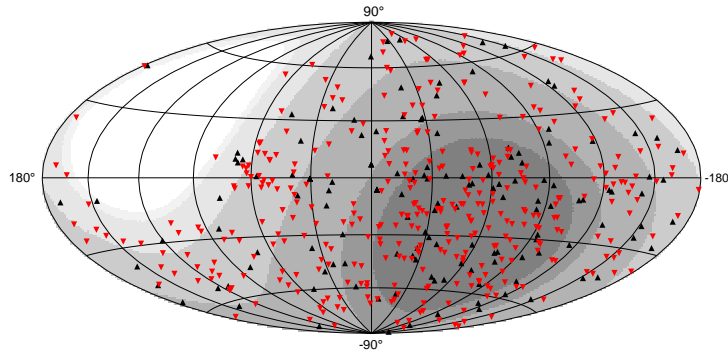


**Figure 3:** Positions of the the GRBs followed by ANTARES (red ticks indicate those detected by Fermi while black ticks those observed by Swift). The shade of grey indicates the ANTARES visibility. The map is in galactic coordinates.

centered on the position of the Parkes beam center. No neutrinos were detected coincident with this transient event. Consequently, a neutrino radiant fluence<sup>4</sup> upper limit at 90% confidence level has been computed together with an upper limit on the total energy emitted in high-energy neutrinos (assuming a redshift of  $z = 0.56$  as constrained by radio data). Results are given in Table 2 for a spectral model  $dN/dE \propto E^{-2}$ .

Fluence U.L. (erg cm <sup>-2</sup> )	Total energy U.L. (erg)
$1.4 \times 10^{-2}$	$1.4 \times 10^{55}$

**Table 2:** Results of the FRB150215 neutrino follow-up performed with ANTARES.

## 6. Conclusion

By simultaneously monitoring at least half of the sky, neutrino telescopes are well-suited to detect transient sources. In this context, multi-messenger approaches are destined for a bright future and will help to probe the physical processes at work in these objects. In addition to offline analyses, that search for time and space coincidences of ANTARES events with electromagnetic, gravitational wave or neutrino signals [2, 30, 31], ANTARES is also able to handle external alerts in real time (as described in this document) and to trigger electromagnetic follow-up of interesting neutrino candidates [7, 8]. Furthermore, the capability of the ANTARES data acquisition system to store a few minutes of raw data coincident with a GCN alert extends the possibility of increasing offline sensitivity to transient astrophysical events. In the near future, KM3NeT, currently under deployment in the Mediterranean sea, will further develop these dedicated multi-messenger programs that will benefit from an increase of both the discovery potential (by a factor of  $\sim 50$  with respect to ANTARES) and the angular resolution of muon tracks and cascade events [32].

<sup>4</sup>Defined as  $\int E dN/dE dE$ .

## References

- [1] Aartsen M G et al. (IceCube), *ApJ*, 809(1), 98 (2015).
- [2] Sánchez-Losa A et al. (on behalf of the ANTARES collaboration), these proceedings.
- [3] Aguilar J et al., *Nucl. Instrum. Meth.*, A570 107 (2007).
- [4] Ageron M et al., *Astropart. Phys.*, 35:530-536 (2012).
- [5] Aguilar J A et al., *Astropart. Phys.*, 34 2011 652-662 (2011).
- [6] Adrián-Martínez S et al., *ApJ*, 760:53 (2012).
- [7] Dornic D et al. (on behalf of the ANTARES collaboration), these proceedings.
- [8] Adrián-Martínez S et al., (ANTARES), *JCAP*, 02:62 (2016).
- [9] Abbott B P et al., *Phys. Rev. Lett.*, 116 061102 (2016).
- [10] Abbott B P et al., *Phys. Rev. Lett.*, 116 241103 (2016).
- [11] Abbott B P et al., *Phys. Rev. Lett.*, 118 221101 (2017).
- [12] Baret B et al., *Astropart. Phys.*, **35** 1:7 (2011).
- [13] The circulars exchanged between collaborating astronomers and LIGO/Virgo regarding GW170104 are archived at <https://gcn.gsfc.nasa.gov/other/G268556.gcn3>.
- [14] Adrián-Martínez S et al., *Phys. Rev. D*, **93** 122010 (2016).
- [15] Adrián-Martínez S et al., *Phys. Rev. D in press*, arXiv:1703.06298 122010 (2017).
- [16] Smith M W E et al., *Astropart. Phys.*, 45:56-70 (2013).
- [17] Dornic D & Coleiro A, on behalf of ANTARES, *ATeL*, 9324 (2016).
- [18] Dornic D & Coleiro A, on behalf of ANTARES, *ATeL*, 9440 (2016).
- [19] Dornic D & Coleiro A, on behalf of ANTARES, *ATeL*, 9715 (2016).
- [20] Dornic D & Coleiro A, on behalf of ANTARES, *ATeL*, 10189 (2017).
- [21] Albert A et al., *Mon. Not. Roy. Astron. Soc.*, 469 906 (2017).
- [22] Adrián-Martínez S et al., *Astron. Astrophys.*, 559 (2013).
- [23] Adrián-Martínez S et al., *Eur. Phys. J. C*, 77:20 (2017).
- [24] Celli S (on behalf of the ANTARES collaboration), these proceedings.
- [25] Sanguineti M et al. (on behalf of the ANTARES collaboration), these proceedings.
- [26] Bouwhuis M (on behalf of the ANTARES collaboration), *Procs. ICRC 2009*, arXiv:0908.0818 (2009).
- [27] Visser E, Doctoral Thesis, Leiden University (2015).
- [28] Keane E F et al., arXiv1706.04459, *submitted to Mon. Not. Roy. Astron. Soc.*.
- [29] Petroff E et al., *Mon. Not. Roy. Astron. Soc.*, 469, 4465:4482, (2017) .
- [30] Pradier T et al. (on behalf of the ANTARES collaboration), these proceedings.
- [31] Illuminati G et al. (on behalf of the ANTARES collaboration), these proceedings.
- [32] Adrián-Martínez S et al., *JPhG*, 43 8 (2016).

## Multi-wavelength follow-up observations of ANTARES neutrino alerts

---

**Damien Dornic\***

*CPPM, Aix-Marseille Université, CNRS/IN2P3, 13009 Marseille, France.*

*E-mail: [dornic@cppm.in2p3.fr](mailto:dornic@cppm.in2p3.fr)*

**D. Turpin (IRAP), M. Ageron, V. Bertin, J. Brunner, A. Mathieu (CPPM), F. Schüssler, B. Vallage (CEA/IRFU), S. Basa (LAM) on behalf the ANTARES, TAROT, MASTER, ZADKO, Swift, MWA, H.E.S.S. Collaborations.**

High-energy neutrinos could be produced in the interaction of charged cosmic rays with matter or radiation surrounding astrophysical sources. Transient phenomena, such as gamma-ray bursts, core-collapse supernovae or active galactic nuclei are promising candidates to emit high-energy neutrinos. To search for coincidences between a transient event and a neutrino emission, a follow-up program of neutrino alerts is in operation within the ANTARES Collaboration since 2009. This program triggers a network of robotic optical telescopes immediately after the detection of a neutrino event and schedule several observations in the following weeks. The most interesting neutrino candidates are also followed by the Swift XRT telescope and the Murchison Wide field Array radio telescope and the H.E.S.S. very high-energy gamma-ray telescope. By combining the information provided by the ANTARES neutrino telescope with information coming from other observatories, the probability of detecting a source is enhanced, allowing the possibility of identifying a neutrino progenitor from a single detected event. No significant counterpart associated with a neutrino emission has been identified during image analysis.

*35th International Cosmic Ray Conference — ICRC2017  
10–20 July, 2017  
Bexco, Busan, Korea*

---

\*Speaker.

## 1. Introduction

High-energy neutrinos may be produced in the interaction of charged cosmic rays with matter or radiation surrounding astrophysical sources. Even with the recent detection of extraterrestrial high-energy neutrinos by the IceCube experiment [1, 2], no astrophysical neutrino source has yet been discovered. Such a detection would provide a direct evidence of hadronic acceleration mechanisms and would therefore solve the origin of very high-energy cosmic rays.

High-energy neutrinos are thought to be produced in several kinds of astrophysical sources, such as the galactic binaries, supernova remnant, gamma-ray bursts (GRB) [3], core-collapse supernovae (CCSN) [4] or active galactic nuclei (AGN) [5]. Most of these sources are also transient events covering a large range in the time domain, from seconds for GRB to weeks for CCSN or AGN. By combining the information provided by the ANTARES neutrino telescope [6] with information coming from other observatories, the probability of detecting a source is enhanced since the neutrino background is significantly reduced in the time window around the event [7].

Based on this idea, a multi-wavelength follow-up program of ANTARES alerts, dubbed TAToO (Telescopes-Antares Target of Opportunity), has been operating since 2009 [8]. It triggers multi-wavelength observations within a few seconds after the detection of selected high-energy neutrino candidates. The document is organized as follows: Section 2 describes the alert sending system and its performances. Follow-up observations of neutrino candidates are now performed over a broad range of the electromagnetic spectrum, from visible to X-ray. Section 3 describes the multi-wavelength facilities used by ANTARES to follow the neutrino alerts. Section 4 reports the main results of the visible and X-ray observations. Section 5 shows the results of the multi-wavelength and multi-messenger follow-up of the alert ANT150901A. The recent search for radio counterpart of few high-energy neutrino events by the Murchison Widefield Array (MWA) [9] is reported in Section 6. On the extreme opposite of the electromagnetic band, a few ANTARES alerts have been followed looking for TeV photons detected by H.E.S.S. [10] (Section 7).

## 2. Characteristics of the ANTARES alert sending system

All the ANTARES events are reconstructed in real-time ( $< 5$  s) by two independent algorithms [11, 12]. These algorithms use an idealized detector geometry and are independent of the dynamical positioning calibration (the positions of the optical modules are not corrected for displacements due to sea currents). This reconstruction and subsequent quality selections allow the rate of events to be reduced from few Hz down to few mHz removing almost all the huge downgoing atmospheric muon contribution. The duty cycle of TAToO is around 90%. From the remaining atmospheric neutrino sample, the selection of the neutrino candidates with an increased probability to be of cosmic origin is performed with three online neutrino trigger criteria currently implemented in the TAToO alert system [8]:

- High energy trigger: the detection of a single high energy neutrino.
- Directional: the detection of a single neutrino for which the direction points toward ( $< 0.4^\circ$ ) a local galaxy ( $< 20$  Mpc) in the GWGC catalogue [13].

**Table 1:** Performances of the three alert criteria. The third column shows the median angular resolution at the mean energy  $\langle E \rangle$ . The fourth column corresponds to the fraction of events inside a  $2^\circ \times 2^\circ$  field of view assuming a flux of GRB [3] and CCSN [4].

Trigger	$\langle E \rangle$	Ang. Res.	Fraction	Muon contamination
Doublet	$\sim 100$ GeV	$\leq 0.7^\circ$	/	0 %
Single HE	$\sim 7$ TeV	$\sim 0.3^\circ$	96% (GRB) 68% (SN)	$< 0.1$ %
Single directional	$\sim 1$ TeV	$\sim 0.4^\circ$	90% (GRB) 50% (SN)	$\sim 2$ %

- Doublet trigger: the detection of at least two neutrinos coming from similar directions ( $< 3^\circ$ ) within a predefined time window (15 min).

The main performances of these three triggers are described in Table 1. Until now, no doublet trigger has been sent to the network. The trigger criteria are inspired by the features expected from astrophysical sources and are tuned to comply with the alert rate to send to the telescope network. An agreement between ANTARES and the optical telescope collaborations allows a rate of around 25 alerts per year to be sent to each optical telescope, while an agreement to send 6 alerts per year to the Swift satellite have been accepted. Due to this reduced rate, a subset of the high-energy trigger with more restrictive requirements on the neutrino energy, provides a dedicated trigger for the Swift satellite. A similar sub-sample is sent to the H.E.S.S. and M.W.A telescopes. The TAToO alert system is able to send alerts within few seconds (3-5 s) after the neutrino detection with an angular resolution better than  $\sim 0.4^\circ$ .

### 3. Multi-wavelength follow-up facilities

The ANTARES neutrino alerts are followed by the small robotic optical telescopes such as TAROT [14], ZADKO [15], MASTER [16] and SVOM/GWAC [17] located all-around the world. TAROT is a network of two identical 0.25 m telescopes with a field of view (FoV) of  $\sim 1.86^\circ \times 1.86^\circ$  located in Calern (France) and La Silla (Chile). Zadko is a 1 meter telescope located at the Gingin observatory in Western Australia. As its FoV is about 0.15 square degrees, seven tiles are needed to cover the ANTARES point spread function. The 6 MASTER telescopes are located in Russia, Canary Islands and in South Africa, and consist of 6 pairs of tubes with a diameter of 0.40 m covering a FoV of up to 8 square degrees for each pair of telescopes. Until the end of 2014, the network also comprises the four optical telescopes ROTSE [18], which have progressively stopped their activity. These telescopes reach a limiting magnitude of  $\sim 19$ -20.5 mag depending on their diameters. In 2017, the follow-up has been extended to the SVOM/GWAC telescopes located in China providing a very large FoV ( $\sim 40^\circ$ ) but with a not very deep sensitivity ( $\sim 15$  mag). The wide FoV and the fast response of these telescopes (images can be taken less than 20 s after the neutrino detection) are well suited to the search for transient sources. For each alert, the optical observation strategy is composed of an early follow-up (within 24 hours after the neutrino detection), to search for fast transient sources such as GRB afterglows, complemented by several observations during the two following months, to detect for example the rising light curves of CCSN. Each observation is composed of series of optical images (with clear filter). Optical images are analyzed with dedicated pipelines based on the image subtraction method to look for new transient sources [22].

The Swift satellite with its XRT [19] provides a unique opportunity to observe X-ray counterparts to neutrino triggers. The detection sensitivity of the XRT is  $\sim 5 \times 10^{-13}$  erg cm $^{-2}$  s $^{-1}$  in 1 ks exposure, and an energy band from 0.3 to 10 keV is covered [20]. Due to the small FoV of the XRT (radius of  $\sim 0.2^\circ$ ) and the typical error radius of an ANTARES alert ( $\sim 0.3$ – $0.4^\circ$ ), each observation of a neutrino trigger is composed of 4 tiles of 2 ks each. This mapping covers about 72% of the ANTARES point spread function for a high-energy neutrino. The observation strategy is composed of an automatic response to the neutrino trigger with observations starting as soon as possible. There is an online analysis of the data and in the case where an interesting candidate to be the counterpart is found, further observations are scheduled.

In the last few years, follow-up observations of a sub-sample of neutrino alerts are also performed by the Murchinson WideField Array (MWA [9]) which is the low frequency (80 - 300 MHz) precursor of the Square Kilometre Array. Its huge field of view (700 square degrees at 150 MHz) is particularly valuable for follow-up of neutrino candidates, which have rather large position uncertainties. A few alerts have also triggered observations by the H.E.S.S. Cherenkov telescope located in Namibia. H.E.S.S. has a typical energy threshold of 100 GeV and a large field of view of around  $5^\circ$  [10].

#### 4. Optical and X-ray follow-up

Since mid 2009, a total of 256 alerts have been sent to optical robotic telescopes while 13 targets of opportunity have been sent to the XRT instrument on board the Swift satellite since mid-2013. The typical follow-up efficiency is around 80% for the network of robotic telescopes and for the Swift satellite.

From mid 2009 to June 2017, 169/256 alerts with early optical follow-up ( $< 24$  h after the neutrino time) have been analyzed ( $\sim 66\%$  of the sent alerts). Among them, 40 have a delay lower than 1 min ( $\sim 16\%$ ). No optical counterparts were found and upper limits on the R-band magnitude of a transient astrophysical source have been derived. These limits correspond to the limiting magnitude of images, which is the faintest signal that can be detected. As we are looking for rapidly-fading sources, the signal is supposed to be more important in the first image of the observation, so the upper limits are the limiting magnitude of each first image computed at  $5\sigma$  and corrected for Galactic extinction [13]. By comparing these upper limits with optical afterglow light curves of gamma-ray bursts (Figure 1), it becomes possible to reject a GRB association with each neutrino alert, in particular when the optical follow-up is performed within a few minutes after the neutrino trigger [22]. A similar analysis has been carried out with Swift-XRT follow-ups of 13 ANTARES alerts [22]. The typical delay of the first Swift observation is around 6h with a minimum delay of 1.1h. The probability to reject the GRB hypothesis reaches more than  $\sim 70\%$  if the X-ray follow-up occurs within few hours after the trigger.

Among the 256 sent alerts, 177 have sufficiently good optical long-term follow-ups, i.e. at least 3 (2) nights of observation for TAROT (MASTER) network. No significant slowly varying transient optical counterparts were found in association with a neutrino trigger. The expected number of accidental SN detections, i.e. a SN detection in coincidence with a background neutrino event, is estimated to 0.3 in the 177 alerts assuming a rate of SN of 1 per year within a sphere of 10 Mpc



( $2.4 \times 10^{-4} \text{ yr}^{-1} \text{ Mpc}^{-3}$ ). This result is consistent with the small expectation SN number with a probability of 0.74.

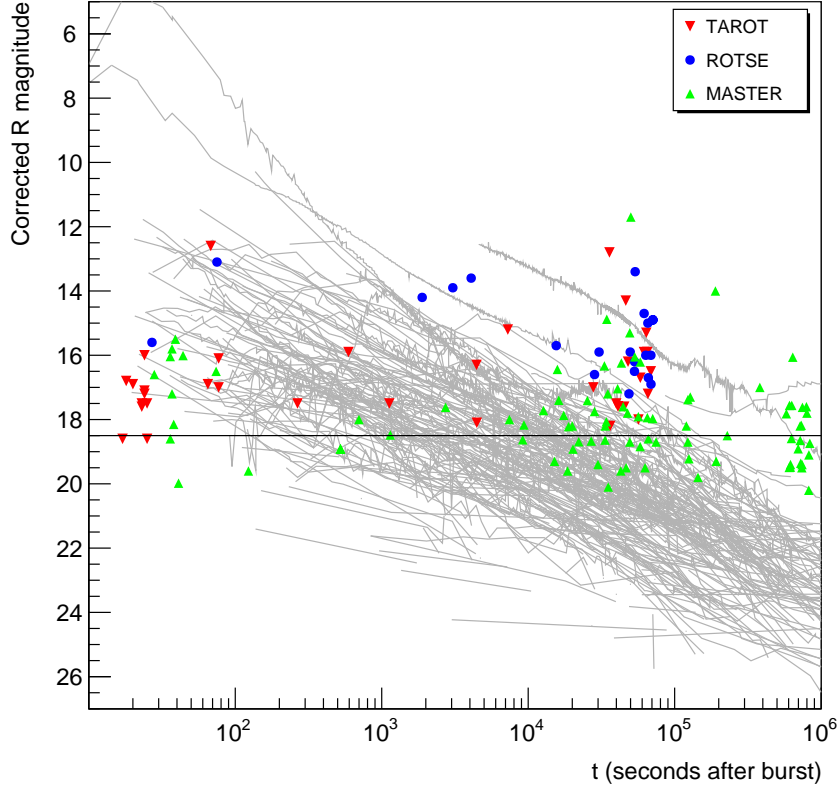


**Figure 1:** Comparison between archived optical light-curves for 301 GRBs detected in the period 1997-2014 and the upper limits obtained for the 169 alerts. Red, blue and green markers indicate upper limits on GRB afterglow magnitudes for neutrino alerts observed by TAROT, ROTSE and MASTER respectively. The horizontal black line corresponds to the typical sensitivity of the optical telescopes.

## 5. Follow-up of ANT150901A

On September 2015 1st, ANTARES detected a bright neutrino (ANT150901A) with an energy around 50 TeV. The direction is RA = 16h25'42, DEC = -27d23'24 with an uncertainty of  $\sim 18$  arcmin (radius, 50% containment). An alert has been sent to our follow-up partners after a delay of 10 s. Swift/XRT has started the follow-up 9h after the neutrino trigger. 8 sources have been identified in the field of view, among them 5 are catalogued, 2 faint sources and one uncatalogued, relatively bright and variable X-ray source above the Rosat All-Sky Survey (RASS) limit [23] ( $= 5 \times 10^{-13} - 1.4 \times 10^{-12} \text{ erg cm}^{-2} \text{ s}^{-1}$  at 0.3 - 10 keV). This source is located at  $0.14^\circ$  from the neutrino direction. Further observations with XRT show an outburst with a typical length of around 2 days (Figure 2 left). In parallel, MASTER has followed the field of view after 10h. No significant new

variable source has been identified. At the position of the X-ray source, MASTER has identified a bright star (USNO-B1.0 0626-0501169) of a magnitude 12.3 with a light curve showing no flux and no color variations. The Figure 2 (right) illustrates the field of view of MASTER.

A GCN notice [24] and an ATeL telegram [25] were emitted to request for more multi-wavelength observations to characterize the star and to test the association between the X-ray flare and this bright star. 19 multi-wavelength observatories have answered to this trigger covering the full electro-magnetic spectrum: 1 radio telescope, 11 optical/IR telescopes, 4 X-ray satellites and 4 very high-energy gamma-ray observatories. IceCube has also reported a non-observation. These observations point to USNO-B1.0 0626-0501169 being a binary RS CVn system, undergoing a flaring episode that produced the X-ray emission. The typical characteristics of this star are a distance of around 100 - 150 pc, an age of around 10 Myr and a mass around  $0.75 M_{\odot}$ . Therefore, this source seems not to be the origin of the bright ANT150901A neutrino with a probability of  $\sim 3\%$  of chance association.

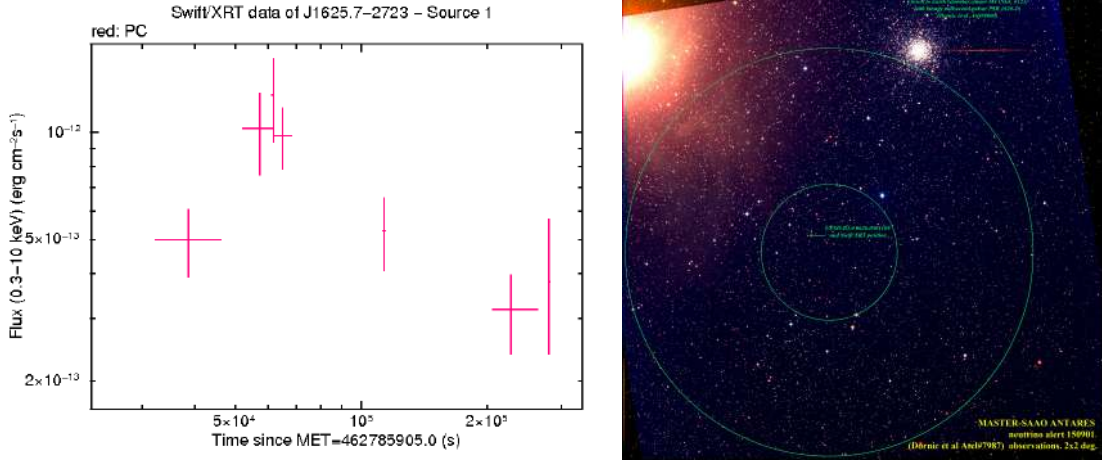


**Figure 2:** Left: Light curve measured by the XRT on board of Swift for the X-ray source identified in the follow-up of ANT150901A. Right: Field of view of MASTER corresponding to ANT150901A.

## 6. Radio follow-up with MWA

A search for radio counterparts to two candidate high-energy neutrino events detected in November 2013 (ANT131121A) and March 2014 (ANT140323A) was performed using the Murchison Widefield Array [26]. Such triggers have directions consistent ( $< 0.4^\circ$ ) with the positions of galaxies within 20 Mpc of Earth [13]. Two galaxies match in each case: NGC1374 and ESO358-015 match ANT131121A, and ESO499-037 and PGC29194 match ANT140323A. PGC29194 (the Antlia Dwarf Galaxy), at a distance of 1.3 Mpc, is located just  $6'$  from the neutrino position. Both neutrino events also had optical follow-up. For ANT131121A, 12 observations of 6 images were performed with the TAROT telescope in Chile from 2 - 61 days after the trigger. No optical transient was identified, to a limiting magnitude of 19. For ANT140323A, a total of 8 images were taken with ROTSE 3b in Texas (starting  $\sim 15$  hr after the trigger) and 10 images with TAROT Chile up to

45 days after the trigger according to the long-term strategy. No transient counterpart was found to limiting magnitudes of 16.4 (prompt) and 18.7 (long-term).

Transient or strongly variable radio sources consistent with the neutrino positions are looked for using MWA archival data at frequencies between 118 and 182 MHz, taken 20 days prior to, at the same time as, and up to a year after the neutrino triggers. As no such counterparts are detected, and  $5\sigma$  upper limit for low-frequency radio emission of  $\sim 10^{37}$  erg s<sup>-1</sup> for progenitors at 20 Mpc. If the neutrino sources are instead not in nearby galaxies, but originate in binary neutron star coalescences, the limits constrain the progenitors to be at  $z \geq 0.2$ . ANTARES is now sending a sub-sample of the neutrino alerts in real-time to MWA. Analysis of MWA data is still on-going.

## 7. Very high-energy gamma-ray follow-up with H.E.S.S.

Since 2016, ANTARES and H.E.S.S. have signed an MoU to exchange information and alerts. Exploiting the intimate connection between high-energy neutrinos and very high-energy gamma rays, the very high gamma-ray H.E.S.S. telescopes have followed two ANTARES alerts shortly after the neutrino detection: ANT150901A and ANT170130A. For ANT150901, the observations started on September 3rd, 2015, at 18:58 UT as soon as the necessary observation conditions were reached. No very-high energy gamma-ray source has been identified in the 1.5 h observations. An upper limit on the gamma-ray flux to  $\Phi(E > 320 \text{ GeV}; 99\% \text{ C.L.}) < 2.7 \cdot 10^{-8} \text{ m}^{-2} \text{ s}^{-1}$  [27]. The neutrino ANT170130A direction has also been followed by H.E.S.S. with a very short delay, 32 s during 1 hour and again 45 min the night after. The preliminary analysis on site shows no source detection in the neutrino field of view [28] (detailed analysis are still in progress).

## 8. Conclusion & perspectives

Follow-up of high-energy neutrino alerts is a very promising method to identify transient sources as sources of neutrino production. The detection of one counterpart associated in time and direction with one neutrino could lead to a high significance discovery. ANTARES is able to send alerts to the external community in 5-7 seconds after the time of the neutrino detection with a precision of the direction better than 0.4 degrees. The triggers are followed by several multi-wavelength facilities such as robotic telescopes located all around the world, a radio telescope, one X-ray satellite and very high-energy gamma-ray telescopes. This provides an unique follow-up network covering the whole EM spectrum. Up to now, no counterpart has been detected significantly in the different searches and constraints have been set on the origin of individual neutrinos.

The two KM3NeT detectors [29], in construction in the Mediterranean Sea, will have a 50 times increased discovery potential compared to the ANTARES telescope from 5 GeV to a few PeV. Dedicated follow-up programs are in development which will allow to send more promising neutrino alerts to the astronomy community.

## References

- [1] M.G. Aartsen et al, *Science*, 342, 1, 2013.
- [2] M.G. Aartsen et al, *ApJ*, 809(1), 98, 2015.

- [3] E. Waxman, J. Bahcall, Phys. Rev. Lett., 78, 2292-2295, 1997. P. Mészáros, E. Waxman, Phys. Rev. Lett., 87(17)171102, 2001. S. Hümmel, M.Rüger, F. Spanier, W. Winter, ApJ, 721, 630-652, 2010.
- [4] S. Ando & J.F. Beacom, Phys. Rev. Lett., 95 (6)061103, 2005.
- [5] M. Böttcher, A. Reimer, K. Sweeney, A. Prakash, ApJ, 768, 54, 2013.
- [6] M. Ageron et al (ANTARES Collaboration), Nucl. Instr. Meth. A, 656, 11-38, 2011.
- [7] S. Adrián-Martínez et al (ANTARES Collaboration), 2015, JCAP, 12, 014.
- [8] M. Ageron et al (ANTARES Collaboration), Astrpart. Phys., 35, 530-536, 2012.
- [9] C.J. Lonsdale, R.J. Capallo, M.F. Morales et al, 2009 IEEE proceedings, 97. 1497. S.J. Tingay, R. Gaeker, J.D. Bowman et al, 2013, PASA, 32, 25.
- [10] F. Aharonian et al (H.E.S.S. Collaboration), A&A 457 (2006) 899.
- [11] J.A. Aguilar et al (ANTARES Collaboration), Astropart. Phys., 34, 652-662, 2011.
- [12] S. Adrián-Martínez et al (ANTARES Collaboration), Astrophys. J. Lett., 743, 14-19, 2011.
- [13] D.J. White, E.J. Daw, V.S. Dhillon, Classical and Quantum Gravity, 28(8):080516, 2011.
- [14] A. Klotz, M; Boer, J.-L. Atteia, B. Gendre, AJ, 137, 4100-4108, 2009.
- [15] D.M. Coward et al, 2016, PASA, 34, 5.
- [16] V. Lipunov et al, Adv. in Astron., 30, 2010.
- [17] Wei J., Cordier B et al (SVOM Collaboration), 2016, arXiv:1610.06892.
- [18] C.W. Akerlof et al, PASP, 115, 132-140, 2003.
- [19] D.N. Burrows et al, Space Sci. Rev., 120, 165-195, 2005.
- [20] P.A. Evans et al, ApJS, 210, 8, 2014.
- [21] D.J. Schlegel, D.P. Finkbeiner, M. Dabvis, ApJ, 500, 525-553, 1998.
- [22] S. Adrián-Martínez et al (ANTARES Collaboration), 2016, JCAP, 02, 062.
- [23] W. Vogues et al, A&A, 349, 389-405, 1999.
- [24] D. Dornic et al (ANTARES Collaboration), GCN, 18231 (2015).
- [25] D. Dornic et al (ANTARES Collaboration), ATeL, 7987 (2015).
- [26] S. Croft et al (MWA & ANTARES Collaborations), The Astrophys. J. 823 (2016) no.2; L24.
- [27] F. Schüssler, Proceedings of the Rencontres de Moriond 2017 (VHEPU), arXiv: 1705.08258.
- [28] F. Schüssler, this conference.
- [29] S. Adrián-Martínez et al, (KM3NET Collaboration), Journal of Physics G: Nuclear and Particle Physics, 43 (8), 084001, 2016.

## Search for muon neutrinos from GRBs with the ANTARES neutrino telescope

---

**Silvia Celli\***

*On behalf of the ANTARES Collaboration*

*Gran Sasso Science Institute, Viale Francesco Crispi 7, 67100 L'Aquila, Italy*

*INFN-Sezione di Roma, P.le Aldo Moro 2, 00185 Roma, Italy*

*E-mail: [silvia.celli@gssi.infn.it](mailto:silvia.celli@gssi.infn.it)*

ANTARES is the largest operational neutrino telescope in the Northern hemisphere, located in the deep water of the Mediterranean Sea, offshore Toulon. One of its main scientific goals concerns the identification of hadronic astrophysical accelerators through the detection of high-energy neutrinos. Among these sources, Gamma-Ray Bursts (GRBs) constitutes promising candidates because they are the most bright sources in the Universe. Their transient nature allows to drastically reduce the expected background when both a temporal and spatial correlation with the observed gamma-ray prompt emission is required. Cosmic neutrinos could be produced in the interaction between accelerated protons and intense radiation fields in the jet. Two different approaches have been adopted in the search: a stacked analysis with a sample of GRBs observable using the full ANTARES data set (from 2008 to 2016) and an individual search from some of the brightest GRBs (with gamma-ray fluence greater than  $10^{-4}$  erg/cm<sup>2</sup>) occurred in the same time period. The methods and the results of these searches for muon neutrinos are here presented. The stacking analysis allows to constrain the contribution to the diffuse flux of neutrinos from this population of sources. In the bright GRB analysis, instead, the internal shock and the photospheric scenarios have been investigated and limits in the parameter space of the fireball model are derived individually. Since no events have been detected in spatial and temporal coincidence with GRBs in any of the searches, upper limits on neutrino fluence are derived both for individual bright sources and for the GRB population sample.

*35th International Cosmic Ray Conference – ICRC2017*

*10-20 July, 2017*

*Bexco, Busan, Korea*

---

\*Speaker.

## 1. Introduction

The first detection of cosmic neutrinos [1] with still unidentified astrophysical sources is one of the main open questions of modern astrophysics. Despite the lack of a clear multi-messenger connection, different interpretations of the signal have come from the theoretical side, addressing both the galactic and the extra-galactic scenario. Many efforts have been carried out from the experimental side as well in order to constraint the contribution to this signal of different source classes. Among them, Gamma-Ray Bursts (GRBs) represents valuable candidates, being the most powerful catastrophic events of the Universe. In baryonic jet models, neutrinos are expected to be produced in the interaction among accelerated protons and the jet radiation field. Thanks to their properties of electrical neutrality, stability and weak interaction, neutrinos are able to reach the Earth undeflected and unabsorbed, directly pointing to the emission site. Both muon and electron neutrinos emerge from  $p\gamma$  interaction: however, the most adequate event sample for astronomical purposes is represented by the muon sample, given the very good angular resolution that can be achieved, particularly in water. Therefore, a search from muon neutrinos from GRBs is here presented, using the ANTARES data set from 2008 to 2016: sources below the detector horizon are here considered in order to strongly suppress the atmospheric muon background, while an unbinned likelihood analysis is performed to distinguish the signal from the irreducible atmospheric neutrino background. A model-dependent search, based on both the internal shock and of the photospheric scenarios of the GRB fireball model is performed. Previous searches in both the ANTARES [2] and the IceCube [3] telescopes did not succeed in the identification of neutrino events spatially and temporally correlated with the detected gamma-ray emissions. The paper is structured as follows: an introduction to the theoretical models connecting gamma-rays and neutrinos in GRBs is introduced in Sec. 2. The analysis method for an optimized search is then discussed in Sec. 3, in order to present in Sec. 4 an individual search from four bright GRBs and in Sec. 5 a diffuse search performed through the stacking technique. In these sections, constraints on the physics of GRBs are derived as well. Conclusions are then given in Sec. 6.

## 2. Gamma-ray bursts modeling

The most accepted scenario describing the emission of the detected gamma-rays (in the so called prompt phase of the GRB) is the fireball model [5]. A central engine injects in the interstellar medium plasma shells with different velocities: particle acceleration is occurring when a faster shell catches up with a slower one. Both protons and electrons are thought to be accelerated in this process, while gamma-rays are mainly produced through inverse Compton scattering over the accelerated electrons. Protons interacting with the radiation field can produce both gamma-rays and neutrinos through the  $\Delta^+$  resonant channel:

$$p + \gamma \rightarrow \Delta^+ \rightarrow \begin{cases} p + \pi^0 \\ n + \pi^+ \end{cases} \longrightarrow \begin{cases} \pi^0 \longrightarrow \gamma + \gamma \\ n \longrightarrow p + e^- + \bar{\nu}_e \\ \pi^+ \longrightarrow \mu^+ + \nu_\mu \\ \mu^+ \longrightarrow e^+ + \nu_e + \bar{\nu}_\mu \end{cases} \quad (2.1)$$

In the internal shock (IS) scenario the radius of shell collisions is located at [6]

$$R_{IS} = 2 \frac{ct_{var}}{1+z} \Gamma^2 \sim 10^{13} \left( \frac{t_{var}}{0.01 \text{ s}} \right) \left( \frac{\Gamma}{10^{2.5}} \right)^2 \left( \frac{1}{1+z} \right) \text{ cm} \quad (2.2)$$

where  $t_{var}$  represents the variability time of the GRB emission,  $\Gamma$  is the jet Lorentz factor and  $z$  is the source redshift. In the photospheric (PH) scenario, instead, the collision radius is located at a lower distance from the central engine where the jet is still optically thick to gamma-rays, respectively at

$$R_{PH} = \frac{L_{iso} \sigma_T}{8\pi m_p c^3} \Gamma^{-3} \sim 10^{11} \left( \frac{L_{iso}}{10^{52} \text{ erg/s}} \right) \left( \frac{\Gamma}{10^{2.5}} \right)^{-3} \text{ cm} \quad (2.3)$$

where  $L_{iso}$  is the isotropic luminosity of the burst,  $\sigma_T$  is the Thomson cross section and  $m_p$  is the proton mass. The radius of emission strongly affects both the energy range and the normalization of the neutrino expected fluence: the IS scenario predicts neutrinos mainly above 100 TeV, while the PH scenario introduces a low-energy component below 10 TeV.

Neutrino spectra are computed individually for each GRB: in the IS case, the numerical code *NeuCosmA* [7] provides spectra for individual neutrino flavors, while in the PH case the analytical description from [8] was adopted.

### 3. Analysis methods

The event selection proceeds through the application of an angular cut, a temporal cut and a cut on the quality of the track reconstruction. The first two cuts are applied in order to get a coincidence with the detected gamma-ray emission: a cone of aperture  $\alpha = 10^\circ$  is defined around the burst position, as identified by a given satellite. Although the ANTARES angular resolution for muon events is about  $0.4^\circ$  at  $E_\nu = 10$  TeV, the size of the angular window is enlarged in order to account for the satellite uncertainty on the burst position, which might reach value of the order of several degrees (especially when Fermi GBM is providing the burst coordinates); however, given the transient nature of the sources, such a large window is not prohibitive in terms of background. The temporal window is selected as the burst T90, which is the time during which 90% of the total fluence is detected, plus a symmetric extension of width 30%T90 which accounts for both the satellite timing uncertainty and the unknown delay between the gamma-ray and the neutrino emission inside the prompt phase of the GRB, plus a symmetric extension of  $\pm 2$  s to account for the time of light propagation from the satellite to the ANTARES site and for ANTARES uncertainty in the data acquisition. Finally, the analysis is based on an unbinned method that relies on the evaluation of a test statistic  $Q$  in a pseudo-experiment procedure defined as:

$$Q = \max_{\mu'_s \in [0; n_{tot}]} \left( \sum_{i=1}^{n_{tot}} \log \frac{\mu'_s S(\alpha_i) + \mu_b B(\alpha_i)}{\mu_b B(\alpha_i)} - \mu'_s \right) \quad (3.1)$$

where  $n_{tot}$  is the number of simulated events in each measurements at an angular distance  $\alpha_i$  from the source position, both for the background only hypothesis and for the signal plus background one. The test statistic is an extended maximum likelihood ratio, defined from the signal probability density function  $S(\alpha)$  and the background probability density function  $B(\alpha)$ . The signal angular



distribution is obtained through Monte Carlo simulations, realized specifically for each GRB, accurately describing the ANTARES conditions at the time of the GRB trigger, while the background distribution is assumed flat in the solid angle considered in the search. The number of expected background event  $\mu_b$  in the temporal and angular window of the search is evaluated from off-time data, while the expected number of signal events  $\mu'_s$  is obtained in the likelihood maximization. Pseudo-experiments are performed at different quality cuts: the final reconstruction quality cut is selected as the one that maximizes the individual Model Discovery Potential (MDP) of each GRB, defined as the probability of the signal hypothesis at a given significance level  $\sigma$ .

#### 4. Individual search: bright GRBs

A search for neutrinos from bright GRBs is performed, as extensively treated in [9]: four sources have been selected with gamma-ray fluence greater than  $10^{-4}$  erg/cm<sup>2</sup> in the time period from 2008 to 2013. The selection yielded GRB080916C, GRB110918A, GRB130427A and GRB130505A. Both the IS and the PH scenarios are investigated for neutrino emissions: in this analysis, a standard value for the bulk Lorentz factor is assumed  $\Gamma = 316$  for each GRB as well as a baryon loading equal to  $f_p = 10$ . In order to increase the sensitivity to the low-energies predicted by the PH model, a special data sample is used in this case: it includes unfiltered data stored during the GRB alert, received through GCN notices [10], as well as unfiltered data buffered before the alert message reception. The overall size of the unfiltered data stored amounts to about 2 minutes, in such a way that they cover the majority of the burst duration. The IS analysis is instead performed through the standard filtered data set. Given the optimization technique described in Sec. 3, the cuts yielding the maximum  $3\sigma$  MDP were applied to unblinded data: no neutrinos were detected in the defined temporal and spatial windows of the search. The absence of signal allows to derive 90% C.L. upper limits to the neutrino fluence, shown individually for each GRB in Fig. 1(a) for the IS model and in Fig. 1(b) for the PH one, in the energy range where 90% of the signal is expected.

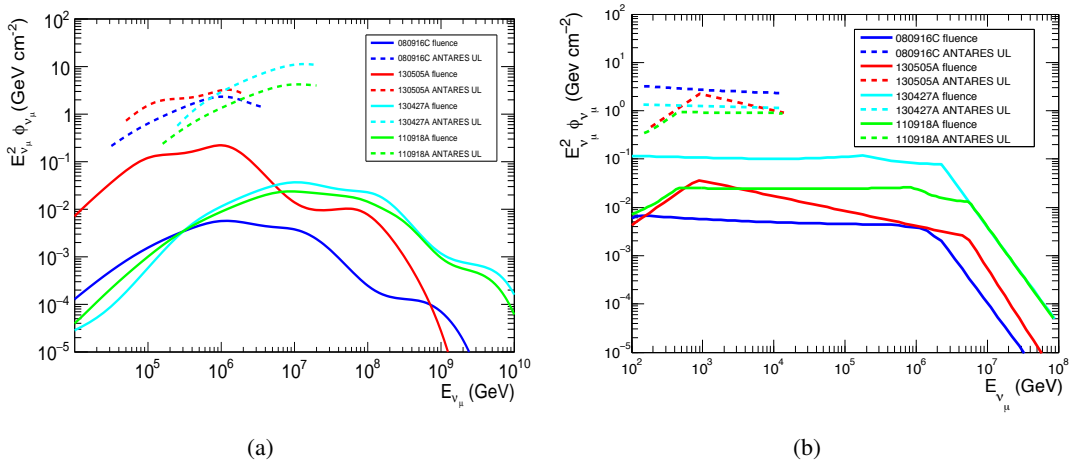


**Figure 1:** Expected  $\nu_\mu + \bar{\nu}_\mu$  fluences (solid lines) and ANTARES 90% C.L. upper limits (dashed lines) on the selected GRBs, in the energy band where 90% of the signal is expected to be detected, for the IS (a) and the PH (b) models.

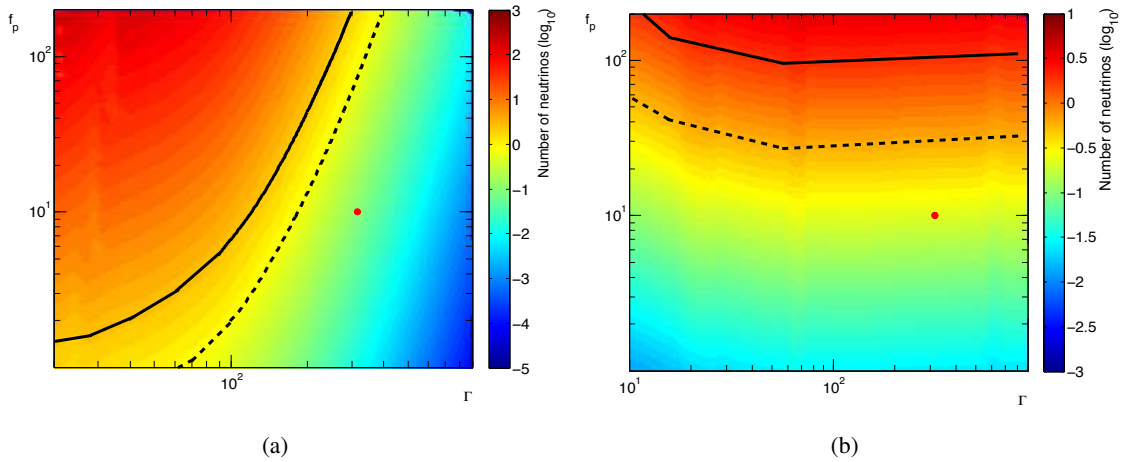


**Figure 2:** Constraints on the  $\Gamma - f_p$  plane. The solid (dashed) black line corresponds to the exclusion limits at 90 (50)% C.L. The red dot shows the benchmark values  $f_p = 10$  and  $\Gamma = 316$ . (a) IS constraints on GRB130505A. (b) PH constraints on GRB130427A.

#### 4.1 GRB model constraints

Given the null results discussed above in the search of neutrinos in angular and temporal coincidence with the gamma-ray emission detected from the bright GRBs, it is possible to derive constraints on the jet parameters affecting neutrino emissions,  $\Gamma$  and  $f_p$  for instance. The most stringent 90% C.L. limit on the IS model is derived for GRB130505A and it is shown in Fig. 2(a), while the PH model is best constrained in the case of GRB130427A, as shown in Fig. 2(b). Low Lorentz factor and high baryonic loading are generally excluded, but still most of the parameter space is available. A different procedure will be adopted in the following stacking analysis: in order to leave the baryonic content as the main free parameter of the model, the bulk Lorentz factor of each burst is inferred through its correlation with the isotropic luminosity.

#### 5. Quasi-diffuse search: the stacking method

The full sample of long GRBs ( $T_{90} \geq 2$  s) observable with ANTARES in the years 2008-2016 was considered: a source selection is performed starting from the Swift and Fermi catalogs, completed through information available on the GCN. GRBs below the ANTARES horizon at the trigger time and with the detector in stable data-taking conditions are considered. Moreover, a stringent selection on the burst spectrum was applied, since a large extrapolation is needed to move from gamma-rays to the expected neutrinos: therefore, GRBs whose gamma-ray spectrum is fitted as a simple power law are excluded. This procedure resulted in 462 GRBs, whose position in the equatorial sky is shown in Fig. 3, where also the detected gamma-ray fluence is shown.

The internal shock scenario is here assumed as signal model. Moreover, a linear correlation among the burst isotropic luminosity and the bulk Lorentz factor is assumed, as derived in [11]: such a correlation reads as

$$\Gamma = 249 \left( \frac{L_{iso}}{10^{52} \text{ erg/s}} \right)^{0.30} \quad (5.1)$$

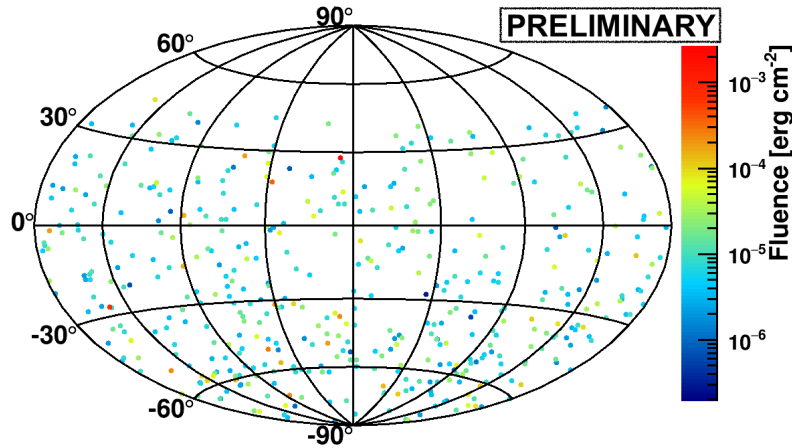


**Figure 3:** Sky map of the GRBs selected for the stacking analysis, in equatorial coordinates: the color code represents the measured gamma-ray fluence.

However, since the isotropic luminosity depends on the redshift and since most of the GRBs in the sample miss this information, we start assigning each burst a redshift by uniformly sampling a distribution of redshifts, as collected by the Swift satellite from long GRBs detected between 2005 and 2017, with the constraint that the resulting  $L_{iso}$  is among  $10^{49}$  and  $10^{53}$  erg/s. Then  $\Gamma$  is inferred through Eq. 5.1: an uncertainty of 50% should be considered in the estimation of the Lorentz factor. The expected neutrino spectrum computed through *NeuCosMA*, assuming a baryon fraction  $f_p = 10$  and the  $L_{iso}$ - $\Gamma$  correlation presented in Eq. 5.1, is shown in Fig.4(a), where the single contributions from each GRB are also shown. With this expected signal, the method described in Sec. 3 is then applied, complemented by the introduction of a statistical penalty factor that accounts for the increased size of the sample: indeed, in the stacking technique, the summed contribution from all sources is considered in the test statistic evaluation, yielding a diffuse flux of events. Given the per burst individual  $MDP_i$ , which is the maximum MDP obtainable among different track quality cuts for a single GRB at a given trial factor, the total MDP obtained when including in the search  $N_{GRBs}$  is defined as

$$MDP(N_{GRBs}) = 1 - \prod_{i=1}^{N_{GRBs}} (1 - MDP_i) \quad (5.2)$$

The total MDP as a function of the number of GRBs included in the search is given in Fig. 4(b).

### 5.1 GRB population constraints

The analysis shows that at a  $3\sigma$  significance level the MDP reaches its maximum value of 11.5% for 254 stacked sources. However, when including all the GRBs of the sample, the MDP decreases only to 11.1%: given the moderate MDP reduction, it is preferable to consider the whole sample of 462 GRBs in the search for a neutrino signal. This results in a total livetime of the analysis equal to 11.2 hours. After the unblinding of data at the optimal cuts, no event is found in angular and temporal coincidence with the prompt gamma-ray emission of any of the GRBs. The 90% C.L. upper limit on the neutrino fluence  $E^2 F_\nu(E)$  stands a factor 18 above the expectations, as

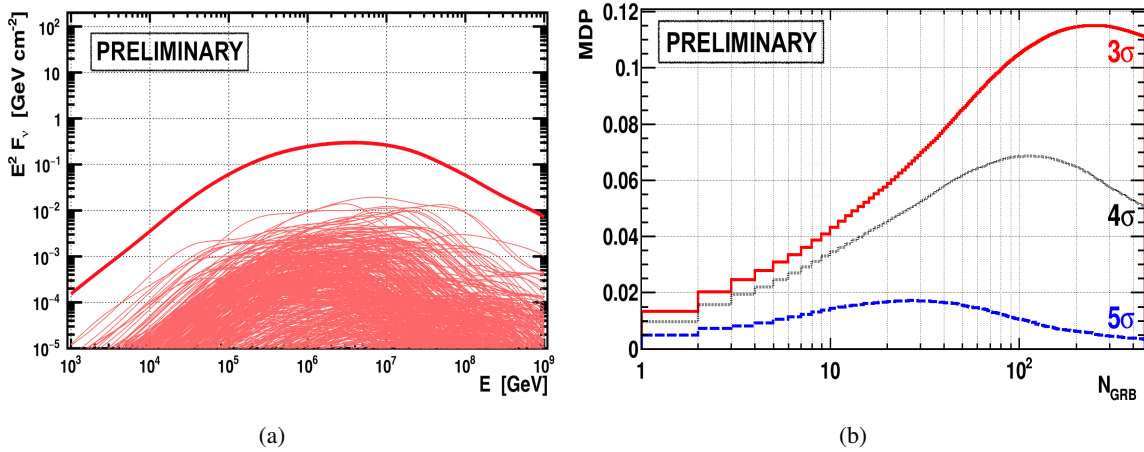


**Figure 4:** (a) Expected  $\nu_\mu + \bar{\nu}_\mu$  fluences from the 462 GRBs of the stacking analysis (thin lines) and summed contribution (thick line), according to the IS modeling of the *NeuCosmA* code. (b) MDP of the stacking analysis as a function of the number of sources included.

shown in Fig. 5: the fluence interval where 90% of the signal is expected ranges between 0.45 and 5.2 GeV/cm<sup>2</sup> in the energy range from  $5 \times 10^4$  to  $8 \times 10^6$  GeV. The fluence limit can be translated into a limit on the quasi-diffuse flux from the GRB population: considering  $N_{GRBs}$  over an average number of 667 long GRBs detected per year, the diffuse flux is

$$E^2 \phi_\nu(E) = \sum E^2 F_\nu(E) \frac{1}{4\pi} \frac{667 \text{ yr}^{-1}}{N_{GRBs}} \quad (5.3)$$

The 90% C.L. on the diffuse flux ranges between  $1.6 \times 10^{-9}$  and  $1.9 \times 10^{-8}$  GeV cm<sup>-2</sup> s<sup>-1</sup> sr<sup>-1</sup>. Moreover, these results directly translate into constraints on the baryonic content of the jets, given that neutrino fluence linearly scales with  $f_p$ : the limit equals to  $f_p \leq 180$  at 90% C.L. and to  $f_p \leq 89$  at 68% C.L. in GRB jets.

The Lorentz factor of the jet is one of the most critical microphysics parameters of the jet for the neutrino spectrum. Propagating the uncertainties in the relation  $L_{iso} - \Gamma$  affects significantly the shape of the neutrino spectrum: reducing the  $\Gamma$  factor, increase the flux of neutrinos at low energies (1 – 100 TeV) and vice versa. A 50% increase in the  $L_{iso} - \Gamma$  relation worsen the limit by a factor 124, while a 50% decrease starts to be constrained by the ANTARES limits. As a result, limits on the baryonic content are also strongly affected: in the optimistic scenario (decrease), the limit on  $f_p$  reaches 10 at 90% C.L., which is a quite restrictive value for scenarios of CR proton acceleration in GRB jets. On the other hand, the limit soften to  $f_p \leq 1240$  (90% C.L.) in case the correlation is increased.

## 6. Conclusions

Through the technique defined in Sec. 3, nine years on ANTARES data were considered for a search of muon neutrinos in time and space coincidence with the prompt emission of 462 GRBs. Both an individual search from bright GRBs and a population study were performed, through an optimization technique based on the maximization of the Model Discovery Potential. However,

no events passed the selection criteria, yielding 90% C.L. upper limits on the expected neutrino fluence and constraints on the parameters affecting the physical emission mechanism of GRBs. Limits and constraints are consistent with previous searches in ANTARES [2, 9] and IceCube [3].

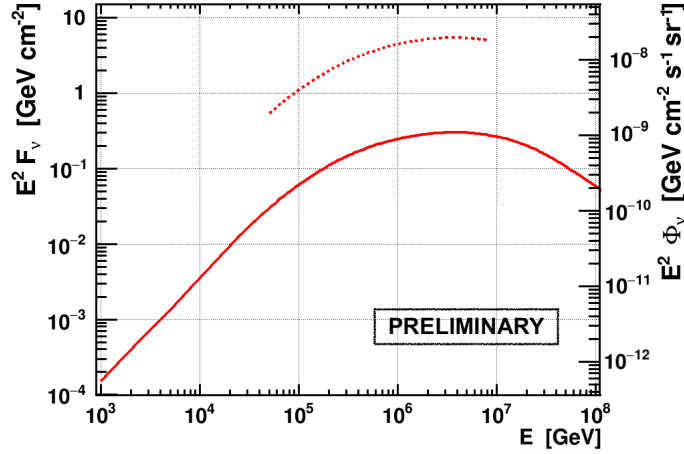


**Figure 5:** Expected  $\nu_\mu + \bar{\nu}_\mu$  fluence (left axis) and diffuse flux (right axis) from the 462 GRBs of the stacking analysis (red solid line) and ANTARES 90% C.L. upper limits (dashed line), in the energy band where 90% of the signal is expected to be detected.

## References

- [1] M. G. Aartsen et al., *Evidence for High-Energy Extraterrestrial Neutrinos at the IceCube Detector*, *Science* **342** (2013) [arXiv:1311.5238]
- [2] S. Adrian-Martinez et al., *Search for muon neutrinos from gamma-ray bursts with the ANTARES neutrino telescope using 2008 to 2011 data*, *Astron. Astrophys.* **559** (2013) [arXiv:1307.0304]
- [3] M. G. Aartsen et al., *Extending the search for muon neutrinos coincident with gamma-ray bursts in IceCube data* [arXiv:1702.06868]
- [4] M. Ageron et al., *ANTARES: the first undersea neutrino telescope*, *Nucl. Instrum. Meth. A* **656** (2011) 11-38 [arXiv:1104.1607]
- [5] T. Piran, *Gamma-ray bursts and the fireball model*, *Phys. Rept.* **314** (1999) 575-667 [arXiv:9810256]
- [6] M. Bustamante, P. Baerwald, K. Murase and W. Winter, *Neutrino and cosmic-ray emission from multiple internal shocks in gamma-ray bursts*, *Nat. Com.* **6** (2015) 6783 [arXiv:1409.2874]
- [7] S. Hummer, P. Baerwald and W. Winter, *Neutrino Emission from Gamma-Ray Burst Fireballs, Revised*, *Phys. Rev. Lett.* **108** (2012) [arXiv:1112.1076]
- [8] B. Zhang and P. Kumar, *Model-dependent high-energy neutrino flux from Gamma-Ray Bursts*, *Phys. Rev. Lett.* **110** (2013) 12 [arXiv:1210.0647]
- [9] A. Albert et al., *Search for high-energy neutrinos from bright GRBs with ANTARES*, *Mon. Not. Roy. Astron. Soc.* **469** (2017) 906 [arXiv:1612.08589]
- [10] [https://gcn.gsfc.nasa.gov/gcn3\\_archive.html](https://gcn.gsfc.nasa.gov/gcn3_archive.html)
- [11] J. Lu, Y. C. Zou, W. H. Lei, B. Zhang, Q. Wu, D. X. Wang, E. W. Liang and H. J. Lu, *Lorentz factor isotropic luminosity/energy correlations of gamma-ray bursts and their interpretation*, *The Astrophysical Journal* **751** (2012) 49 [arXiv:1109.3757]

## Search for neutrinos from Fast Radio Bursts with ANTARES

---

### Damien Turpin

*Université de Toulouse; UPS-OMP; IRAP; Toulouse, France*  
*CNRS; IRAP; 14, avenue Edouard Belin, F-31400 Toulouse, France*  
*E-mail: [damien.turpin@irap.omp.eu](mailto:damien.turpin@irap.omp.eu)*

### Damien Dornic

*CPPM, Aix-Marseille Université, CNRS/IN2P3, 13009 Marseille, France*  
*E-mail: [dornic@cppm.in2p3.fr](mailto:dornic@cppm.in2p3.fr)*

### Alexis Coleiro

*APC, Univ Paris Diderot, CNRS/IN2P3, CEA/Irfu, Obs de Paris, Sorbonne Paris Cité, France*  
*IFIC - Instituto de Física Corpuscular (CSIC - Universitat de València) c/ Catedrático José Beltrán, 2 E-46980 Paterna, Valencia, Spain*  
*E-mail: [alexis.coleiro@ific.uv.es](mailto:alexis.coleiro@ific.uv.es)*

### Matteo Sanguinetti\*

*Università degli Studi di Genova, INFN Genova*  
*E-mail: [matteo.sanguinetti@ge.infn.it](mailto:matteo.sanguinetti@ge.infn.it)*

### on the behalf of the ANTARES collaboration and the SUPERB collaboration

Fast Radio Bursts are one of the most mysterious transient sources. They are characterised by an intense radio-pulse lasting few milliseconds and mainly detected in the GHz energy band. Many unknowns remain concerning the nature of the transient progenitor, the nature of the radio emission and their distribution in the Universe. Recently, the first evidence on the association between the repeating burst FRB121102 and a star-forming dwarf galaxy located at the cosmological distance  $z = 0.19$  was reported. These observations imply that at least some of the fast radio bursts indeed originate from the distant Universe and have to be associated with extremely violent events to explain their observed brightness. So far, the radiative processes powering the radio emission are unknown but efficient particle acceleration may occur in the vicinity of the progenitor. A multi-wavelength and a multi-messenger approach are therefore crucial to identify the nature of these acceleration mechanisms. In this context, a search for a high-energy neutrino signal from the most recent radio bursts has been performed with the ANTARES neutrino telescope. By design, ANTARES mainly observes the Southern sky ( $2\pi$  steradian at any time) and is perfectly suited to search for a neutrino signal from sources of transients that have been mainly detected at the Parkes observatory in Australia. In this contribution, we will present the results of our searches with ANTARES and their implications for hadronic models of FRBs.

*35th International Cosmic Ray Conference — ICRC2017*  
*10–20 July, 2017*  
*Bexco, Busan, Korea*

---

\*Speaker.



## 1. Introduction

Energetic transient sources are promising candidates for a high-energy neutrino (TeV-PeV) detection as they would originate from explosive processes that release a huge amount of energy in a short timescale and heat the surrounding environment in violent shocks. In the shock fronts, the acceleration of hadrons could be efficient enough to explain the origin of the most energetic cosmic rays and the cosmological high-energy neutrinos discovered few years ago by the IceCube Collaboration [1]. In addition, the shorter the transient duration is the more significant will be the detection since typically the searches for a neutrino signal from a transient event below the minute timescale can be almost considered as background free and hence, the detection of a single neutrino event might be enough to claim a significant association with the transient source. The Gamma-ray Bursts (GRB) are one of the best example of such promising target for point like-source neutrino searches but without any success so far [2, 3, 4].

A decade ago, the Fast Radio Bursts (FRB) have been serendipitously discovered in the radio domain [5] and, up to now, constitute one of the most intriguing fast transient sources. They are characterised by a very bright radio-pulse (few Jy·s) lasting only few milliseconds and even less than a millisecond which make them the brightest radio source in the sky during their short lifetime. The measure of the uncommonly large delay between the high and the low radio frequencies, due to the dispersion of the radio signal by the column of the cold plasma crossed by the radio wave, points out toward an extragalactic and even a cosmological origin for these transients. This has been only confirmed for FRB121102 [6, 7, 8] and from the dispersion measures (DM) the cosmological distance distribution of FRBs is found in the range of redshift:  $z_{DM} = [0.19-1.4]$  according to the public FRB catalogue<sup>1</sup>. To explain both the short timescale and the large energy budget of the FRBs they may be associated to extremely energetic events possibly to cataclysmic phenomena such as NS-NS merger [9, 10], short Gamma-ray Bursts (SGRB) [11, 12], the collapse of supramassive neutron star (SMNS) [13, 14] or maybe to giant flaring activities from highly magnetised neutron stars [15]. In the close environment of these extreme objects, hadronic acceleration processes may occur and would also lead to the production of TeV-PeV neutrinos mainly through photo-hadronic interactions between the ambient energetic photon field (typically x-ray/gamma-ray photons) produced by different radiative processes and the accelerated protons at a minimum energy  $E_p \gg \text{GeV}$ . Because of their remarkable transient properties similar to the Gamma-ray Bursts, if FRBs are indeed cosmic accelerators of hadrons, they offer a great opportunity for an unambiguous detection of cosmic neutrinos by the large neutrino telescopes.

The progenitors of the FRBs are still unidentified mainly because they have been only detected in the radio domain despite active searches at different wavelength [16, 17, 18]. Note that the observation of a  $\gamma$ -ray transient source associated to FRB131104 with the Swift satellite but under quite low significance ( $3.2\sigma$ ) was reported by [19]. In such observational context, the multi-messenger observations with the high-energy neutrino telescopes can help to solve the “FRB mystery“ and offer an unique way to address the following question : could the FRB progenitor be efficient cosmic accelerator of hadrons ? As a consequence, a search for a high-energy neutrino signal from the

<sup>1</sup>see<http://www.astronomy.swin.edu.au/pulsar/frbcat/>



most recent FRBs has been performed with the ANTARES neutrino telescope [20]. The results are presented in this contribution.

## 2. The FRB sample

During the period 2013-2017, 12 FRBs have been detected by Australian radio facilities in different narrow bands such as the Parkes ( $\nu_{obs} \sim [1.2 - 1.5]$  GHz), the ASKAP ( $\nu_{obs} \sim [0.7 - 1.8]$  GHz) and the UTMOST ( $\nu_{obs} \sim [0.83 - 0.85]$  GHz) telescopes. Among them, 9 FRBs were visible by ANTARES at the trigger time and the detector was taking data in good conditions. Below we describe the characteristics of these 9 FRBs.

**Table 1:** Properties of the 9 FRBs visible by ANTARES in the period 2013-2017

FRB	$z_{DM}$	date (UTC)	RA ( $^{\circ}$ )	dec ( $^{\circ}$ )	radio trigger
131104	0.59	2013-11-04 18:03:59	101.04	-51.28	Parkes
140514	0.44	2014-05-14 17:14:09	338.52	-12.31	Parkes
150215	0.55	2015-02-15 20:41:41	274.36	-4.90	Parkes
150418	0.49	2015-04-18 04:29:04	109.15	-19.01	Parkes
150807	0.59	2015-08-07 17:53:55	340.10	-55.27	Parkes
160317	0.70	2016-03-17 08:30:58	118.45	-29.61	UTMOST
160410	0.18	2016-04-10 08:16:54	130.35	6.08	UTMOST
160608	0.37	2016-06-08 03:52:24	114.17	-40.78	UTMOST
170107	0.48	2017-01-07 20:05:45	170.79	-5.02	ASKAP

## 3. Searching method

The analysis focused on the data collected during the acquisition period  $[T_0 - 6h; T_0 + 6h]$  where  $T_0$  is the trigger time of the considered FRB. The search for a significant neutrino flux is based on the detection of up-going muon-track events spatially and temporally coincident with the radio burst emission. For each FRB, a search cone of  $2^{\circ}$ , corresponding to the ANTARES point spread function at  $3\sigma$ , is set around the FRB position (for which the error on the position is negligible wrt to the ANTARES PSF). To remove a significant contamination of mis-reconstructed muon background events in the neutrino sample, selection cuts are applied event by event on quality variables of the track reconstruction algorithm: the local zenith angle,  $\theta$ , the error estimate of the reconstructed direction  $\beta$  and the quality parameter of the reconstruction algorithm,  $\Lambda$ . We require that each selected up-going event ( $\cos\theta > 0$ ) has a direction error  $\beta < 1^{\circ}$ . The selection criterion on  $\Lambda$  has been optimised FRB per FRB to give a potential discovery of  $3\sigma$  for one neutrino event in a searching time window of  $\Delta T = [T_0 - 6h; T_0 + 6h]$ . This relatively large time window allows us to cover different scenarios for the delay between the radio and the possible neutrino emission with a high potential of discovery.

Before applying the searching method to the sample of FRBs, the detector stability has been

checked by looking at the total event rates detected in time slices of 2 hrs within  $\Delta T_{\text{back}} = [T_0 - 6\text{h}; T_0 + 6\text{h}]$ . No significant variability was found in the event rates which guarantees the stability of the detector.

We finally found no up-going events temporally and spatially correlated with the 9 selected FRBs. Then, the number of atmospheric background events,  $\mu_b$ , has been directly estimated from the data using the  $\Delta T_{\text{back}}$  time window. The expected number of background events in a ROI of  $2^\circ$  is found to be  $\mu_B \sim 5 \cdot 10^{-8} \text{ event} \cdot \text{s}^{-1}$  which corresponds to a Poisson probability of observing zero event knowing the background noise,  $\mu_b$ ,  $P \geq 99\%$ . Hence, the null result is compatible with the neutrino background expectation.

#### 4. Constraints on the neutrino emission from FRBs

As no significant neutrino signal has been detected from the selected FRBs by ANTARES, we can set upper limits on the neutrino fluence,  $F_\nu$ , that would yield to a detection at 90% C.L. First of all, the observable quantity that can be constrained with ANTARES data is the expected number of neutrinos,  $N_\nu$ , that directly depends on the acceptance of the detector,  $\text{Acc}(\delta)$  and the neutrino flux. As the neutrino emission time is unknown, the instantaneous ANTARES acceptance was estimated at the FRB trigger times and is valid for all time in the search window. Then,  $N_\nu$  mainly depends on the declination coordinate ( $\delta$ ) of the source and its spectral model,  $\frac{dN}{dE_\nu} = \phi E_\nu^{-p}$ . In this analysis, two source models have been tested, a soft one with a spectral index  $p = 2$  and a hard spectrum model with  $p = 1$ . According to the Poisson statistics, a neutrino signal of  $N_\nu = 2.3$  events gives a 90% C.L upper limit on the flux normalisation factor given by  $\phi_{90\%} = N_\nu / \text{Acc}(\delta)$ . Then, the corresponding 90% C.L. neutrino fluence upper limit,  $F_{\nu,90\%}$ , can be expressed as:

$$F_{\nu,90\%} = \int_{E_{\min}}^{E_{\max}} \frac{dN}{dE_\nu} \cdot E_\nu \cdot dE_\nu \quad \text{in erg} \cdot \text{cm}^{-2} \quad (4.1)$$

where  $E_{\min}$  and  $E_{\max}$  are the energies that define the 5-95% range of the energy distribution of events passing the applied quality criteria ( $\cos\theta > 0$  and  $\Lambda_{\text{cut},3\sigma} + \beta < 1^\circ$ ) for the corresponding spectrum.

To compute such upper limits we used Monte-Carlo simulations to reproduce the data taking conditions of the detector at each FRB trigger time. A sample of neutrino MC events is therefore modeled and the event times have been set at the FRB trigger time (instantaneous limits). The equatorial coordinates of each event (RA, Dec) are computed from the simulated local coordinates and the event times. Then, each event of energy,  $E_\nu$ , passing the cuts ( $\beta < 1^\circ$  and  $\Lambda > \Lambda_{\text{cut},3\sigma}$ ) contributes to the neutrino flux with a weight given by the instantaneous ANTARES acceptance.

The results on the neutrino fluence upper limits,  $F_{\nu,90\%}$ , for the two considered neutrino spectra are given in table 2.

The fluence upper limits can be converted into a constraint on the isotropic total energy released in neutrinos in the rest frame according to the equation 4.2:

$$E_{\nu,90\%}^{\text{iso}} = 4\pi D(z)^2 \times F_{\nu,90\%} / (1+z) \quad (4.2)$$

**Table 2:** Upper limit on the neutrino fluence,  $F_{V,90\%}$  (given in unit of  $\text{erg} \cdot \text{cm}^{-2}(\text{GeV} \cdot \text{cm}^{-2})$ ), estimated for the 9 selected FRBs according to the instantaneous ANTARES sensitivity. The limits are given where 90% of the neutrino signal is expected between  $[E_{\min} - E_{\max}]$  given in  $\log_{10}[\text{GeV}]$ .

FRB	$E^{-2}$		$E^{-1}$		$\Lambda$ cut
	$F_{V,90\%}$	$[E_{\min} - E_{\max}]$	$F_{V,90\%}$	$[E_{\min} - E_{\max}]$	
131104	$1.4 \cdot 10^{-2}(8.8)$	[3.4-6.8]	$20.7 \cdot 10^{-1}(1294)$	[5.8-7.9]	-5.52
140514	$2.3 \cdot 10^{-2}(14.4)$	[3.6-6.9]	$45.0 \cdot 10^{-1}(2805)$	[5.8-7.9]	-5.50
150215	$2.8 \cdot 10^{-2}(17.7)$	[3.1-6.5]	$41.4 \cdot 10^{-1}(2583)$	[5.8-7.9]	-5.56
150418	$2.1 \cdot 10^{-2}(13.2)$	[3.5-6.9]	$24.1 \cdot 10^{-1}(1502)$	[5.8-8.0]	-5.52
150807	$1.9 \cdot 10^{-2}(12.2)$	[3.6-6.9]	$5.4 \cdot 10^{-1}(339)$	[5.8-8.0]	-5.60
160317	$2.1 \cdot 10^{-2}(12.8)$	[3.5-6.9]	$42.6 \cdot 10^{-1}(2659)$	[5.8-7.9]	-5.58
160410	$1.9 \cdot 10^{-2}(11.8)$	[3.6-6.9]	$7.1 \cdot 10^{-1}(444)$	[5.8-7.9]	-5.56
160608	$2.6 \cdot 10^{-2}(16.3)$	[3.6-7.0]	$24.3 \cdot 10^{-1}(1516)$	[5.8-7.9]	-5.68
170107	$1.4 \cdot 10^{-2}(8.8)$	[3.5-6.9]	$4.3 \cdot 10^{-1}(267)$	[5.7-7.9]	-5.58

where  $z$  is the redshift of the source. The distance of the neutrino source,  $D(z)$ , is computed as follows :

$$D(z) = \frac{c}{H_0} \int_0^z \frac{(1+z')dz'}{\sqrt{\Omega_m(1+z')^3 + \Omega_\Lambda}} \quad (4.3)$$

where  $\Omega_m = 0.308$  and  $\Omega_\Lambda = 0.692$ ,  $H_0 = 67.80 \text{ km} \cdot \text{s}^{-1} \cdot \text{Mpc}^{-1}$  following [21] and  $c$  is the light speed. As the distance of each FRB is poorly constrained, we test different kind of scenarios : a galactic origin ( $D \in [1-50]$  kpc), an extragalactic origin ( $D \in [0.05-100]$  Mpc) and a cosmological origin ( $z \in [0.02-z_{DM}]$ ). The 90 % upper limits on  $E_{V,90\%}^{\text{iso}}$  for the two neutrino spectra,  $E^{-2}$  and  $E^{-1}$ , are shown in the figures 1 and 2.

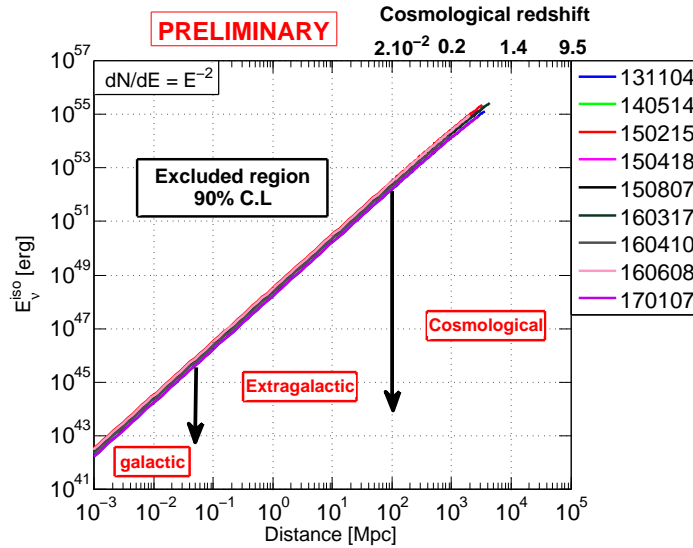


**Figure 1:** Upper limits on the neutrino energy released by the 9 selected FRBs as function of their plausible distances assuming a  $E^{-2}$  spectrum.

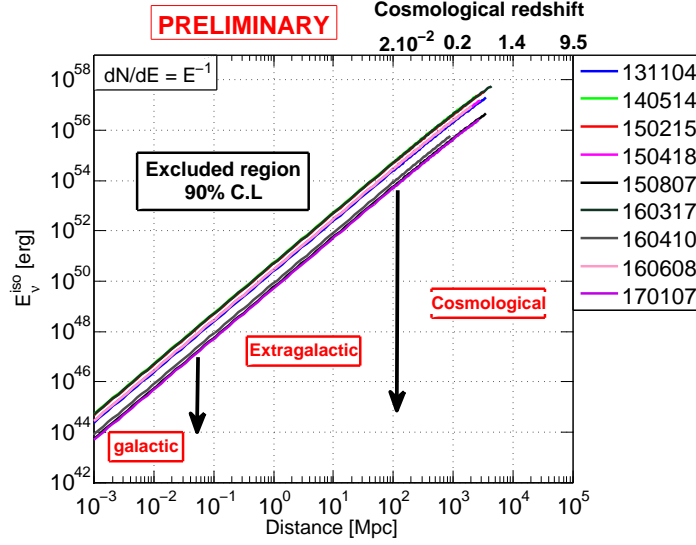


**Figure 2:** Same as the figure 1 assuming a  $E^{-1}$  spectrum.

If these FRBs are neutrino emitters, ANTARES puts interesting constraints on their plausible origin. Indeed, at distances  $d \lesssim 50$  Mpc, the ANTARES constraints, for a  $E^{-2}$  source model, are at the level of  $E_{v,90\%}^{\text{iso}} \lesssim 10^{52}$  erg. In the case of a  $E^{-1}$  spectrum, the energy is mainly deposited in the PeV domain where the ANTARES sensitivity is largely degraded by the Earth absorption. Thus, the limits on  $E_{v,90\%}^{\text{iso}}$  are lowered by an order of magnitude. In any spectral case, the cosmological scenario is poorly constrained by ANTARES.

## 5. Conclusion

In this contribution, the first search into the ANTARES data for a high-energy neutrino signal from a population of Fast Radio Bursts detected these last four years has been reported. No neutrino events were spatially found in correlation with the nine selected FRBs in a time window extended up to six hours before and after the radio bursts. These non detections allow us to derive 90% C.L. upper limits on the neutrino fluence at the FRB trigger times. As the neutrino production during a FRB event is largely unknown, the limits were derived assuming standard hard and soft power law neutrino spectra with spectral indexes  $p = 1$  and  $2$ , respectively. The limits are of the order of  $F_{v,90\%} \lesssim 10^{-1} - 10^{-2}$  erg  $\cdot$  cm $^{-2}$  for a  $E^{-1}$  and  $E^{-2}$  source model, respectively. Since the FRB distances are poorly constrained, the corresponding isotropic energies released in neutrinos were then computed under different distance hypothesis: a galactic, an extragalactic or a cosmological origin. The constraints on  $E_{v,90\%}^{\text{iso}}$  for different distances are given in the figures 1 and 2. First, it is clear that the ANTARES sensitivity is too low to significantly constrain any cosmological scenario for the FRB progenitors ( $E_{v,90\%}^{\text{iso}} \lesssim 10^{55} - 10^{54}$  erg for  $z \sim 0.1$  for a  $E^{-1}$  and  $E^{-2}$  source model, respectively). However, the galactic and very close extragalactic scenarios ( $D < 1-10$  Mpc) start to be interestingly restricted below  $E_{v,90\%}^{\text{iso}} \sim 10^{52}$  erg. To go further into the FRB neutrino model constraints, larger scale neutrino detectors (km $^3$ ) are needed to catch the neutrino signal from the potential FRB progenitors such as giant flares from magnetars or short GRBs. This

might be achievable in the next few years with the new generation of european neutrino telescopes KM3NeT/ARCA that will be 50 times more sensitive than ANTARES [22].

## References

- [1] The IceCube Collaboration, 2013, *Science*, 342
- [2] Abbasi, R., Abdou, Y., Abu-Zayyad, T., et al. 2012, *Nature*, 484, 351
- [3] Adrián-Martínez, S., Albert, A., Samarai, I. A., et al. 2013, *A&A*, 559, A9
- [4] Ackermann, M. and Adams, J. and Aguilar, J. A. and Ahlers, M., et al. 2016, ArXiv e-prints : arXiv1601.06484
- [5] Lorimer et al., 2007, *Science*, 318, 777
- [6] Tendulkar, S. P., Bassa, C. G., Cordes, J. M., et al. 2017, *ApJL*, 834, L7
- [7] Chatterjee, S., Law, C. J., Wharton, R. S., et al. 2017, *Nature*, 541, 58
- [8] Marcote, B., Paragi, Z., Hessels, J. W. T., et al. 2017, *ApJL*, 834, L8
- [9] Totani, T. 2013, *PASJ*, 65
- [10] Wang, J.-S., Yang, Y.-P., Wu, X.-F., Dai, Z.-G., & Wang, F.-Y. 2016, ArXiv e-prints : arXiv1603.02014
- [11] Zhang, B. 2014, *ApJL*, 780, L21
- [12] Palaniswamy, D., Wayth, R. B., Trott, C. M., et al. 2014, *ApJ*, 790, 63
- [13] Ravi, V. & Lasky, P. D. 2014, *MNRAS*, 441, 2433
- [14] Li, X., Zhou, B., He, H.-N., Fan, Y.-Z., & Wei, D.-M. 2014, *ApJ*, 797, 33
- [15] Popov, S. B. & Postnov, K. A. 2013, ArXiv e-prints : arXiv1307.4924
- [16] Petroff, E., Keane, E. F., Barr, E. D., et al., 2015, *MNRAS*, 451, 3933
- [17] H. E. S. S. Collaboration and Abdalla, H., Abramowski, A., Aharonian, F., et al., 2017, *A&A*, 597, A115
- [18] Petroff, E. and Burke-Spolaor, S. and Keane, et al., 2017, *MNRAS*, 469, 4465-4482
- [19] DeLaunay, J. J., Fox, D. B. and Murase, K. and Mészáros, P., et al., 2016, *ApJL*, 832, L1
- [20] Ageron, M., Aguilar, J. A., Al Samarai, I., et al. 2011, *Nuclear Instruments and Methods in Physics Research A*, 656, 11
- [21] Planck Collaboration, Ade, P. A. R., Aghanim, N., et al., 2016, *A&A*, 594, A13
- [22] Adrián-Martínez, S., Ageron, M., Aharonian, F., et al. 2016, ArXiv e-prints : arxiv1601.07459

# Search for a correlation between ANTARES high-energy neutrinos and ultra high-energy cosmic rays detected by the Pierre Auger Observatory and the Telescope Array

---

**Julien Aublin**

*Université Pierre et Marie Curie, 75005 Paris, France, and  
Laboratoire APC, CNRS/IN2P3.*

*E-mail: [aublin@lpnhe.in2p3.fr](mailto:aublin@lpnhe.in2p3.fr)*

**Antonio Capone**

*Università di Roma La Sapienza, I-00185 Roma, Italy and  
Istituto Nazionale di Fisica Nucleare, Sezione di Roma, Italy;*

*E-mail: [Antonio.Capone@roma1.infn.it](mailto:Antonio.Capone@roma1.infn.it)*

**Irene Di Palma\***

*Università di Roma La Sapienza, I-00185 Roma, Italy and  
Istituto Nazionale di Fisica Nucleare, Sezione di Roma, Italy;*

*E-mail: [Irene.DiPalma@roma1.infn.it](mailto:Irene.DiPalma@roma1.infn.it)*

**on behalf of the ANTARES Collaboration**

A search for angular correlations between high-energy neutrinos detected by ANTARES and the cosmic rays events measured by the Pierre Auger Observatory and the Telescope Array experiments is presented. An unbinned likelihood-ratio method is used, using both the angular information and an energy estimation of the reconstructed neutrinos. The search has been applied to the nine-years ANTARES all-flavour point-source sample, leading to a non significant correlation. A 90% upper limit on the flux emitted by the candidate neutrino sources associated to the cosmic ray population is reported:  $\Phi_{\text{tot}}^{\text{UL}} = 1.5 \cdot 10^{-7} \text{ GeV}^{-1} \text{ cm}^{-2} \text{ s}^{-1}$ .

*35th International Cosmic Ray Conference — ICRC2017  
10–20 July, 2017  
Bexco, Busan, Korea*

---

\*Speaker.

## 1. Introduction

The connection between ultra-high energy cosmic rays (UHECRs), with energies in the EeV range and high energy neutrinos in the TeV-PeV range can be investigated to understand whether the same astrophysical sources can produce both of them. The observation of such kind of correlation could provide clues to understand the origin of these cosmic messengers. Previous searches that have been performed report only hints of correlations but without the level of significance needed for a discovery [1].

In this search, we use the public data from the Pierre Auger Observatory (PAO) [2] and the Telescope Array (TA) [3] experiments. These two experiments measure UHECRs through the detection of extensive air showers produced in the Earth's atmosphere. They have collected 318 events in total with energies above 52 EeV.

## 2. ANTARES neutrino events and UHECR data

The ANTARES detector [4] is the largest underwater neutrino telescope in the Northern hemisphere. The ANTARES data-set analyzed here covers a period of time between January 29th, 2007 to December 31st, 2015, for a total of 2423.6 days of live-time. The sample is composed of 7629 track-like (mostly muon neutrinos) and 180 shower-like events (mostly induced by  $\nu_e$  charged current and by all flavor neutral current  $\nu$  interactions). The selection procedure of the data has been optimized for point source searches, and is described precisely in [5].

The Pierre Auger Observatory is located near the town of Malargüe in the Mendoza Province, Argentina, at 1400 m above sea level and covers an area of  $\sim 3000 \text{ km}^2$  which makes it the largest cosmic ray observatory ever constructed. The PAO is a hybrid detector, it consists of a Surface Detector (SD) array of 1600 water-Cherenkov particle detector stations overlooked by 24 air fluorescence telescopes. In addition, three high elevation fluorescence telescopes overlook a surface of  $23.5 \text{ km}^2$  where additional 61 water-Cherenkov particle detector stations are installed. The public data set used in the present work, taken from [6], consists of 231 cosmic-ray events with zenith angle  $\theta \leq 80^\circ$  and energy  $E_{\text{CR}} \geq 52 \text{ EeV}$  recorded by the SD from January 1st, 2004 up to March 31st, 2014.

The Telescope Array (TA), situated in Utah, USA, consists of 507 plastic scintillator detectors, each of  $3\text{m}^2$ , located on a  $1.2 \text{ km}$  square grid, covering an area of  $\sim 700 \text{ km}^2$  [3]. The detector has been fully operational since March 2008. For this analysis, we use the 87 events collected between May 11th, 2008 and May 4th, 2014.

It should be noted that the absolute energy scale of UHECRs may contain a systematic error which may be, in principle, different for the two experiments. According to the results of the specific investigations of the TA-Auger Energy Spectrum working group [7], the UHECR spectra measured by TA and Auger could be made coincident in the region around  $10^{19}\text{eV}$  (the ankle region) by down-shifting the TA energies by  $\sim 13\%$  or equivalently by up-shifting the Auger energies. A down-shift of the TA energies by  $13\%$  has been chosen for this analysis.



### 3. Description of the analysis

#### 3.1 Magnetic deflection of UHECRs

Cosmic rays, unlike neutrinos, are deflected by magnetic fields (galactic and extra-galactic) during their propagation, the magnitude of the deflection being inversely proportional to their magnetic rigidity  $R = pc/Ze \simeq E/Ze$ . Unfortunately, the chemical composition of UHECRs is not yet reliably measured at the highest energies in consideration here [8][9], essentially due to lack of statistic available in the fluorescence data that has a smaller duty cycle than surface arrays. This situation could change in the next few years when the upgrade of the Pierre Auger Observatory (AugerPrime) [10] will be fully operational.

The cosmic magnetic fields that deflects cosmic rays are separated into a galactic and an extra-galactic contribution, both being poorly known. The galactic field has a magnitude of the order of  $\mu G$ , containing both a coherent component following the spiral structure of the gas and stellar population, and a turbulent component.

Extragalactic magnetic fields, which are even less known, should provide a sub-dominant contribution for nearby CR sources (closer than several hundreds of Mpc), upper limits on the average field being of the order of  $1nG$  [11]. Among the recent models of the galactic magnetic field [12] [13], the average deflections predicted are comparable in magnitude, but show very different patterns on the sky, making reliable predictions difficult.

In the following analysis, we use the median deflection angle that is predicted by those models for protons, assuming only a gaussian deflection around the position of the observed UHECRs. Hence for each UHECR we parametrize the individual magnetic deflection as:

$$\sigma_B(E_j^{CR}) = 3^\circ \times \frac{100}{E_j^{CR}(EeV)}. \quad (3.1)$$

#### 3.2 Statistical method

The method uses an unbinned maximum-likelihood approach, where the cosmic rays are considered as tracers of candidate neutrino sources. The search compares the null hypothesis  $H_0$ : the neutrinos detected by ANTARES come from atmospheric background, with an alternative hypothesis  $H_1$ : a fraction of the detected neutrinos are emitted with a common spectral index  $\gamma$  from astrophysical point sources located around the position of UHECRs in the sky.

We assume that there is an underlying neutrino source associated to each cosmic ray, injecting the same flux  $\Phi = \Phi_0 (E/1 \text{ GeV})^{-\gamma}$ , where the normalization  $\Phi_0$  is expressed as a flux per flavor (accounting for both  $\nu$  and  $\bar{\nu}$ 's), in units of  $\text{GeV}^{-1} \text{cm}^{-2} \text{s}^{-1}$ . However, as we test the correlation between  $\nu$ 's and the stacking of  $N_{\text{CR}}$  cosmic ray positions, the relevant quantity in the following analysis will be the total flux injected  $\Phi_{\text{tot}} = N_{\text{CR}} \Phi$ .

The conversion from the flux  $\Phi$  injected by a point source at a given declination and the corresponding number of signal events  $n_s$  detected is given by the acceptance of the ANTARES detector.

The acceptance is computed in bins of declination and spectral indexes, using Monte-Carlo simulations where the same set of cuts than for data are applied. For example, in this analysis, the average number of signal events expected for a total injected flux  $\Phi_{\text{tot}} = 10^{-8} (\text{E}/1 \text{ GeV})^{-2} \text{ GeV}^{-1} \text{ cm}^{-2} \text{ s}^{-1}$  is  $\simeq 2$  tracks and  $\simeq 0.5$  showers.

Each neutrino event is characterized by its reconstructed direction  $(\alpha_i, \delta_i)$  in equatorial coordinates and its energy through the number of hits  $Nh_i$  used in the reconstruction procedure. For one particular channel (tracks or showers), the log-likelihood for the hypothesis  $H_1$  can be written as:

$$LL(\text{data}|H_1) = \sum_{i=1}^N \log \left[ \frac{n_s}{N} S_\gamma(\alpha_i, \delta_i, Nh_i) + \left(1 - \frac{n_s}{N}\right) B(\delta_i, Nh_i) \right] \quad (3.2)$$

where  $N$  is the total number of  $\nu$  events detected in the considered channel, the function  $S_\gamma$  is the probability density function (PDF) describing the expected astrophysical signal and the function  $B$  represents the background PDF, both function being normalized to unity. The free parameters are:  $n_s$  the number of signal events and the spectral index  $\gamma$  of the neutrino sources.

The log-likelihood for the background only hypothesis  $H_0$  is simply:

$$LL(\text{data}|H_0) = \sum_{i=1}^N \log B(\delta_i, Nh_i) \quad (3.3)$$

The test statistic that is used to compare the two hypothesis is the log-likelihood ratio:

$$Q = LL(\text{data}|H_1)^{\text{max}} - LL(\text{data}|H_0) \quad (3.4)$$

using the values of the parameters  $(\tilde{n}_s, \tilde{\gamma})$  that maximize the likelihood under hypothesis  $H_1$ .

We use pseudo-experiments to compute the test statistic distribution under the  $H_0$  hypothesis, that will be used to estimate the significance of the result. The discovery potential of the method can be estimated by generating pseudo-experiments where a neutrino flux  $\Phi$  is injected for a given spectral index  $\gamma$ .

The combination of the track and shower channels is performed using a global log-likelihood function:

$$LL(\text{data}|H_1) = \sum^{\text{N}_{\text{tracks}}} \log \left[ \frac{n_{\text{tr}}}{N_{\text{t}}} S_\gamma^{\text{tr}} + \left(1 - \frac{n_{\text{tr}}}{N_{\text{t}}}\right) B^{\text{tr}} \right] + \sum^{\text{N}_{\text{showers}}} \log \left[ \frac{n_{\text{sh}}}{N_{\text{s}}} S_\gamma^{\text{sh}} + \left(1 - \frac{n_{\text{sh}}}{N_{\text{s}}}\right) B^{\text{sh}} \right]$$

where the free parameters are the number of signal track events  $n_{\text{tr}}$ , the number of shower events  $n_{\text{sh}}$  and the common spectral index  $\gamma$ .

### 3.3 Ingredients for the likelihood

The signal PDF  $S(\alpha, \delta, Nh)$  represents the probability for an astrophysical neutrino emitted with energy  $E$  from a source located in  $(\alpha_s, \delta_s)$ , to be detected and reconstructed by ANTARES

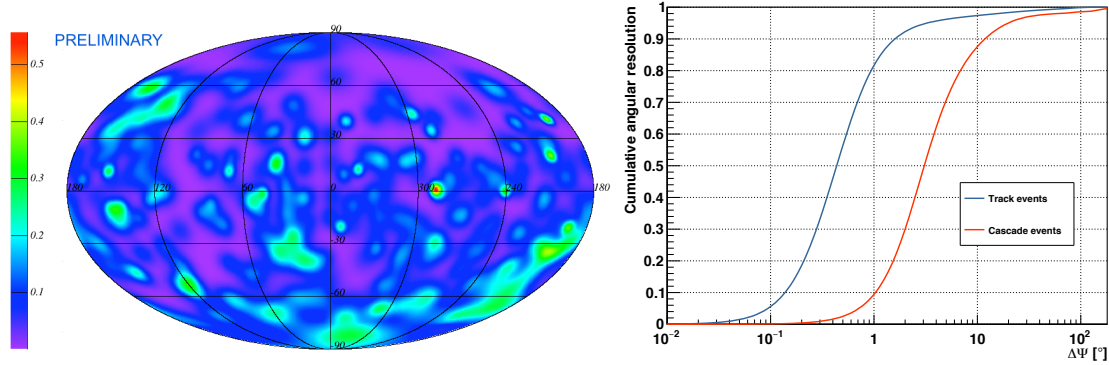


**Figure 1:** **Left:** map in equatorial coordinates of the source term  $f_{CR}$ , representing the probability to find a neutrino source in a given direction. The intensity of the color scale reflects only the contrast of the map, as the integral of the source term over the solid angle is made equal to 1. **Right:** average Point Spread Function for an  $E^{-2}$  spectrum: the cumulative distribution of the angle between the reconstructed direction of track (blue) and shower (red) events and the true Monte-Carlo neutrino direction is shown.

with  $(\alpha_{rec}, \delta_{rec}, Nh_{rec})$ . The signal PDF is built as a product of two terms: an angular, and an energy dependent term:

$$S_{\gamma}(\alpha, \delta, Nh) = f_{\gamma}(\alpha, \delta) \times g_{\gamma}(Nh) \quad (3.5)$$

The angular term  $f_{\gamma}(\alpha, \delta)$ , is defined as:

$$f_{\gamma}(\alpha, \delta) = A_{\gamma}(\delta) \times (f_{CR} * \text{PSF}_{\gamma})(\alpha, \delta) \quad (3.6)$$

where  $A_{\gamma}$  is the ANTARES acceptance,  $f_{CR}(\alpha_s, \delta_s)$  represents the probability for a neutrino source associated to a cosmic ray to be located at  $(\alpha_s, \delta_s)$ . Finally, to obtain the probability of reconstructing a neutrino at  $(\alpha_{rec}, \delta_{rec})$ , this source term is convoluted with the Point Spread Function (PSF) of the considered channel (right of figure 1). The acceptance and the PSF are tabulated as a function of declination and spectral index  $\gamma$ .

The source term  $f_{CR}$  is obtained by applying an energy dependent gaussian smearing  $\sigma(E)$  over the position of cosmic rays:

$$f_{CR}(\alpha_i, \delta_i) = \sum_{j=1}^{N_{CR}} \frac{\Phi}{2\pi\sigma_j^2} \exp\left(-\frac{d_{ij}^2}{2\sigma_j^2}\right) \quad (3.7)$$

where  $d_{ij}$  is the angular distance between the position of the neutrino and the cosmic ray. The standard deviation  $\sigma_j(E) = \sqrt{(\sigma_{Auger/TA}^2 + \sigma_B^2(E_j^{CR}))}$ , is obtained by summing in quadrature the angular resolution of the cosmic rays experiments:  $\sigma_{Auger} = 0.9^\circ$  [6] and  $\sigma_{TA} = 1.5^\circ$  [14], with the magnetic deflection term  $\sigma_B(E)$  given by equation 3.1. The function  $f_{CR}$  is represented in equatorial coordinates on figure 1 (left).

The energy term  $g_{\gamma}(Nh)$  uses the number of hits information to better discriminate atmospheric neutrinos and muons from the candidate astrophysical signal, due to their very different spectrum

( $\Phi_{\text{atm}} \propto E^{-3.7}$ ). The figure 2 shows for track and shower channels the expected distribution of the number of hits for the atmospheric background and for an  $E^{-2}$  astrophysical flux, together with the values observed in the real data sample.

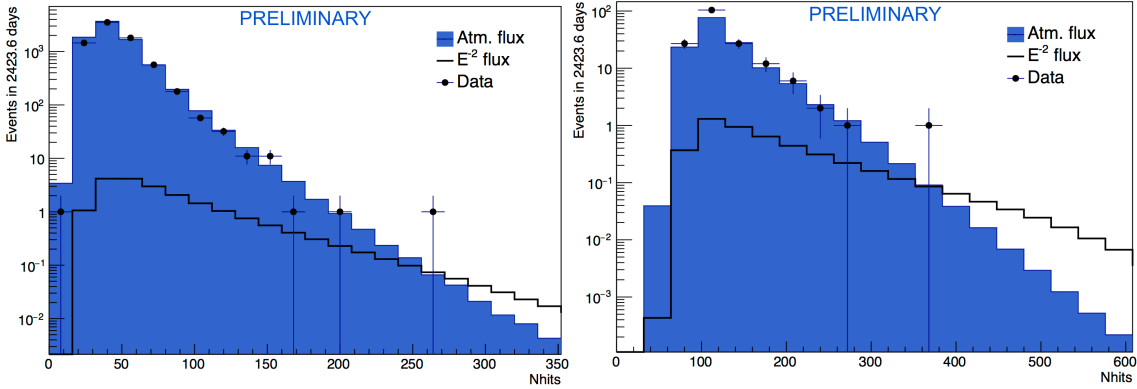


**Figure 2:** Distributions of the number of hits in the track (left) and shower (right) channels. The expectation for the atmospheric background (blue histogram) and for a diffuse astrophysical  $\Phi_0 E^{-2}$  flux (black line) are represented, together with the data (black dots). The vertical scale indicates the number of events expected for the total live time considered in the analysis, the normalization of the diffuse flux used for comparison is  $\Phi_0 = 10^{-8} \text{ GeV}^{-1} \text{ cm}^{-2} \text{ s}^{-1} \text{ sr}^{-1}$ .

The background PDF  $B(\delta, Nh)$  that accounts for the atmospheric flux is assumed to be uniform in right ascension. As for the signal PDF, it is factorized into an angular term and an energy term:

$$B(\delta, Nh) = f(\delta) \times g(Nh) \quad (3.8)$$

where  $f(\delta)$  is the declination distribution and  $g(Nh)$  is the distribution of the number of hits shown in figure 2. The expected contribution of an astrophysical signal being small, the actual declination distribution observed in data is used for the function  $f(\delta)$  (see figure 3), whereas the function  $g(Nh)$  is obtained from Monte-Carlo. To get a stable behavior of the minimization procedure, a smooth function fitted on the declination distribution is effectively used in the likelihood.

### 3.4 Discovery Potential

To evaluate the sensitivity of the analysis, a large number of pseudo-experiments have been generated for the background and signal. Background events are simulated by sampling directly the declination and the number of hits from the parameterization of  $B$ , while the right ascension is sampled from a uniform distribution in  $[0; 2\pi]$ .

The signal events are generated for a given flux  $\Phi_0$  per source with the following procedure: for each cosmic ray, a random neutrino source position is determined from a 2d gaussian function corresponding to equation 3.7. A random number of neutrino events is then generated according to a Poisson distribution with a mean equal to  $\Phi_0 \times A_\gamma(\delta)$ . The final coordinates of the events are obtained by adding a random deviation sampled from the  $\text{PSF}_\gamma(\delta)$ , and a number of hits from the histograms of figure 2.

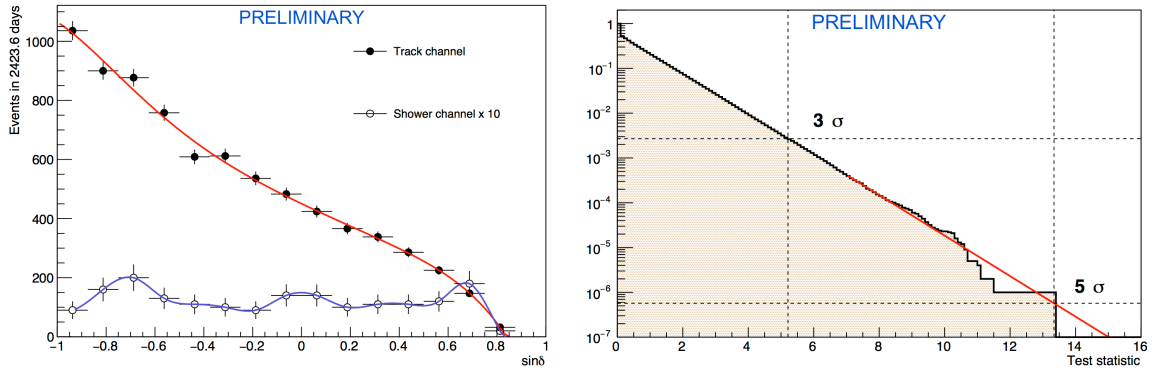


**Figure 3:** **Left** : Declination distribution observed in data in the track (black dots) and shower (empty circles) channels, together with the smooth curves that are used to compute the background PDF for the likelihood (for presentation purposes, the shower channel is multiplied by a factor 10). **Right**: Anti-cumulative distribution of the test statistic  $Q = LL(\text{data}|H_1)^{\text{max}} - LL(\text{data}|H_0)$  in the background only hypothesis, for the combined sample tracks+showers. The dotted lines show the  $3\sigma$  and  $5\sigma$  significance levels and the corresponding values of the test statistic. An exponential fit (red line) is performed on the tail of the distribution to estimate the position of the  $5\sigma$  level.

The distribution of the test statistic for the combined sample in the background only hypothesis is shown in figure 3. It is obtained by performing the full minimization procedure on a large number ( $10^6$ ) of pseudo-experiments. The value of the test statistic  $Q_{3\sigma}$  and  $Q_{5\sigma}$  corresponding to p-values of  $2.7 \times 10^{-3}$  and  $5.7 \times 10^{-7}$  are reported for illustration.

The median discovery potential at 3 or  $5\sigma$  is defined as the minimum flux  $\Phi_{3/5\sigma}$  (or number of events  $n_{3/5\sigma}$ ) that is required to get a test statistic value  $Q > Q_{3/5\sigma}$  in 50% of the pseudo-experiments. The table 1 summarizes the results that have been obtained for an  $E^{-2}$  spectrum.

Discovery potential	$n_{3\sigma}$	$n_{5\sigma}$	$\Phi_{3\sigma}^{\text{tot}}$ ( $\text{GeV}^{-1}\text{cm}^{-2}\text{s}^{-1}$ )	$\Phi_{5\sigma}^{\text{tot}}$ ( $\text{GeV}^{-1}\text{cm}^{-2}\text{s}^{-1}$ )
Tracks	64	117	$3.1 \cdot 10^{-7}$	$5.7 \cdot 10^{-7}$
Showers	21	40	$4.4 \cdot 10^{-7}$	$8.3 \cdot 10^{-7}$
Combined	51 tr +12 sh	94tr + 22 sh	$2.5 \cdot 10^{-7}$	$4.6 \cdot 10^{-7}$

**Table 1:** Discovery potential of the analysis for tracks (tr) showers (sh) and for the combined sample.

#### 4. Results and conclusion

The application of the likelihood fit on the full data sample tracks+showers gives the following results:  $n_{\text{tr}} = 10^{-3}$ ,  $n_{\text{sh}} = 11.4$ , with a spectral index  $\gamma = -3$ . The test statistic is  $Q_{\text{data}} = 0.26$ , leading to a p-value of  $p = 0.46$  (computed from the curve of figure 3).

From this non-significant result, we can compute the 90%C.L upper-limit on the total all-flavor flux  $\Phi_{\text{tot}}$  that is emitted by the potential neutrino sources associated with the UHECRs population. We estimate with pseudo-experiments the smallest flux that is required to get at least

90% of the test statistics values  $Q > Q_{\text{data}}$ , leading to a value:  $\Phi_{\text{tot}}^{\text{UL}} = 1.5 \cdot 10^{-7} \text{ GeV}^{-1} \text{ cm}^{-2} \text{ s}^{-1}$ . For comparison with other analyses, this limit can be converted into an equivalent diffuse flux of  $\Phi_{\text{dif}} = \Phi_{\text{tot}}^{\text{UL}} / 4\pi = 1.2 \cdot 10^{-8} \text{ GeV}^{-1} \text{ cm}^{-2} \text{ s}^{-1} \text{ sr}^{-1}$ .

The neutrinos from the all-flavors point source sample collected by ANTARES during nine years of data acquisition shows no evidence of correlation with the 318 UHECRs above 52 EeV measured by the Pierre Auger Observatory and the the Telescope Array.

We note that the observation of such a correlation relies on several assumptions that may not be fulfilled: the magnetic deflections that we assume could be largely underestimated, especially if the cosmic ray mass composition is heavy.

The potential strong difference in range between the UHECRs above  $\sim 50$  EeV that suffer from energy losses and the neutrinos that can come from cosmological distances reduces the amount of common sources that can be observed. The propagation time of cosmic rays in magnetic fields compared to neutrinos could also lead to the absence of correlation if the UHECRs sources are transient.

In addition, the energies of the cosmic rays considered here are  $\sim 6$  orders of magnitude higher than those of the neutrinos, hence only a fraction of the neutrinos sources could potentially be the same accelerators of UHECRs.

The discovery potential of future searches will be enhanced with more statistic and when a measure of the mass composition of the cosmic rays at the highest energies will be available.

## References

- [1] IceCube Collaboration, Pierre Auger Collaboration, & Telescope Array Collaboration 2016, JCAP, 01-037I 2016
- [2] A. Aab et al., Nucl. Instrum. Meth. A798, 172-213 2015.
- [3] T. Abu-Zayyad et al., Nucl. Instrum. Meth. A 689 (2012) 87.
- [4] J. A. Aguilar et al, *Nuclear Inst. and Methods in Physics Research A* 656 11 2011.
- [5] Antares Collaboration, arXiv:1706.01857.
- [6] A. Aab et al., *Astrophys.J.* 804 (2015) no.1, 15
- [7] II. Maris, presentation at the UHECR symposium (2014), Springdale, USA, [http://uhecr2014.telescopearray.org/maris/TAAuger\\_Springdale.pdf](http://uhecr2014.telescopearray.org/maris/TAAuger_Springdale.pdf).
- [8] R.U. Abbasi et al., *Astropart. Phys.* 64 (2014) 49.
- [9] A. Aab et al., *Phys. Rev. D* 90 (2014) 12 122005.
- [10] The Pierre Auger Collaboration. 2016, Upgrade - Preliminary Design Report, ArXiv:1604.03637
- [11] M. S. Pshirkov, P. G. Tinyakov, F. R. Urban, *Phys. Rev. Lett.* 116, 191302 (2016).
- [12] R. Jansson and G.R. Farrar, *Astrophys. J.* 757 (2012) 14.
- [13] M.S. Pshirkov, P.G. Tinyakov, P.P. Kronberg and K.J. Newton-McGee, *Astrophys. J.* 738 (2011) 192.
- [14] M. G. Aartsen et al., JCAP 1601 (2016) no.01, 037.